The Influence of Seasonal Forcing on the Population Dynamics of Ecological Systems

Rachel Anne Taylor

Submitted for the degree of
Doctor of Philosophy

Heriot-Watt University

Department of Mathematics,
School of Mathematical and Computer Sciences.

June 24, 2014

Abstract

Seasonal forcing represents a pervasive source of environmental variability and it has been shown to be important in generating the cycles observed in many ecological and epidemiological systems. We use a combination of bifurcation analysis and simulation to understand the impact of seasonality on population dynamics, with a focus on predator-prey and host-macroparasite systems. Multi-year cycles with a wide range of periods, quasi-periodicity and chaos are found.

We consider the importance of the unforced dynamics in a predator-prey system by contrasting the effect of seasonality when the underlying behaviour is oscillatory decay to the equilibrium or limit cycles. The limit cycles case shows a wider range of dynamics and multiple solutions. The effect of variations in the seasonal forcing term are analysed in a predator-prey model by changing the breeding season length, using the vole system in Fennoscandia as a case study. It is found that the period of the multi-year cycles increases as the breeding season length decreases. By studying a general host-macroparasite system, in which the effect of seasonality has not previously been explored in detail, we find a larger potential for multiple solution behaviour compared to predator-prey systems.

Overall, we show the critical role that seasonality can play in ecological systems.

Acknowledgements

I am extremely grateful to both my supervisors, Andrew White and Jonathan Sherratt, for their insights, support and encouragement, without whom this process would not have been as smooth or as enjoyable. They always gave freely of their time, encouraged me to publish, and motivated me to work hard. Specific thanks go to Andy for always reminding me to bring it back to the biology and to Jonathan for pointing out thought-provoking questions or areas which I would not have considered.

My flatmates, department friends and church family have made my time here so wonderful. And to the city of Edinburgh – what an inspiring place to live! I extend my gratitude particularly to my officemates, for providing motivation, advice, and a chance to procrastinate and have completely random conversations. They have been a fabulous group and even put up with my noisy typing!

I am indebted to my family for the support and encouragement I received to do the Ph.D. and throughout the whole journey. Simon, John and Lyndsey always brought me back down to earth. I would especially like to thank my parents for everything they've done for me. For Mum putting up with boring maths conversations and for Dad wanting to have them.

I offer thanksgiving to God for the talents and desires that I have been blessed with which have brought me here, and for the support He has given me throughout the whole Ph.D. These words strengthened me through the final few months:

> *"May the God of hope fill you with all joy and peace as you trust in Him, so that you may overflow with hope by the power of the Holy Spirit."*
> Romans 15:13.

Contents

List of Figures

Chapter 1

Introduction

This thesis studies the effect of seasonal forcing on different ecological systems, with a focus on predator-prey and host-macroparasite interactions. It considers in depth the possible dynamics that can result from seasonal forcing applied to parameters within these models, the bifurcations leading to these dynamics and the potential for multiple solution behaviour. The aim of this thesis is to understand in full the resultant population dynamics when seasonal forcing is applied to model parameters. In particular, we detail how seasonal forcing can drive changes in the population dynamics leading to population cycles with a wide range of periods, quasi-periodicity and chaos.

Population cycles are a frequent occurrence across many different species, with a significant impact on human and natural systems (Kendall et al., 1998; Turchin, 2003). Cyclic populations can cause management or economic concern, with prime examples being cyclic outbreaks of pest species destroying crops (e.g. larch budmoth (Baltensweiler et al., 2008)), reductions in fish stocks (e.g. salmon (Krkošek et al., 2011)), or outbreaks of diseases (e.g. measles (Earn et al., 2000)). Population cycles are also an interesting ecological puzzle due to the many different causes of cyclicity, the potential for extinction during low phases of the cycles, the need to anticipate future peaks or troughs, or trying to understand the loss of cycles within systems.

There are many reasons for populations to cycle, with these different factors often interacting within each system (Krebs et al., 2001). Intrinsic cyclic behaviour of the system is a commonly attributed cause, with the most well-known example being predator-prey cycles as described first by Lotka and Volterra (Lotka, 1920; Volterra, 1928). Predator-exclusion experiments have indicated that population cycles can be directly caused by predation, such as in the Fennoscandian vole system in which predator removal led to loss of the vole cycles (Korpimaki and Norrdahl, 1998; Korpimaki et al., 2002). Oscillations can be sustained by stochastic noise (Nisbet and Gurney, 1982; Kuske et al., 2007), or stochasticity can lead to alternating steady states (Dakos et al., 2013). This thesis concentrates on one of the most ubiquitous drivers of cyclic

dynamics – seasonal forcing. Seasonal forcing can lead to cycles on its own, such as in influenza epidemics (Dushoff et al., 2004) or it can be present alongside one of more of these other factors inducing cycles (Gammaitoni et al., 1998; Mabille et al., 2010). The desire to understand the causes and consequences of population cycles is one motivation for studying in detail the effect of seasonal forcing on population dynamics.

1.1 Seasonal Forcing

The study of seasonal forcing, or seasonality, considers largely predictable yearly or seasonal fluctuations which affect populations externally through their life-history parameters (Altizer et al., 2006). These fluctuations could be caused by changing resource levels throughout the year (Scheffer et al., 1997), changing transmission rates, for example because of a rainy season (Watts et al., 1987), changing predation rates (Korpimaki and Krebs, 1996) or many other factors (Sultan et al., 2005; Altizer et al., 2006; Cornell et al., 2008; Oraby et al., 2014). We choose to study perhaps the most pervasive form of seasonality, the yearly fluctuations in the birth rate in which populations restrict their breeding to a portion of the year, usually spring or summertime. This restricted breeding season is common to a large percentage of different animal species located in temperate regions, including insects, fish, mammals, birds, amphibians and reptiles; even humans show seasonal peaks in their birth rate (He and Earn, 2007). It is thus natural to wish to understand fully how these fluctuations can impact on the population dynamics.

It is widely accepted that seasonal forcing can be a driver of population cycles in a range of different systems (Kendall et al., 1999; Altizer et al., 2006; Keeling and Rohani, 2008; Sherratt and Smith, 2008; Smith et al., 2008). In both interacting populations and microparasite systems, seasonality has been well-established as a factor in generating the observed cycles found in data. For example, seasonal forcing has been shown to induce $2-3$ year cycles in measles incidence due to yearly variation in the rate of transmission caused by school terms (Earn et al., 2000; Finkenstadt and Grenfell, 2000). Another example is that of the lake plankton cycle in which clear water phases can be absent or occur up to 4 times in a year. Scheffer et al. (1997) showed that that these clear water phases could be replicated using a seasonally forced predator-prey model of Daphnia (predator) and algae (prey).

Furthermore, seasonal forcing is important when considering the effect of climate change as this can lead to changes in the yearly fluctuations (Intergovernmental Panel On Climate Change, 2001). Knowing how population dynamics alter when the breeding season length varies or when the size of the fluctuations in the birth rate increases is a key part of studying seasonal forcing and can help in the understanding of how

a changing climate could impact on the ecosystem. Climate change has been implicated already in the loss of cycles for different species (Ims et al., 2008) which can have damaging and widespread effects on many other species within the ecosystem. Thus, studying seasonal forcing is also motivated by this desire to understand populations within a changing climate.

1.2 The Study of Seasonal Forcing

In the seminal work of Dietz (1976), seasonal forcing was studied in an epidemiological model by introducing a sinusoidal term in one of the parameters to represent the fluctuations throughout the year. This work showed that seasonal forcing could produce multi-year cycles (specifically, 2 year cycles of measles incidence) through the occurrence of subharmonic resonance. Following on from Dietz, seasonal forcing is commonly incorporated in models through a periodic term in one or more of the parameters. Step functions, in place of sinusoidal functions, have been used as they can be a more realistic interpretation of the actual system, but it is unclear whether the resulting dynamics are significantly altered by this change (Altizer et al., 2006) and sinusoidal terms often lead to more tractable models.

However, different methods of investigating the subharmonic resonance and other resulting dynamics have been used, such as a bifurcation approach, a resonance-based approach and others. We outline these methods and their various advantages and disadvantages here and explain why we have studied seasonal forcing in the manner we utilise in Chapters 2 - 4.

1.2.1 A Bifurcation Approach

The bifurcation approach to understanding seasonally forced systems has been advanced primarily by Rinaldi and co-workers (Kuznetsov et al., 1992; Rinaldi et al., 1993; Rinaldi and Muratori, 1993; Kuznetsov and Piccardi, 1994; Gragnani and Rinaldi, 1995). This approach focusses on producing a two-dimensional bifurcation diagram of the system to show when different dynamics exist and are stable, outlined by the various bifurcation curves. Each diagram is thus split into different dynamical regions by the bifurcation curves. Numerical bifurcation software is used to produce these bifurcation diagrams; there are two main software programs, namely AUTO (Doedel, 1981) and LOCBIF (Khibnik et al., 1992) as well as adaptations for Windows and Matlab – CONTENT (Kutznetsov and Levitin, 1997), MatCont (Dhooge et al., 2003) and XPPAUT (Ermentrout, 2012). For periodically forced systems the software is capable of detecting and tracing period-doubling, fold and Neimark-Sacker bifurcation curves, which can give rise to multi-year cycles, quasi-periodicity and chaos (for a

description of these bifurcations, please see §2.3). However, many of the software programs are also able to detect codimension-2 points and higher, which indicate when different bifurcation curves intersect or branch off from each other (Kuznetsov, 1995). Thus, it is possible to work out whether all bifurcation curves have been found using these codimension points.

Often the bifurcation diagrams will have the amplitude of the forcing on one axis with the mean value of the forced parameter on the other. This allows for a comprehensive exploration of the impact of the forced parameter on the dynamics. On the axis with forcing amplitude equal to zero, the system effectively reduces to the unforced model and thus as the forcing amplitude increases, it is possible to directly compare how forcing interacts with the unforced dynamics.

Numerical bifurcation continuation is a powerful mathematical method, and will only increase in power with advances in software. Using this method, one is able to categorically state whether the yearly and multi-year solutions exist and are stable and through what bifurcations these processes happen. Thus, a full mathematical understanding is possible for that parameter regime. It indicates whether regions with multiple solutions exist as well as whether shifts in the seasonal forcing can lead to "catastrophes" when the dynamics change dramatically. However, issues with this bifurcation approach include the lack of information on the relative frequency of multi-year cycles when there are multiple solutions, and its inability (at present) to indicate when chaos arises due to the quasi-periodicity disappearing through torus destruction.

This bifurcation approach is the most comprehensive way of analysing the system's dynamical structure under the influence of seasonal forcing. However, the method is quite technical and perhaps has not been well enough explained to a more biological audience.

1.2.2 A Resonance Approach

The resonance approach has been pioneered by Greenman and collaborators (Greenman et al., 2004; Ireland et al., 2004; Greenman and Norman, 2007; Greenman and Pasour, 2011) on the basis that explaining the dynamics in terms of the natural period and resonance would be more intuitive than using bifurcation diagrams. Through a rescaling of both the model parameters and time by a new parameter p, the system is converted into one in which the external forcing period can vary. Therefore, for each value of p the system can be considered in two different ways – either as the original parameter values with non-annual periodic forcing or as a different parameter set under annual forcing. A resonance diagram is then produced by simulation to show the change in solution amplitude and period as this parameter p is varied. Numerous simulations are required for each value of p due to the possibility of multiple solution

behaviour. Peaks in solution amplitude occur when the parameter p is equal to the natural oscillation of the system (i.e. when the forcing and the natural oscillation of the system resonate) or integer factors of this value (i.e. subharmonic resonance), and these solutions have period determined by this integer factor. These peaks also start to "bend over" creating a wave shape and leading to multiple solution behaviour.

This method provides a clear illustration of the link between the multi-year cycles and the underlying oscillation of the system, and while doing so, shows the change in solution amplitude for the different multi-year cycles, and the yearly cycle at resonance. (This link between the cycles and the underlying oscillation is included in the bifurcation diagram approach but is not so obvious at first glance, although a plot showing the period of the unforced system makes it clear.) Also, the fact that it is possible to trace a curve in parameter space to explore the dynamics under yearly forcing for different parameters is convenient, but all the parameters are changing by the same proportion which limits its usefulness.

In general, there are numerous drawbacks with this approach. Firstly, it is based on simulation and so there is always the possibility of missing one or more solutions due to small basins of attraction, even though understanding of the underlying oscillations will indicate where multi-year solutions should be located. It becomes simulation intensive, especially because each resonance diagram is for only one value of the forcing amplitude and thus multiple diagrams have to be produced. This leads to difficulties in understanding the effect of increasing the forcing amplitude on the dynamics as it is not obvious how one resonance diagram morphs into another for different values of forcing amplitude (a more likely change to a real-world system than a change in the forcing period). Solutions which exist but are not stable are not found nor are the bifurcations which lead to the appearance and disappearance of each of the multi-year cycles. Therefore, a full understanding of the system under seasonal forcing is not possible with this approach.

1.2.3 Other Approaches

King and Schaffer (1999, 2001); Schaffer et al. (2001) also used bifurcation theory to explain seasonally forced dynamics but from a different perspective than the approach described in §1.2.1. Their aim was to present an overarching framework for seasonal forcing, with the idea that previous studies were in effect particular cases within this framework. To do this, they represented predator-prey models as perturbations of a Hamiltonian limit. Again using numerical bifurcation software, they explore the Hamiltonian limit through two-dimensional bifurcation diagrams and sections of the Poincaré map, as well as constructing a "rainbow bridge" from the Hamiltonian limit back to the original system. Much of the structure within the Hamiltonian limit is still present in the original system under seasonal forcing.

From a completely different perspective, Stone et al. (2007); Olinky et al. (2008) did not focus on the overall dynamical structure but instead on predicting whether there will be a peak in the current year and how many non-peak years to expect after. They were considering recurrent epidemics (caused by seasonal forcing) but it would be of interest if their methods are applicable to a wider range of models. Predictability of an epidemic is particularly useful when the system has chaotic dynamics or when noise is present leading to switches between multiple solutions. While all the above methods are much more useful at exploring the effects of seasonal forcing generally, this method is suitable for learning how to predict and control the cyclic dynamics.

1.2.4 Our Approach

The bifurcation approach is definitely the most comprehensive and effective at analysing the impact of seasonal forcing in population systems, thus it will be the key aspect of the methodology in this thesis. However, to overcome some of the shortcomings of this approach, namely the lack of information on the relative frequency of the multiple solutions and the rather technical nature of the bifurcation approach, we will supplement the bifurcation analysis with extensive simulations that directly correspond to the bifurcation diagrams. The relative sizes of the basins of attraction when there is multiple solution behaviour are therefore calculated, as well as information on the solution amplitude for the different multi-year cycles. We then present these simulations in an innovative way, using a grid of pie charts. The fact that the simulations directly relate back to the bifurcation diagram helps in the understanding of the effect of each bifurcation curve as it is clear from simulations whether solutions have become stable (or unstable) from their appearance (or disappearance) in the simulation diagrams.

We use AUTO bifurcation software (Doedel, 1981) to perform this bifurcation analysis. We present here a detailed outline of the procedure we implement in AUTO to find the bifurcation curves. Suppose that we have a system of ODE's of the form:

$$\dot{\underline{u}} = f(\underline{u}, p) \tag{1.1}$$

where p is a parameter that we wish to force. In order to use AUTO for forced systems we need to augment each of our models with a pair of decoupled ODEs to produce the term required for the forcing, following the procedure in Doedel and Oldeman (2009, §14.5). This limits our forcing term to be continuous rather than a step function.

More precisely, we input into AUTO the following system of ODE's:

$$\dot{\underline{u}} = f(\underline{u}, p(x)) \tag{1.2a}$$

$$\dot{x} = x + 2\pi y - x(x^2 + y^2) \tag{1.2b}$$

$$\dot{y} = -2\pi x + y - y(x^2 + y^2) \tag{1.2c}$$

The last two equations produce the solution $x = \sin(2\pi t)$ and thus the usual sinusoidal forcing term is produced with

$$p(x) = p_0(1 + \epsilon x) = p_0(1 + \epsilon \sin(2\pi t)) \tag{1.3}$$

where p_0 is the mean value of the forced parameter, ϵ is the amplitude of the forcing and the period of the forcing is 1 year. For more detail on how these equations are inputted into AUTO please see Appendix A for actual code from each of our models in Chapters 2 - 4. Using Matlab simulation or by directly analysing the differential equations, the equilibrium values are found for our chosen starting parameter values. These are inputted into the AUTO code as initial conditions.

We assume for this outline of our procedure that p_0 and ϵ are the axes for our two-dimensional bifurcation diagrams, which is the presentational format that we use in Chapter 2. Information on the specific bifurcations is given in §2.3.

1. We begin first by considering purely the unforced system, thus we use the "stationary solutions of ODEs" setting (specifically this means that the constant IPS = 1 in the AUTO constants file; a sample constants file is in Appendix A). Tracing the equlibrium solution by varying p_0 leads to hitting the Hopf bifurcation, whose presence should be known through direct analysis of the differential equations. Changing IPS = 2 and adding parameter 11 to the list of free parameters allows AUTO to switch at the Hopf bifurcation onto the limit cycles solution branch and parameter 11 informs us of the period of these limit cycles. The amplitude can also be found. This indicates which multi-year cycles to expect and the specific values of p_0 at which they occur.

2. We now consider the forced system. For this IPS must equal 2 and parameter 11 must be a free parameter. We trace the equilibrium solution by increasing ϵ from 0. This may find the Neimark-Sacker bifurcation directly; otherwise we switch to tracing in p_0 to find it. The Neimark-Sacker bifurcation hits the axis where the unforced system has a Hopf bifurcation which gives a good indication of where to find the Neimark-Sacker bifurcation curve. We trace this Neimark-Sacker bifurcation curve by changing ISW = 2 to indicate that we are tracing a locus of a bifurcation, and have three free parameters (p_0, ϵ and the period).

3. When tracing the Neimark-Sacker bifurcation curve, AUTO will flag whenever there is a codimension-2 point, indicating that another bifurcation curve is hitting the Neimark-Sacker curve. AUTO tells us which type of curve has hit the Neimark-Sacker bifurcation curve.

4. If the period of the unforced system started below 2, this is a good indication that there will be a period-doubling curve present which can be found by knowledge of whether it hits the Neimark-Sacker bifurcation curve, or purely by tracing along the yearly solution for p_0 and ϵ.

5. Once a period-doubling curve has been found it can be traced in the same way as the Neimark-Sacker bifurcation curve. Again, codimension-2 points should indicate the presence of a 2 year fold curve. However, AUTO cannot switch onto another type of bifurcation curve at a codimension-2 point thus we have to change back onto the solution curve, find the other bifurcation curve, and then trace it.

6. Directed simulation in Matlab can find multi-year solutions, based on the values of p_0 where the specific period is present in the stable limit cycles. To start on this multi-year cycle, we run AUTO without the initial conditions for the equilibrium solution and instead input a whole period of numerical data for each of the variables, in the manner of Doedel and Oldeman (2009, §14.4). This numerical data can come straight from Matlab.

7. Once we are on the multi-year solution, the fold bifurcation and any period-doubling or Neimark-Sacker bifurcations which may occur to the solution can then be traced in a similar manner to that described above.

In Chapters 2 and 3 the bifurcation diagrams are supported by extensive numerical simulations which are all performed in Matlab using `ode15s`. The solutions are tested to determine whether there is a periodic solution with a period up to our maximum test period. This maximum test period is different for the three models in Chapters 2 - 4, based on the periods expressed in the unforced dynamics. The choice is arbitrary; there could in principle be solutions with any finite integer period but an upper limit is required for numerical study. If a periodic solution with period less than or equal to the maximum test period is not found, then the solution is declared to be quasi-periodic. Hence, simulations showing quasi-periodicity could actually be periodic with a period higher than this maximum test period, or they could be chaotic. To test whether a solution had a period of, for example, four years, the value of the solution is recorded for 20 time points at intervals of 4 years, after an initial time period of sufficient length that transients have decayed. If the difference between the maximum and minimum of these numbers is less than 2.5% of their mean value, then

it is declared a four year solution. Tests of some difficult cases near bifurcation curves or within multiple solution regions led to the choice of the run time length, the 20 test points used and the threshold level of 2.5% variation as they enabled periodic and quasi-periodic solutions to be distinguished. We also investigated the use of the fast Fourier transform to find power spectra as a means of calculating the period but it was found to be less effective. However, it still gives a good indication of how often the solution peaks, thus we used it to help determine the "dominant period." Solutions are replicated 50 times using different (random) initial conditions between 0 and 1, independently chosen for all variables. We determine the basins of attraction by examining the frequency of particular solutions from these 50 simulations. However, points in parameter space which show multiple attractors are recomputed with 500 simulations to gain increased accuracy of the relative sizes of the basins of attractions.

1.3 Our Aims

A major aim of this thesis is to discern the importance of the unforced dynamics when seasonality is applied to ecological and epidemiological models. Resonance between the underlying period of the system and the forcing period indicates that the underlying period is crucial to the forced dynamics. The bifurcation theory of how this resonance occurs is well developed (see §2.3 for details on Arnol'd tongues) but there are still many issues that are not clearly understood. This includes how seasonality affects systems that are experiencing oscillatory decay to the equilibrium compared to systems with limit cycles. Both of these are oscillatory with a period that can resonate with the forcing period, but it is not apparent whether the overall dynamics are different for the two regimes. Another aspect that is still ambiguous is the effect on the dynamics of varying the period of the unforced limit cycles through changes in the parameter values. Does this lead to multi-year cycles of different period only or do the bifurcation diagrams change in other ways too? Related to this is the issue of how the structure of the unforced dynamics impacts on the forced system, such as the potential for multiple solution behaviour and the range of stable multi-year cycle periods. Within this thesis, we consider these aspects of the interaction between the unforced system and the seasonality in detail and provide insight into this important topic within seasonal forcing.

This thesis focusses on seasonal forcing in predator-prey and host-macroparasite systems. By studying different systems, we are able to assess whether seasonal forcing acts in a similar manner for many types of models or whether there are significant differences depending on the unforced model dynamics. These two models are comparable since cycles are possible without any forcing for both. However, does this indicate that when forcing is added to these models they will respond with simi-

lar dynamics? Gragnani and Rinaldi (1995) found that the bifurcation diagrams for the seasonally forced Rosenzweig-McArthur predator-prey model were topologically equivalent to a chemostat model (an extension of the Rosenzweig-McArthur model). Further, this was true for all the forced parameters which they considered (Rinaldi et al., 1993). Thus, the suggestion is that models with similar unforced dynamics will also have similar forced dynamics, and that the models respond in the same way regardless of which parameter is being forced. In this thesis we provide some insight into both of these ideas.

Another aim of this thesis is to broaden the scope of seasonal forcing study. Primarily the focus has been on exploring the effect of increasing the amplitude of the forcing. But the level of seasonality in a system is likely to change for numerous reasons and these may do more than purely increase the amplitude of the forcing. For example, the length of a breeding season or a rainy season could vary, and these variations should be included so that the seasonal forcing is as biologically realistic as possible. We consider how these changes could impact on the possible forced dynamics.

A final aim is to study the effects of seasonal forcing in a system in which it has not been previously considered in depth, namely in host-macroparasite systems. The focus of seasonal forcing literature has predominantly been for interacting populations and host-microparasite systems. We wish to widen the scope of the literature by showing that seasonal forcing can have a significant impact on host-macroparasite systems as well.

In Chapter 2, we consider a general predator-prey model with seasonally forced prey growth rate. While this model subject to seasonal forcing has been studied previously, the case of seasonally forced prey growth rate was omitted. The prey growth rate is a unique parameter in this model as it is the only one not involved in the condition for a Hopf bifurcation to occur. Thus, we can tailor our parameter choice in order to analyse separately the effect of a seasonally forced growth rate when the system has monotonic decay to the equilibrium, oscillatory decay or limit cycles in the unforced system. We outline the necessary bifurcation theory for periodically forced systems which will be required for the whole thesis, and present both bifurcation and simulation diagrams for the different unforced dynamical regimes. Additionally, we explore how the bifurcation diagrams transform into each other as the parameters are changed from one regime to another.

Chapter 3 also considers a predator-prey model with forcing on the prey growth rate, although this model includes both generalist and specialist predation. In this chapter we address the idea, mentioned above, that deviations in the seasonal forcing can occur in more ways than purely through the amplitude of the forcing and we

ask whether this can result in different dynamics. These variations in the seasonal forcing could be caused by latitude, altitude, proximity to the coastline or other factors. Fennoscandian voles are used as a case study as they are spread over a large geographical location and show significant differences in their cyclic dynamics along this latitudinal gradient. We explore whether this geographical gradient in population cycles can be explained by changes in the breeding season, alongside variation in the level of generalist predation. To do this, the seasonal forcing term is adapted to represent changes in the length of the breeding season. Again we use bifurcation and simulation diagrams to show the range of dynamics possible as both breeding season length and level of generalist predation vary.

In Chapter 4 we focus on a host-macroparasite system with seasonal forcing in the host birth rate. The model includes the free-living larval stage explicitly, leading to limit cycles in the unforced system. We first study the system with parameters adapted for red grouse in England and Scotland, and using bifurcation analysis we show how changing the forcing amplitude and the impact of the macroparasite on host fecundity affects the population cycles. We then extend the parameter range in order to understand more generally the effect of the period of the limit cycles in the unforced system on the resulting dynamics when forcing is applied. To do this, we analyse the bifurcation diagrams for different values of the host birth rate, as varying this parameter leads to changes in the period of the limit cycles of the unforced system.

Finally, in Chapter 5 we discuss overall implications and conclusions of this research as well as areas in which further work would be useful so that the application of seasonal forcing within ecological systems can be more completely understood.

Chapter 2

Seasonal Forcing and Multi-Year Cycles in Interacting Populations: Lessons from a Predator-Prey Model

The majority of this chapter forms the following publication:
Rachel A. Taylor, Jonathan A. Sherratt, Andrew White. Seasonal Forcing and Multi-Year Cycles in Interacting Populations: Lessons from a Predator-Prey Model. *Journal of Mathematical Biology*, 67(6-7):1741-1764, 2013.

2.1 Introduction

Many natural systems are subject to significant seasonal fluctuations in their life history parameters. This has been studied in the context of epidemiology, and seasonal forcing has been proposed as the cause of multi-year cycles for a number of diseases in human and wildlife populations (Dietz, 1976; Finkenstadt and Grenfell, 2000; Dushoff et al., 2004; Altizer et al., 2006; Keeling and Rohani, 2008; Smith et al., 2008). Literature on interacting populations which include seasonal forcing is also plentiful. Interacting population systems can often cycle without forcing, implying a richer range of potential effects of seasonality, and conclusions from previous studies indicate that seasonal forcing can have critical effects on the population behaviour (Scheffer et al., 1997; Holt and Colvin, 1997; Stenseth et al., 1998; Mabille et al., 2010).

The main mathematical approach to investigating the effects of seasonal forcing in epidemiological and ecological models is the bifurcation approach of Rinaldi and co-workers (Kuznetsov et al., 1992; Rinaldi et al., 1993; Rinaldi and Muratori, 1993; Kuznetsov and Piccardi, 1994; Kuznetsov, 1995) and continued by others (Mancusi

et al., 2004; Bolzoni et al., 2008). This uses numerical bifurcation software to construct bifurcation diagrams of solution behaviour as the forcing parameters are varied. It provides a systematic method for investigating solution structure and revealing all possible solutions. However, when there are multiple stable solutions, it gives no information on the relative frequency with which these arise. Alternative approaches include the resonance approach pioneered by Greenman (Greenman et al., 2004; Ireland et al., 2004; Greenman and Norman, 2007; Greenman and Pasour, 2011) and bifurcation analysis in the manner of King and Schaffer (1999, 2001); Schaffer et al. (2001). The resonance approach constructs resonance diagrams to demonstrate increases in solution amplitude when the forcing period and the underlying period of the unforced system are integer multiples of one another. The approach used by King and Schaffer examines the bifurcation structure by formulating the model as a perturbation of a Hamiltonian limit, and then presents the work through a combination of two-dimensional bifurcation diagrams and sections of the Poincaré map.

In this chapter, we will focus on the bifurcation approach to understand solution behaviour and augment it by a systematic program of numerical simulations in order to give more information on basins of attraction. We consider the specific case of the Rosenzweig-MacArthur predator-prey model with sinusoidal forcing of the prey growth rate. In reality, biological systems are very complex with the likelihood that all parameters are in some way affected by the seasons but with different forcing strengths and phases. We assume that the growth rate varies while the carrying capacity remains constant. This reflects the situation where the host has a defined breeding season but resources remain constant (and therefore breeding and resources are driven by different environmental factors). This differs to the work of Rinaldi et al. (1993) who applied temporal forcing to the growth rate and additionally forced the carrying capacity (with the same temporal forcing term). The prey growth rate is distinguished as the only model parameter that does not affect the stability of the predator-prey coexistence equilibrium (details in §2.2) thus allowing us to study the effects of the forcing from a different perspective, namely studying the three cases of monotonic decay to the coexistence equilibrium, oscillatory decay and cycles in the unforced system separately. This provides a novel outlook on the impact of seasonal forcing, illustrating how the resulting cyclic behaviour is dependent on the unforced dynamics.

In §2.2 we describe the predator-prey model, its properties in the unforced case, and the different forcing scenarios we will consider. In §2.3 we summarise the necessary bifurcation theory, and the results of this bifurcation approach follow in §2.4. Simulation work is shown in §2.5 while in §2.6 we consider the importance of our choices for a controlling parameter. In §2.7, we discuss how the methods support and verify each other as well as possible extensions and applications.

2.2 Model

We consider the widely used Rosenzweig-MacArthur predator-prey model (Rosenzweig and MacArthur, 1963):

$$\frac{dx}{dt} = r\left(1 - \frac{x}{K}\right)x - \frac{axy}{b+x} \tag{2.1a}$$

$$\frac{dy}{dt} = \frac{caxy}{b+x} - dy \tag{2.1b}$$

where $x(t)$ and $y(t)$ are the prey and predator density at time t. All parameters are positive; r and K represent the growth rate and carrying capacity of the prey population respectively; d is the natural death rate for the predator population; and c relates birth of new predators to prey intake. The Holling Type II predation term is a saturating function in which a is the maximum predation rate and b is the density of prey at which the predation rate is half its maximum (Holling, 1959a,b).

The model (2.1) has a coexistence steady state which is stable when:

$$K_1 \equiv \frac{bd}{ca-d} < K < \frac{b(ca+d)}{ca-d} \equiv K_2. \tag{2.2}$$

There is a transcritical bifurcation at $K = K_1$ denoting a change to the prey-only equilibrium ; at $K = K_2$ there is a supercritical Hopf bifurcation, and a stable limit cycle arises. For $K_1 < K < K_2$ there is either monotonic decay or oscillatory decay to equilibrium, with oscillatory decay occurring for larger K, say $K > K^* \in (K_1, K_2)$ (see Figure 2.1). K^* is defined as when the characteristic equation of the Jacobian of (2.1) has zero discriminant, indicating the change from real to complex eigenvalues. Notice that the growth rate r is significant as the only parameter not involved in the formula for K_1 and K_2; however, r does affect K^* and the values of x and y at the steady state.

We introduce yearly forcing through the growth rate of the prey and following many previous studies (Dietz, 1976; Rinaldi et al., 1993; Greenman et al., 2004; Choisy et al., 2006; He and Earn, 2007) we use a sinusoidal form:

$$r(t) = r_0(1 + \epsilon \sin(2\pi t)). \tag{2.3}$$

When $\epsilon = 0$ then the seasonally forced model collapses to the unforced case with $r_0 = r$. Throughout, we will use r to denote the growth rate in the unforced system, with $r(t)$ being the growth rate in the forced system and r_0 being the mean value of the growth rate in the forced system. This is to emphasise when we are referring to the unforced case. The parameter ϵ is the forcing amplitude. We will vary the two parameters in the forcing term, r_0 and ϵ, for fixed values of the other parameter

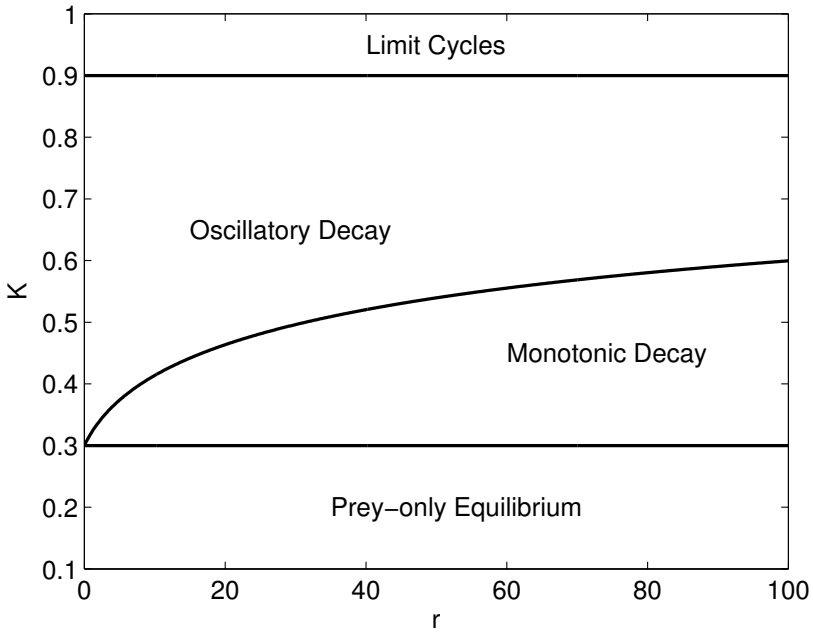

Figure 2.1: The change in stability of the coexistence steady state as r and K vary. The other parameters are fixed at $a = 4\pi, b = 0.3, d = 2\pi, c = 1$. The switch between monotonic decay and oscillatory decay ($K = K^*$) increases with r. As $r \to \infty$, $K^* \to K_2 = 0.9$.

values; following Rinaldi et al. (1993) we choose $a = 4\pi, b = 0.3, d = 2\pi, c = 1$. For these values $K_1 = 0.3$ and $K_2 = 0.9$.

We will focus on three different values of K: $K = 1$, giving a stable limit cycle in the unforced system; $K = 0.8$, giving oscillatory decay to the coexistence equilibrium; and $K = 0.35$, giving monotonic decay unless r_0 is small. We can consider these three cases separately because the threshold value K_2 is independent of the forcing parameter. Therefore we can analyse how the strength of oscillations in the unforced system affects the complexity of behaviour when seasonality is introduced.

2.3 Bifurcation Theory of Periodically Forced ODEs

For the benefit of readers unfamiliar with the bifurcation theory of periodically forced ODEs, we now give a brief summary. Kuznetsov (1995) provides full details of all bifurcation theory necessary while Guckenheimer and Holmes (1983); Seydel (1994) are perhaps more accessible for those unfamiliar with the theory. Useful background on Arnol'd Tongues is given in King and Schaffer (1999); Greenman and Benton (2004). The standard procedure for locating bifurcations uses the Poincaré (or stroboscopic) map $\mathcal{P}$ that transforms the continuous system into a discrete one by sampling the solution once in each forcing period; one year in our case. Note that the stable/unstable annual cycles become stable/unstable fixed points of $\mathcal{P}$. Discrete bifurcation theory

reveals that this fixed point is unstable if one of the eigenvalues of its linearisation has modulus larger than 1. Changes in stability are of three possible types. If the eigenvalue is equal to -1, it is a *period-doubling (flip) bifurcation*; if the eigenvalue is equal to $+1$ it is a *fold (saddle-node, tangent) bifurcation*; and if there is a pair of complex conjugate eigenvalues with modulus 1, it is a *Neimark-Sacker (torus) bifurcation*.

Period-Doubling Bifurcation At a period-doubling bifurcation, the fixed point of $\mathcal{P}$ loses stability but no new fixed points appear. However, the same fixed point of the second iterate of $\mathcal{P}$ ($\mathcal{P}^2$) undergoes a pitchfork bifurcation leading to two fixed points of $\mathcal{P}^2$. Thus the solution alternates between two different points on the Poincaré section. For the continuous system this produces a two year cycle, which will typically become more distinctively biennial as one moves away from the bifurcation. A period-doubling bifurcation can then happen to the new two year cycles leading to a four year cycle, etc.; this can yield an infinite cascade of period-doublings, ultimately ending in chaos. On our bifurcation diagrams, we will denote by PDk a period-doubling bifurcation curve across which a stable cycle of period k loses stability and a stable cycle of period $2k$ arises.

Fold Bifurcation When the eigenvalue is $+1$ the system undergoes a fold bifurcation. On one side of the bifurcation point there is no solution but on the other side there are both stable and unstable solution branches, which curve around ("fold") at the bifurcation point. By stability, we mean locally stable as a solution to the ODEs. Thus, when crossing a fold curve on the bifurcation diagram, a new solution appears to arise from nowhere. In fact, it is arising when the forcing period ($p = 1$ year) and the underlying period of the model (denoted by p_0) have the ratio $\frac{p}{p_0} = \frac{1}{n}$ ($n \in \mathbb{N}$). These bifurcations are the boundaries of Arnol'd Tongues, with each tongue denoting a region in which a specific periodic solution occurs. Thus, when crossing a fold bifurcation curve on the bifurcation diagram, denoted by FDk, a stable cycle of period k arises.

Neimark-Sacker Bifurcation A Neimark-Sacker bifurcation is a discrete version of a Hopf bifurcation. For a standard supercritical Neimark-Sacker bifurcation, when the eigenvalues are complex with modulus 1 the fixed point on the Poincaré section becomes unstable and a stable closed invariant curve arises around the point on the Poincaré section (provided that certain non-degeneracy conditions hold including that strong resonances should be excluded). If this is a space-filling curve, that is, if there is no number l such that l iterations of the Poincaré map $\mathcal{P}$ will bring the solution back to the same point on the curve, then it produces a *quasi-periodic* solution. More precisely, this means that the points of the solution on the Poincaré section are dense

within this closed invariant curve. When considered in the continuous setting, a quasi-periodic solution may superficially appear periodic but in fact it has no finite period. The Neimark-Sacker bifurcation is also known as a torus bifurcation, due to the shape produced as it goes around the Poincaré section. Far away from the bifurcation point, the torus can undergo torus destruction leading to an area of chaotic behaviour, caused by a global bifurcation.

The condition for the closed invariant curve in the Poincaré map to be a space-filling curve is that the ratio of the two frequencies describing motion along the axis and along the cross-section of the torus is irrational. This ratio is the same as that between the forcing period and the underlying period of the unforced model, which we discussed earlier. Due to the larger cardinality of irrational numbers over rational numbers, quasi-periodicity is the typical behaviour beyond a Neimark-Sacker bifurcation curve in the bifurcation diagram. This bifurcation curve is denoted by NSk where it is a cycle of period k which loses stability.

If the two frequencies have a rational ratio $\frac{m}{n}$ then there is *phase-locking* or *frequency-locking.* The solution becomes entrained on a periodic cycle within the curve on the Poincaré section and the period of the solution will be given by n. For example, if the forcing period and the underlying period have a ratio of $\frac{1}{3}$, then the system will respond with a solution of period 3. The fold bifurcation discussed earlier also gives phase-locking, with $m = 1$. As in the $m = 1$ case, solutions with a given $m \neq 1$ (and $n > 1$) occur within an Arnol'd Tongue, whose boundaries are fold bifurcations of the solution within the tongue. The fact that m can now take any positive integer value leads to different "families" of tongues which are numerated by m. However, the family with $m = 1$ usually has the largest tongue on the bifurcation diagram. Thus, period ratios of $\frac{2}{3}$ and $\frac{1}{3}$ will both produce 3 year solutions within their respective Arnol'd Tongue, but the latter will usually be more prominent in the bifurcation diagram (see later, Figure 2.3(b), where several FDk curves representing different Arnol'd Tongues are plotted). Typically, most tongues are so thin that they are difficult to find via simulation.

Finally in this section, we comment that throughout this thesis we will use the term "subharmonics" to refer to any solution which has a period that is an integer multiple of the external forcing period (Seydel, 1994). As the external period in question is one year, subharmonics will be multi-year cycles of period 2, 3, 4 years etc. Therefore, both the period-doubling and fold bifurcations produce subharmonics. We state this explicitly because confusion can arise from the fact that period-doubling bifurcations are sometimes called subharmonic bifurcations. Further, subharmonics are often described as being associated with the ratio of the different periods interacting, although this is only really true for the fold bifurcation and not the period-doubling bifurcation.

2.4 The Bifurcation Approach

We used the software package AUTO (Doedel, 1981; Doedel et al., 1991, 2006; Doedel and Oldeman, 2009) to calculate bifurcation diagrams for (2.1) augmented with (2.3). We describe separately the results for $K = 0.8$ (oscillatory decay), $K = 1$ (limit cycles) and $K = 0.35$ (monotonic decay). We restrict attention almost entirely to $\epsilon < 1$, which guarantees that the prey growth rate is always positive.

2.4.1 Two-Dimensional Bifurcation Diagram for $K = 0.8$

Figure 2.2 shows a bifurcation diagram in the $\epsilon - r_0$ plane; recall that ϵ is the forcing amplitude and r_0 is the mean value of the forced growth rate.

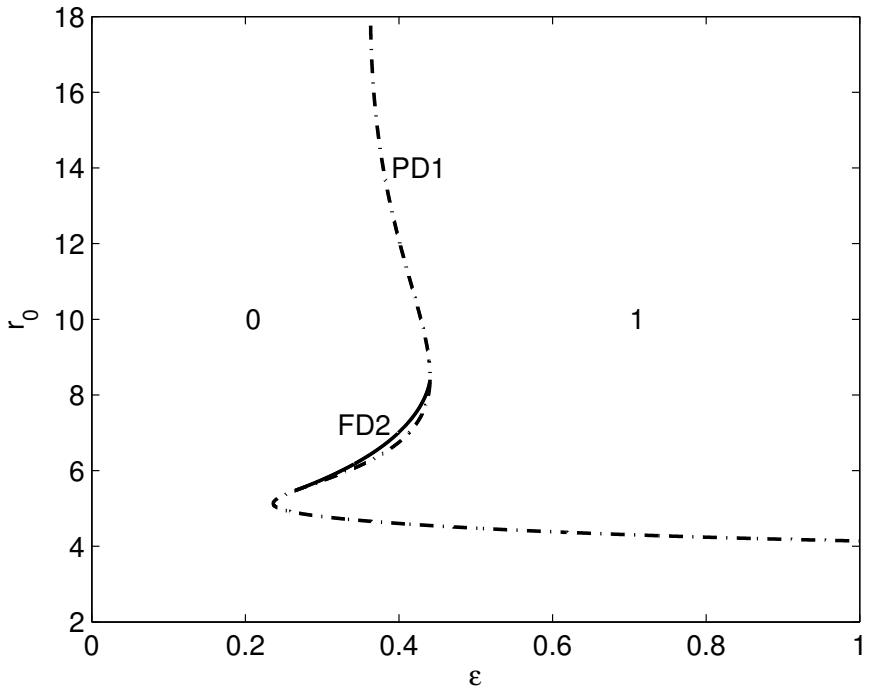

Figure 2.2: A two-dimensional bifurcation diagram for $K = 0.8$ when the unforced system has oscillatory decay to the coexistence steady state. The two parameters varied in the diagram are those involved in the forcing term (equation (2.3)), that is the mean value of the forcing, r_0, and the amplitude of the forcing, ϵ. The other parameters are $a = 4\pi, b = 0.3, d = 2\pi, c = 1, K = 0.8$. Dot-dash lines represent period-doubling bifurcation curves while solid lines are for fold bifurcation curves. In region 0 the system responds to the forcing with yearly cycles but after crossing the period-doubling curve PD1, indicating that a cycle of period 1 loses stability, the solution behaviour is two year cycles (region 1). The fold bifurcation curve shows an area where two year cycles can occur outside of the period-doubling region, thus between the two curves both the one year and the two year solutions are stable.

For low levels of forcing (i.e. small ϵ), there are yearly solutions in region 0, which emulate the forcing oscillation. As ϵ is increased a period-doubling curve is crossed and thus the stable solution in region 1 is a two year cycle; the yearly solution also exists but is unstable. There is a fold bifurcation curve which implies a (small) region of parameter space outside the period-doubling region 1, containing two year solutions. The yearly solutions are also stable in this region: they do not lose stability until the period-doubling bifurcation curve is crossed. Thus between the two curves there are two different stable solutions. This is the full range of behaviour possible when $K = 0.8$ as there are no more fold bifurcation curves for higher period cycles. However, in §2.5, we produce detailed simulation diagrams to investigate the basins of attraction for Figure 2.2.

2.4.2 Two-Dimensional Bifurcation Diagram for $K = 1$

The two-dimensional bifurcation diagram for the case $K = 1$ (stable limit cycles) is shown in Figure 2.3 with and without the Arnol'd Tongues related to solutions of period greater than 2. Note that when r_0 is varied with no forcing ($\epsilon = 0$), the period of the limit cycles increases with decreasing r_0.

Figure 2.3(a) shows that a larger range of complex population behaviour is possible compared to when there is oscillatory decay in the unforced system (Figure 2.2). A Neimark-Sacker bifurcation curve, labelled as NS1 occurs for this set-up. As we increase ϵ from 0 in a system with a limit cycle, the system typically responds with quasi-periodic solutions due to the appearance of the Neimark-Sacker bifurcation, and this is the generic behaviour in regions 1 and 1*. These quasi-periodic solutions will be very similar, for very low levels of forcing, to the limit cycles on the $\epsilon = 0$ axis, but increasing forcing pushes the solutions away from this period. Crossing the NS1 curve from region 1 to region 0 leads to the torus disappearing and the yearly cycle becomes stable. Therefore the stable behaviour in region 0 is one year cycles. This implies that increasing the level of forcing is actually able to produce more regular behaviour – stable yearly cycles rather than quasi-periodicity. Although counter-intuitive, this does make sense as we are imposing yearly forcing on to an inherent cyclic solution (limit cycle) and with enough forcing, i.e. once ϵ is large enough, this cycle becomes entrained onto the yearly cycle. Note that if r had been part of condition (2.2) for a Hopf bifurcation, then the Neimark-Sacker bifurcation curve would have hit the $\epsilon = 0$ axis at the value of r where the Hopf bifurcation occurs.

As for $K = 0.8$, crossing from region 0 to region 2 across the period-doubling bifurcation curve PD1 leads to stable two year cycles in region 2 and the loss of stability of the yearly cycles. This new two year cycle itself undergoes period-doubling as indicated by the curve PD2. Thus the stable solution behaviour in region 6 is four year cycles. There is another period-doubling curve PD4, and a subsequent cascade of

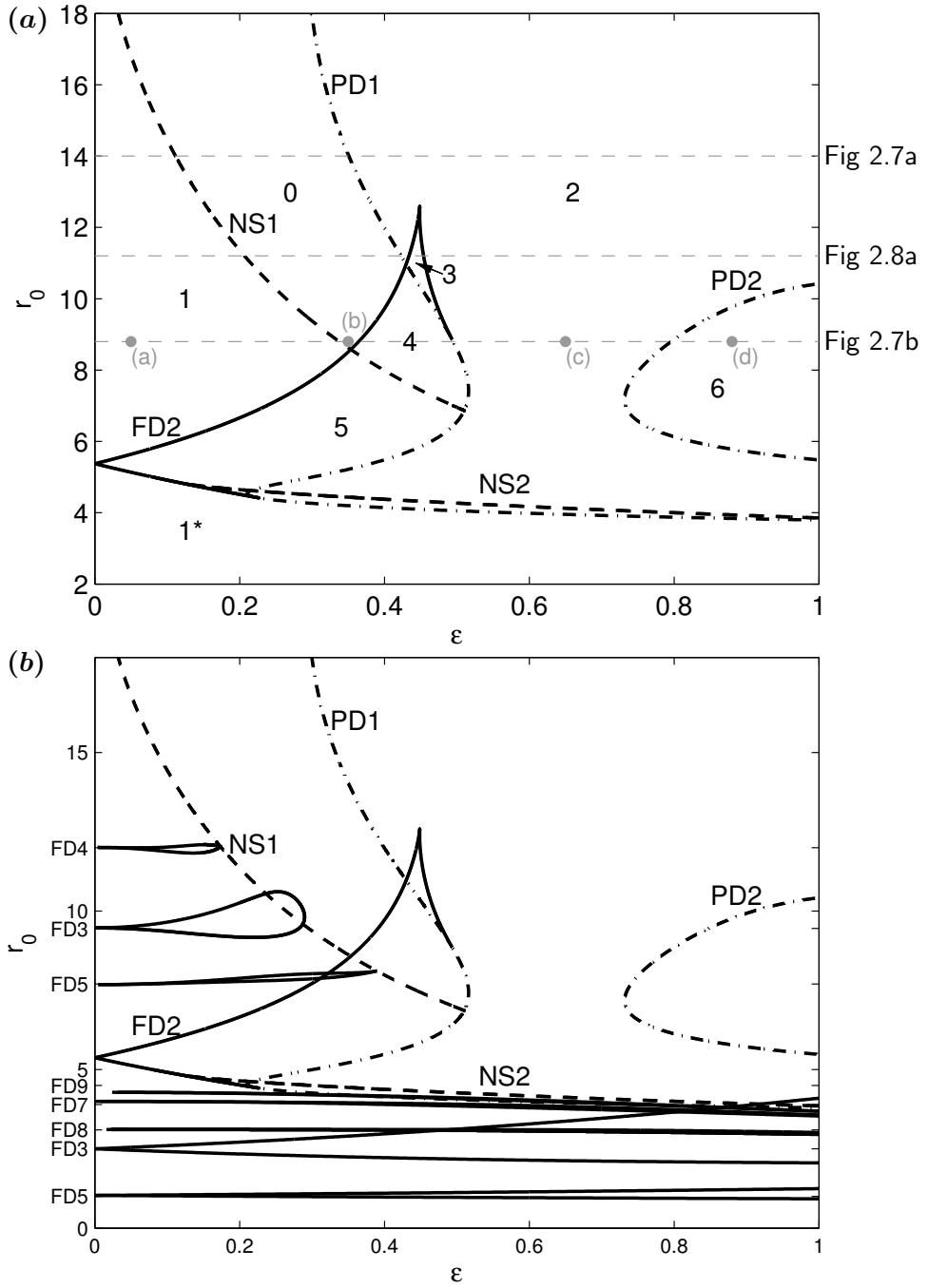

Figure 2.3: A two-dimensional bifurcation diagram for $K = 1$ when the unforced system has stable limit cycles. Other parameters and details of the bifurcation diagram are as in Figure 2.2. Dot-dash lines represent period-doubling bifurcation curves, solid lines are for fold bifurcation curves and dashed lines represent Neimark-Sacker bifurcation curves. (a) Stable behaviour by region: region 0 - one year solution; region 1/1* - quasi-periodic cycles; region 2 - two year solution; region 3 - two different two year solutions; region 4 - one year and two year solutions; region 5 - quasi-periodic solution and two year solution; region 6 - four year solution. Grey dashed lines refer to one-dimensional bifurcation diagrams in the relevant figures. Points (a) - (d) refer to the simulations shown in Figure 2.4. (b) This includes the fold bifurcation curves relating to all multi-year simulations found. There are two FD3 curves indicating the appearance of three year cycles in different regions, one FD4 curve, two FD5, one FD7, FD8 and FD9 curves. We believe that the fold curves FD8 and FD9 do in reality extend to the $\epsilon = 0$ axis, with the earlier end a numerical artefact.

period-doubling to chaos, in the region $\epsilon > 1$. There is also a second Neimark-Sacker bifurcation curve, NS2, in region 2. As r_0 decreases past this curve, it indicates the loss of stability of the two year cycles in region 2 and the onset of stable quasi-periodic solutions. However, this region is very thin and further decrease in r_0 causes a loss of stability due to crossing the period-doubling curve PD1.

Thus in Figure 2.3(a) there are four main types of behaviour shown on this two-dimensional bifurcation diagram, namely one year, two year, four year and quasi-periodic cycles. There is also the possibility that there may be chaotic dynamics in some parts of the "quasi-periodic regions"; we have not investigated this. Examples of these behaviours are shown in Figure 2.4; the corresponding parameters sets are labelled (a) - (d) in Figure 2.3(a).

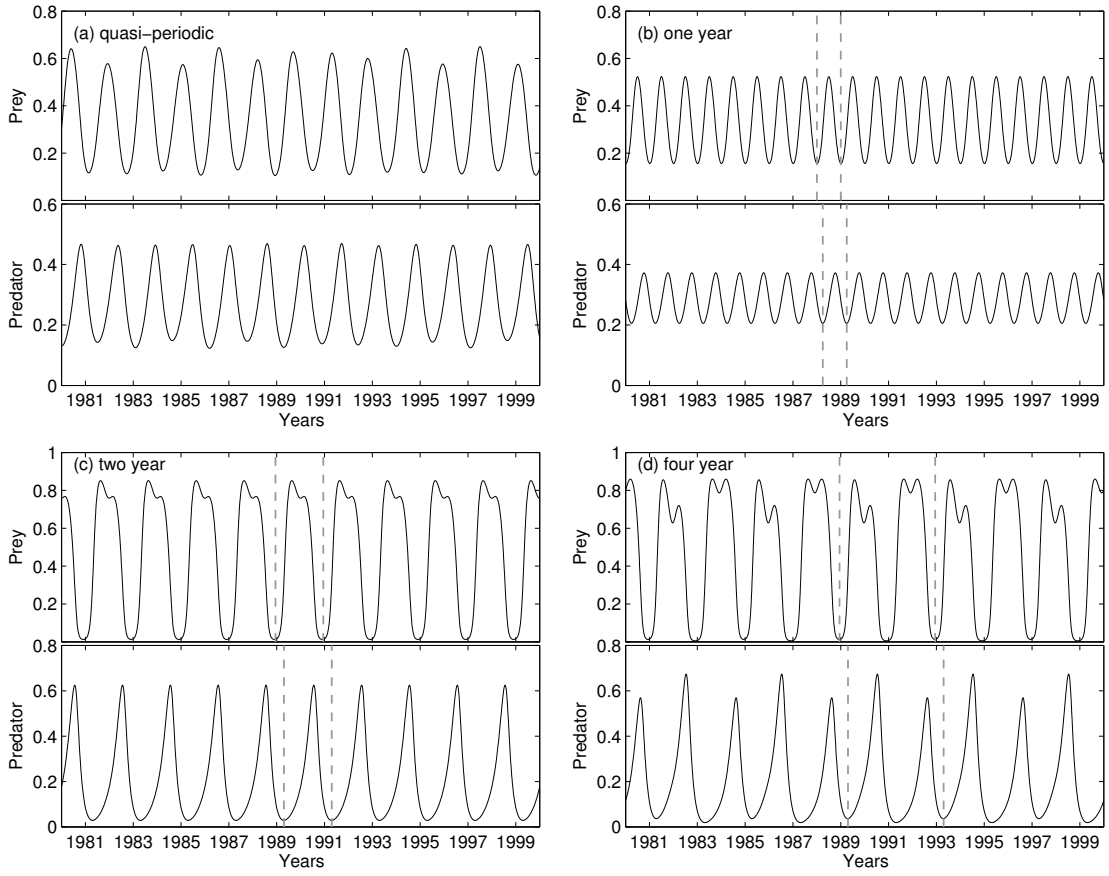

Figure 2.4: Simulation examples of different solutions found through the bifurcation diagram approach. Parameter values are $(\epsilon, r_0) =$ (a) $(0.05, 8.8)$, (b) $(0.35, 8.8)$, (c) $(0.65, 8.8)$, (d) $(0.88, 8.8)$ and correspond to the four points labelled on Figure 2.3(a) with other parameters as in Figure 2.3 ($K = 1$). The prey and predator solutions are plotted against time (years), with the simulations run for 2000 years so that they have settled to equilibrium. The Matlab ode solver (`ode15s`) was run with tolerances: reltol $= 10^{-8}$ and abstol $= 10^{-6}$. Grey dashed lines highlight a full period of the solution. The initial conditions were $(x_0, y_0) = (0.3, 0.3)$ in all cases.

We now consider Figure 2.3(b) which includes the higher period Arnol'd Tongues. We used simulation in order to obtain initial conditions as starting solutions for numerical continuation. Specifically we input into AUTO one whole period of the solution from a Matlab simulation and trace the solution branch to see what bifurcations occur along it, in particular the fold bifurcation curve enclosing the periodic solutions.

We see that the three year fold curve which has a root on the $\epsilon = 0$ axis at approximately $r_0 = 3$ is the largest of these additional tongues. However, there are many different period solutions, as well as multiple regions of the same period solution. In Figure 2.5 we explore the two separate regions of three year stability by showing a representative solution from each of these regions, plotted as a function of time. Recall that a tongue is characterised by the rotation number $\frac{m}{n}$ within the torus. Here n is the period and m is the number of peaks in the solution per period. Thus the three year simulations found in Figure 2.5(a) have $m = 1$, $n = 3$ while Figure 2.5(b) corresponds to $m = 2$, $n = 3$. However, this rotation number also relates to the forcing period (1 year) and the underlying period of the unforced system. The larger 3 year fold curve hits the axis where the unforced system has a period of 3 years, thus leading to this rotation number of $\frac{1}{3}$. Furthermore, the smaller three year fold curve hits the axis at $r_0 = 9.5$ when the unforced system has a period of 1.5 years. Thus the rotation number is $\frac{1}{1.5} = \frac{2}{3}$ as expected.

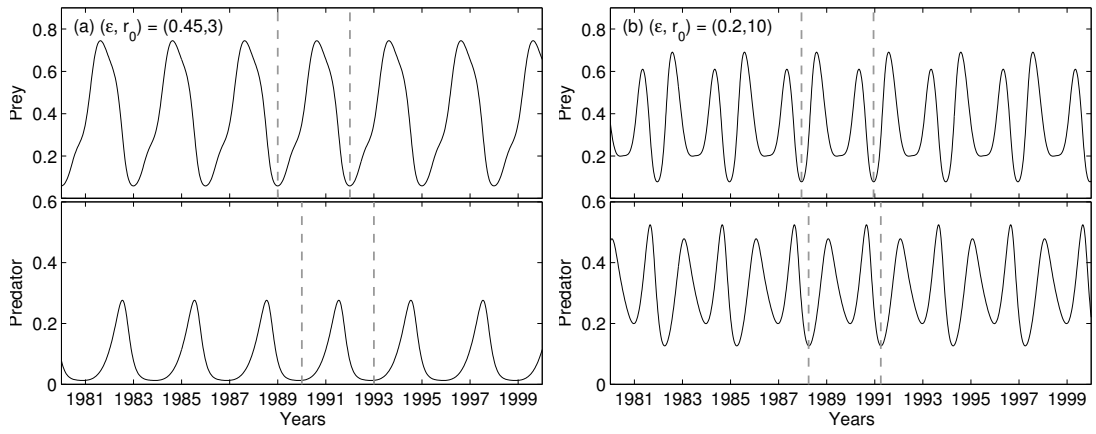

Figure 2.5: Two different simulations of three year solutions. The simulations are taken from two different regions on the bifurcation diagram in Figure 2.3(b). The prey and predator solutions are plotted against time (years), with the simulations run for 2000 years so that it will have settled to equilibrium. The ode solver (`ode15s`) was run with tolerances: reltol = 10^{-8} and abstol = 10^{-6}. Initial conditions were taken as $(x_0, y_0) = (0.5479, 0.7230)$ and $(0.1440, 0.6490)$. Grey dashed lines highlight a full period of the solution. The number of peaks over each three year period indicates which Arnol'd tongue the solutions belong to.

This rotation number relationship is the same for all the Arnol'd tongues in Figure 2.3(b) and we show this in Figure 2.6. For example, the four year tongue in Figure 2.3(b) touches the $\epsilon = 0$ axis where the limit cycles have period 1.25 so that the solution has $\frac{m}{n} = \frac{1}{1.25} = \frac{3}{4}$. Thus we state $\frac{m}{n} = \frac{\text{peak}}{\text{period}}$ for each of the plots in Figure 2.6(a)-(f) respectively, as $\frac{3}{4}$, $\frac{1}{5}$, $\frac{3}{5}$, $\frac{3}{7}$, $\frac{3}{8}$, $\frac{4}{9}$. These cycles may of course change in qualitative behaviour (although still being of the same period) as the ϵ and r_0 values move closer to the edge of the Arnol'd Tongue. In particular, the quasi-periodic behaviour near the tongue often looks similar to the periodic solution at the edge of the tongue.

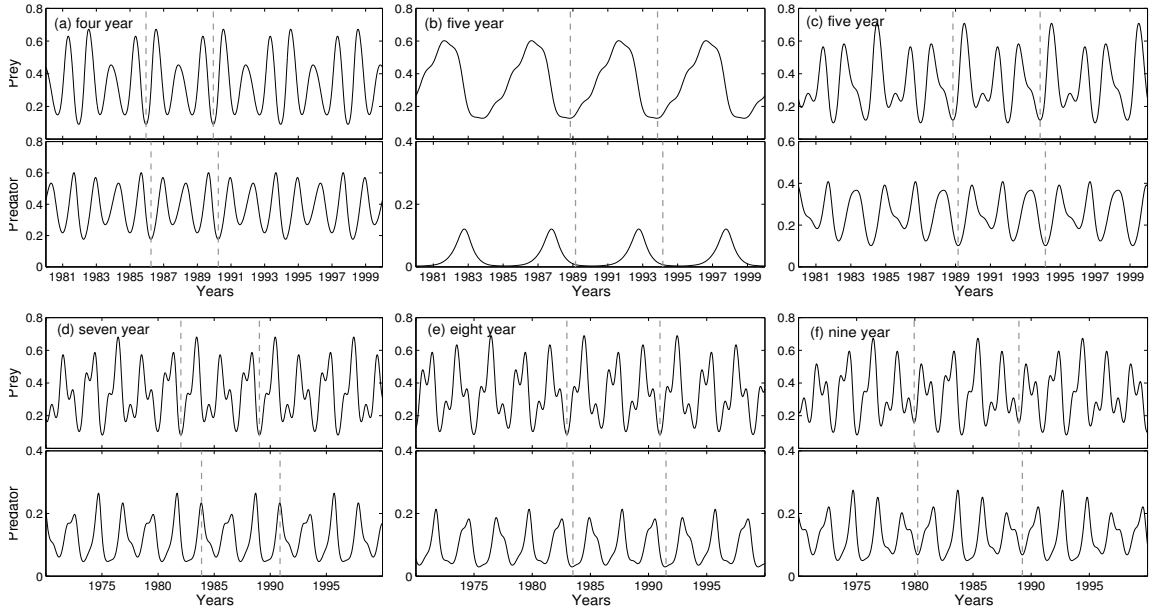

Figure 2.6: Examples of solutions found in the bifurcation diagram for the case $K = 1$ (Figure 2.3(b)). Parameter values are $(\epsilon, r_0) = (a)\ (0.1, 12)$, $(b)\ (0.5, 1)$, $(c)\ (0.3, 8)$, $(d)\ (0.7, 3.8)$, $(e)\ (0.95, 3)$, $(f)\ (0.65, 4)$ and the cycle period for each case is indicated in each subplot. The prey and predator solutions are plotted against time (years). Further details are in Figure 2.5. Grey dashed lines highlight a full period of the solution. Two different five year solutions are shown as two different regions of five year solution behaviour were found. Note that the time scale differs between cases as does the predator density plotting range. Initial conditions were taken as (x_0, y_0) $= (0.3, 0.3)$ except for the seven year cycles $(0.8147, 0.9058)$ and eight year cycles $(0.3448, 0.2718)$.

Figure 2.3(b) shows a large number of tongues close to the $\epsilon = 0$ axis, and in fact general theory implies that there are an infinite number (see §2.3 and Kuznetsov (1995)). However, in practice for small ϵ most of the tongues are very thin and

the corresponding cycles will actually be very similar to the nearby quasi-periodic cycles. As ϵ increases, the tongues usually get thicker and the cycles begin to be more distinctively multi-year. Note also that in principle period-doubling can occur within the tongues. However, we have only found this within the three year fold near $r_0 = 3$, leading to six year cycles, and this occurs for $\epsilon > 1$. Also there are more Neimark-Sacker bifurcation curves which we did not calculate to avoid even more complexity on the diagram.

General theory also implies that close to the $\epsilon = 0$ axis the Arnol'd tongues are non-overlapping since they are each governed by a different ratio of underlying period to forcing period at the root of the tongue (Kuznetsov, 1995). However, for larger ϵ overlap can occur because the ratio determines only the root and period of the tongue; this is seen easily in Figure 2.3(b) where the seven, eight and nine year tongues overlap the three year tongue. The points where different bifurcation curves intersect, for example where the fold curve FD2 hits the period-doubling curve PD1, are called codimension-2 bifurcation points. These are flagged when tracing the curves in AUTO, indicating the presence of other bifurcation curves and providing a useful tool for finding all curves on the bifurcation diagram. The theory behind codimension-2 bifurcation curves is well developed (see Kuznetsov (1995)).

2.4.3 One-Dimensional Bifurcation Diagrams for $K = 1$

We wish to analyse more closely the area enclosed by the fold bifurcation curve FD2 in Figure 2.3(a), where there are stable two year cycles. To do this, we switch to one-dimensional bifurcation diagrams, plotting the size (L_2-Norm over 1 period) of the prey population against ϵ, for fixed r_0. We compare the solution behaviour when crossing the period-doubling curve PD1 for different values of r_0, in order to clarify how the fold bifurcation interacts with the period-doubling bifurcation.

When $r_0 = 14$ the fold curve is not present, and results show a supercritical period-doubling bifurcation, with the additional region of instability of the yearly cycle due to the Neimark-Sacker bifurcation (for $\epsilon < 0.12$) (Figure 2.7(a)). Once the yearly solution becomes stable, $\epsilon > 0.12$, it remains stable until it hits the period-doubling bifurcation curve ($\epsilon = 0.35$). At this point the yearly solution becomes unstable and a stable two year cycle arises.

When $r_0 = 8.8$ (Figure 2.7(b)), we see a similar profile for the yearly cycle, going from unstable to stable to unstable as it first crosses the Neimark-Sacker bifurcation curve and then the period-doubling bifurcation curve. However, there is a marked change in the behaviour of the two year cycle. Again it bifurcates from the yearly cycle at the period-doubling bifurcation curve ($\epsilon = 0.49$), but now the bifurcation is subcritical. Thus it is initially unstable and only exists for $\epsilon < 0.49$, until it folds (at $\epsilon = 0.36$), at which point it becomes stable. Thus for values of ϵ between the

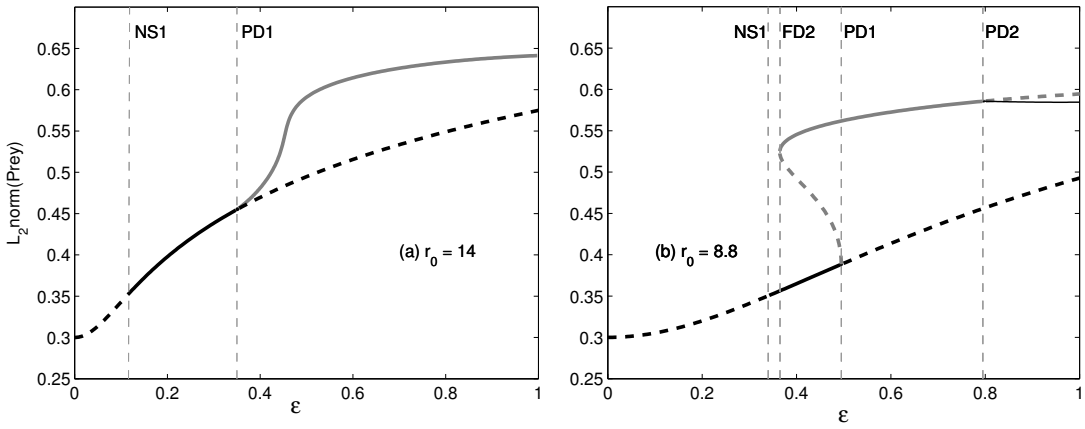

Figure 2.7: A one-dimensional bifurcation diagram for fixed r_0 and varying ϵ with the other parameters as in Figure 2.3(a) ($K = 1$). Along the vertical axis is the L_2-Norm of the prey solution. Thick black curves: 1 year equilibria, thick grey curves: 2 year equilibria, thin black curves: 4 year equilibria. Solid curves are stable while dotted curves are unstable. In (a) a supercritical period-doubling bifurcation occurs while in (b) the period-doubling bifurcation is subcritical and the solution then undergoes a fold. The thin grey dashed lines indicate when curves on the two-dimensional bifurcation diagram are crossed, labelled appropriately.

fold bifurcation curve and the period-doubling bifurcation curve ($0.36 < \epsilon < 0.49$) there are two stable solutions – a one year solution and a two year solution. Lastly, Figure 2.7(b) shows that for larger ϵ the two year cycle loses stability (at $\epsilon = 0.8$) and a stable four year cycle appears. This arises from crossing the period-doubling curve PD2.

Further understanding of the fold curve in Figure 2.3(a) can be gained by examining a one-dimensional bifurcation diagram for $r_0 = 11.2$ (Figure 2.8(a)). In particular, variation in ϵ will mean that region 3 in Figure 2.3(a) will be explored. For $\epsilon < 0.4$ the one year solution has a similar behaviour to that shown in Figure 2.7 (unstable, stable and then unstable due to the Neimark-Sacker bifurcation and the period-doubling bifurcation). In Figure 2.8(a) one can see that the two year solution arises and is stable from the period-doubling bifurcation at $\epsilon = 0.42$. It then undergoes two folds giving it an "S shape" before continuing for increasing ϵ as a stable solution. More precisely, it hits the fold bifurcation curve FD2 twice, at $\epsilon = 0.435$ and $\epsilon = 0.452$. In Figure 2.3(a), this is reflected by the fact that region 3 is bounded on both sides by the fold curve FD2. Thus for $0.42 < \epsilon < 0.435$ and $\epsilon > 0.452$ there is one stable two year solution, whereas for $0.435 < \epsilon < 0.452$ there are two stable two year solutions. Examples of the two different two year solutions are shown in Figure 2.8(b), (c) for the prey population; these solutions are for the same parameter values but different initial conditions.

From all of these one-dimensional bifurcation diagrams, one can see that increasing

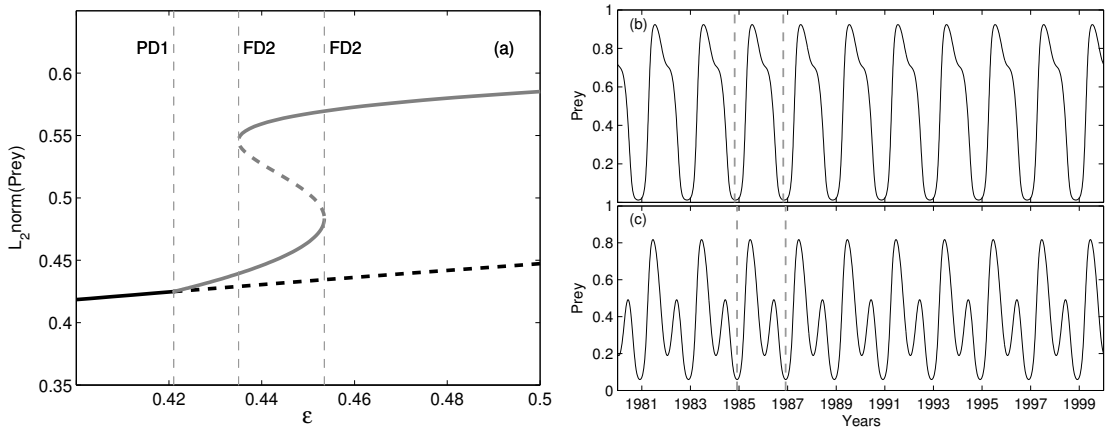

Figure 2.8: Exploring region 3 in Figure 2.3(a). In (a) there is a one-dimensional bifurcation diagram for $r_0 = 11.2$, focussed in on $0.4 < \epsilon < 0.5$; behaviour outside this range is similar to Figure 2.7(a). A stable two year cycle appears when the yearly solution hits the PD1 curve. This undergoes two "folds", with instability in between, before continuing as a stable solution. Two stable two year solutions are shown in (b) and (c) with the same parameter values $(\epsilon, r_0) = (0.44, 11.2)$ but different initial conditions; namely (b) $(x_0, y_0) = (0.8245, 0.5211)$ and (c) $(x_0, y_0) = (0.9189, 0.7191)$. Here, the prey population is plotted against time over an interval of 20 years, once the solution has settled to equilibrium. For details on the numerical method see Figure 2.4.

ϵ leads to an increase in the L_2-Norm of the solution and in that sense the two year cycle is larger than the one year cycle. This is also seen in Figure 2.4 and complements the work of Greenman et al. (2004) and others (e.g. Bolzoni et al. (2008); Childs and Boots (2010)). It ties in with the resonance peaks seen on Greenman's resonance diagram: subharmonics are a type of "resonant solution," with a higher amplitude than that of the applied forcing (Choisy et al., 2006). However, it should also be noted that the four year cycle is smaller in L_2-Norm than the two year cycle. This can be understood by looking at Figure 2.4(c) and 2.4(d) where the two solutions have similar amplitude except that the four year solution only reaches this value every other peak.

2.4.4 Two-Dimensional Bifurcation Diagram for $K = 0.35$

We now consider the final case of monotonic decay to the coexistence steady state. We have mentioned previously the importance of the interaction between the oscillations in the unforced model and the forcing term as a driver of complex behaviour. Thus, it is expected that the lack of any oscillations in the unforced model will cause the system to respond simply by emulating the forcing term. Both bifurcation and simulation analysis for $K = 0.35$ indicate that yearly cycles are the only possible population behaviour. A plot of the period-doubling curve (PD1) for different values of K (Figure 2.9) indicates that the period-doubling region reduces in size as K decreases

and entirely disappears at a value of K slightly greater than 0.6. As discussed in §2.2, the value K^* at which there is a switch from monotonic to oscillatory decay in the unforced model is an increasing function of r, with $K^* < 0.6$ throughout the range of values of $r(t) = r_0(1 + \epsilon \sin(2\pi t))$ that we are considering. Thus, the period-doubling curve has disappeared while the system is still oscillatory and so one does not expect multi-year cycles in the monotonic decay regime.

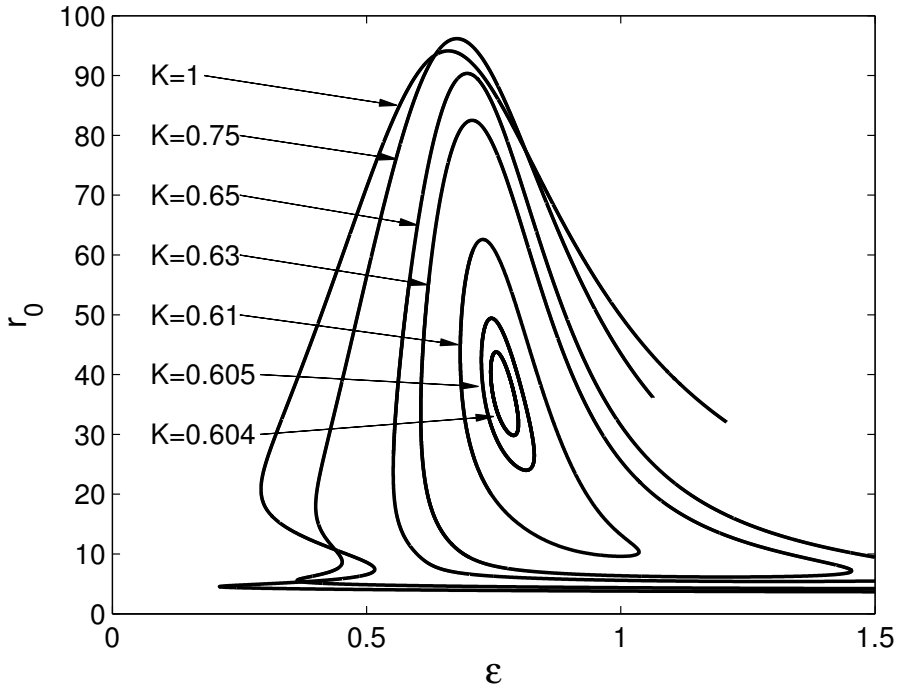

Figure 2.9: Investigating whether complex behaviour can occur when the unforced system has monotonic decay to the coexistence steady state. The period-doubling curve indicating the appearance of stable two year solutions is drawn in the two-dimensional bifurcation diagram for decreasing values of K. As K decreases towards 0.6, the curve shrinks.

This result suggests that a reasonable level of oscillatory decay is necessary in order for forcing to induce population behaviour that is more complex than annual cycles. When the period-doubling curve does not exist, our results indicate that the two year fold curve (FD2) also cannot exist. Further, we have not found Arnol'd tongues for these values of K (e.g. Figure 2.13, below). This suggests that yearly cycles are the only possible behaviour when annual forcing is introduced into the system with monotonic decay to steady state.

2.4.5 AUTO Details

The bifurcation diagrams discussed in this section were created in AUTO (Doedel, 1981; Doedel et al., 1991, 2006; Doedel and Oldeman, 2009) using essentially standard numerical continuation techniques. However, a few complications are worth mentioning. (*i*) We impose periodic forcing by augmenting (2.1) with a decoupled pair of ODEs which have an oscillatory solution of the form required for the forcing (Doedel and Oldeman, 2009, §14.5). (*ii*) We found that versions of AUTO earlier than 07p-0.8 (2011) were not capable of continuing the Neimark-Sacker bifurcation curve. (*iii*) Although it can be useful to overspecify parameters so that it is always possible to see clearly the r_0 and ϵ values and to extract data easily, it has to be remembered that this is not possible when tracing the Neimark-Sacker bifurcation curve since AUTO will assume that a fourth specified parameter relates to the rotation angle around the torus. (*iv*) When trying to trace the period-doubling, fold and Neimark-Sacker bifurcation curves it is important to use a small step size so that the restart point for tracing the curve is determined accurately. Otherwise AUTO tends to have problems tracing the bifurcation curve from the restart point. (*v*). The labels for our curves were chosen to be Period-Doubling - PD, Fold - FD and Neimark-Sacker - NS. In AUTO the corresponding labels are PD, LP and TR respectively.

2.5 Simulation

This section will produce simulations of the model equations in order to elucidate the results presented in the bifurcation diagrams. In the previous section the bifurcation diagrams showed that there exist regions which have more than one type of possible solution behaviour. Simulation results can be used to estimate the likelihood of each of the solutions i.e. the relative sizes of their basins of attraction. Thus, simulation can expand our knowledge of subharmonic solutions. A comparison of the simulation results and bifurcation diagrams can therefore provide a clearer understanding of how forcing drives the population dynamics.

2.5.1 Simulation Details

The predator-prey model equations (2.1), (2.3) were solved using Matlab (`ode15s`) for 2,000 years and the solutions were tested to determine whether there was a periodic solution with period $1-9$ years; if not, the solution was taken to be quasi-periodic. The choice of 9 years as a maximum test period is arbitrary; there could in principle be solutions with any finite integer period, but an upper limit is required for numerical study. To test whether a solution had a period of, for example, four years, the value of the prey solution was recorded for 20 time points at intervals of 4 years, after an initial

time period of sufficient length that transients had decayed. If the difference between the maximum and minimum of these numbers was less than 2.5% of their mean value, then it was declared a four year solution. Tests of some difficult cases near bifurcation curves or within multiple solution regions led to the choice of 2,000 years run time, 20 test points and 2.5% variation as they enabled periodic and quasi-periodic solutions to be distinguished. We also investigated the use of the fast Fourier transform to find power spectra as a means of calculating the period but it was found to be less effective. We considered the parameter region $1 < r_0 < 20$, $0 < \epsilon < 1$. For each set of parameter values, solutions were replicated 50 times using different (random) initial conditions between 0 and 1, independently chosen for both prey and predator. We determine the basins of attraction by examining the frequency of particular solutions from these 50 simulations. However, points in parameter space which showed multiple attractors were recomputed with 500 simulations to gain increased accuracy of the relative sizes of the basins of attractions. This straightforward method for estimating basins of attraction is effective (particularly as numerical investigations indicate that the basins of attraction have a complicated profile, see Figure 2.12). Other, more sophisticated methods such as using Lyapunov functions (Giesl, 2007) could also be used.

2.5.2 Simulation Results for $K = 0.8$

Again we first explore the simpler case of when there is oscillatory decay to the coexistence steady state. In this case the two-dimensional bifurcation diagram (Figure 2.2) showed only two types of behaviour — one year cycles and two year cycles.

Figure 2.10(a) shows the results from the $K = 0.8$ simulation program. Again, the only behaviours to occur are one year cycles (light blue) and two year cycles (pink). At $(\epsilon, r_0) = (0.4, 7)$ in Figure 2.10(a), there is a pie chart indicating that multiple solution behaviour is predicted. This is close to the fold bifurcation curve in Figure 2.2 and so we examine this region in more detail in Figure 2.10(b). We expect both one and two year solutions to be possible in the region between the fold bifurcation curve and the period-doubling curve in Figure 2.2. In Figure 2.10(b) we see that this behaviour is found through simulation at more than one grid location and the relative proportion of the two colours indicates that the two year solutions are more likely at these parameter sets. Even in the zoomed-in simulation diagram (Figure 2.10(b)), only eleven of the pie charts show multiple solutions since the region is so small.

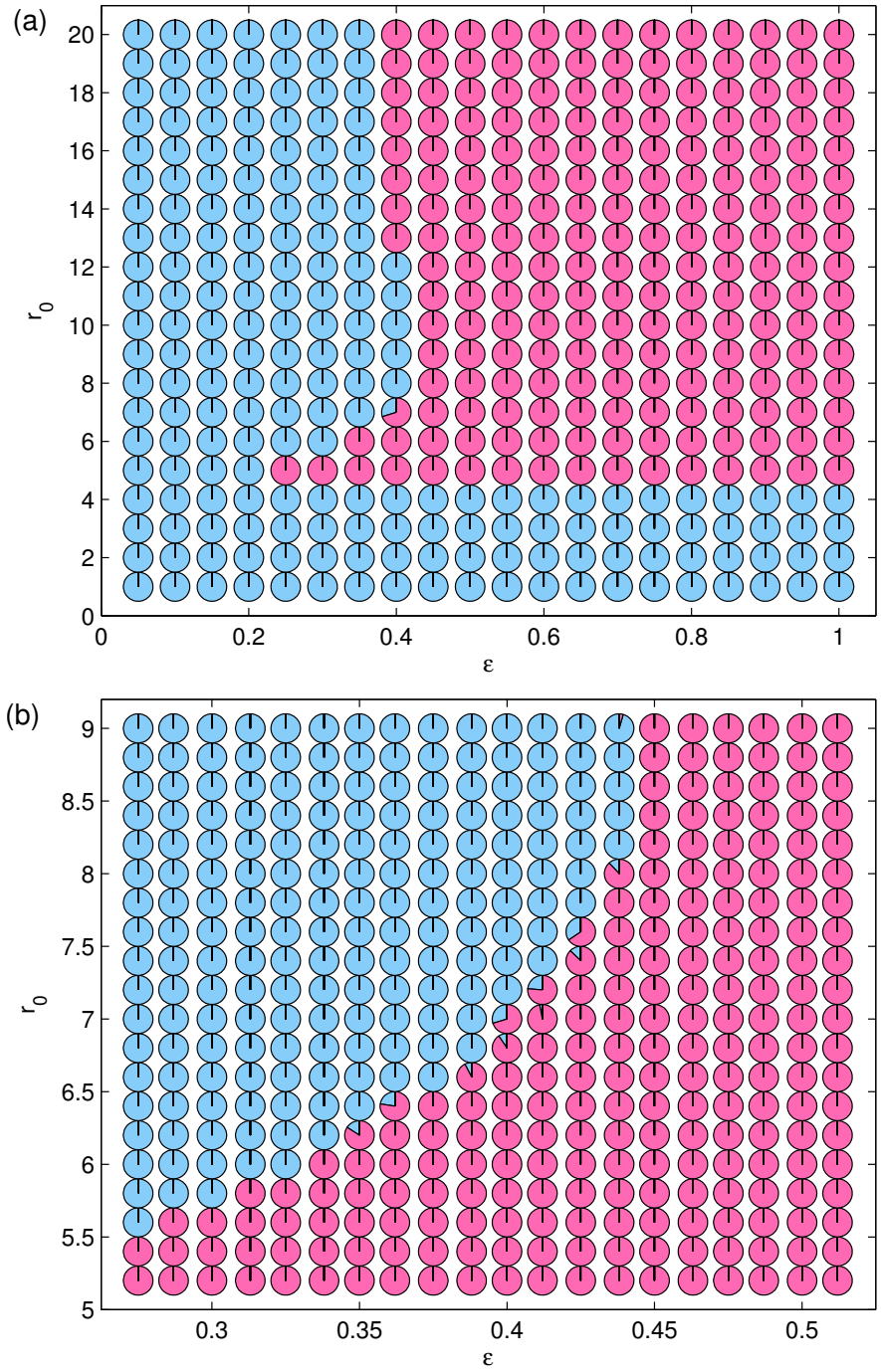

Figure 2.10: In (a) there is a simulation diagram for $K = 0.8$ when the unforced system has oscillatory decay to the coexistence steady state. At each point tested on the (ϵ, r_0) grid, a pie chart shows what proportion of the 50 (or 500) simulations had a particular period. Points which showed multiple solution behaviour were run with 500 simulations for increased accuracy of the basins of attraction. The other parameters are kept constant at $a = 4\pi, b = 0.3, d = 2\pi, c = 1$. Each simulation was run with random initial conditions (between 0 and 1 for both prey and predator) and the period was tested after 2,000 years. The Matlab ode solver (`ode15s`) was run with tolerances: reltol $= 10^{-8}$ and abstol $= 10^{-6}$. The period is illustrated by the colour with light blue being one year cycles and pink being two year cycles. In (b) a close-up of the diagram to focus on the area where more than one solution appeared at the same point. This shows eleven points tested had multiple solution behaviour.

2.5.3 Simulation Results for $K = 1$

We now turn to the case when there is a limit cycle present in the unforced model (Figure 2.11).

In Figure 2.11 one immediately notices the prominence of the two year cycles (pink). There are also large regions of one year, four year and quasi-periodic cycles. In fact, for the most part, the behaviour is well represented by Figure 2.3(a), indicating that the multi-year cycles arising from the Arnol'd tongues are the minority behaviour.

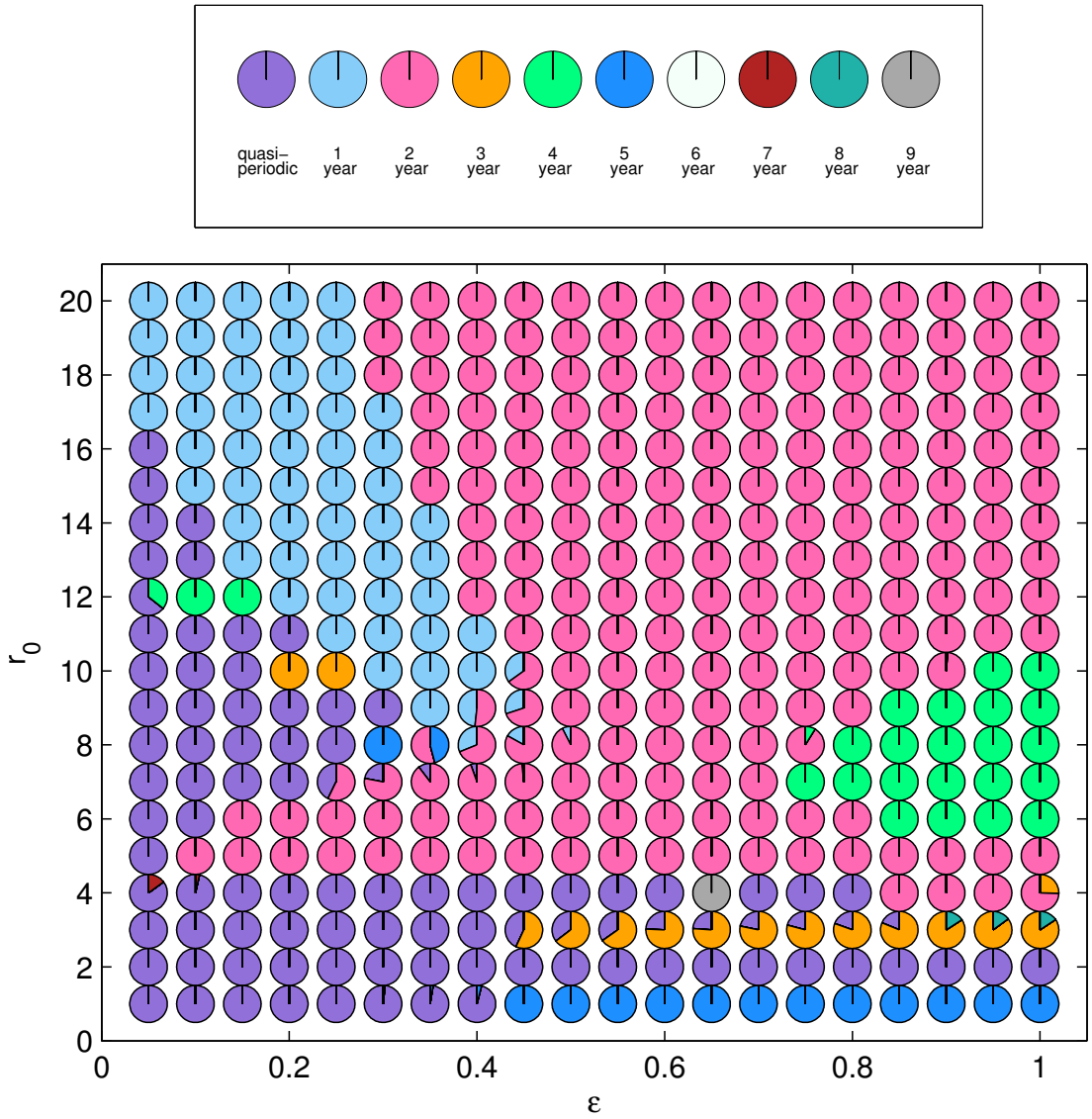

Figure 2.11: A simulation diagram for $K = 1$ so that the unforced system has stable limit cycles. At each point tested on the (ϵ, r_0) grid, a pie chart shows what proportion of the 50 (or 500) simulations had a particular period indicated by the legend. Each simulation was run with random initial conditions (between 0 and 1 for both prey and predator) . The Matlab ode solver (`ode15s`) was run with tolerances: reltol = 10^{-8} and abstol = 10^{-6}.

All of the tongues shown in Figure 2.3(b) are represented by some simulation results. We note that on most occasions the multi-year solution has a larger basin of attraction than the quasi-periodicity which is usually also stable at that location. In fact, often the multi-year solution attained all 50 of the simulations. The only real exception is the 7 year cycles. Furthermore, most of the multi-year cycles occur further away from the $\epsilon = 0$ axis where the tongues are thicker (again, the 7 year cycles are an exception). This is obviously due to the fact that the larger tongue means that one is more likely to capture the solution through simulation results. We reiterate here the fact that the "quasi-periodic" solutions could actually be chaotic as we do not distinguish between these cases.

There are a large number of five year cycles near $r_0 = 1$ which indicate that the five year tongue might be quite large. However, we know from Figure 2.3(b) that the tongue is quite thin, but just happens to lie directly over the line $r_0 = 1$, which forms part of the parameter grid for our simulation. This emphasises the important point that simulation results depend significantly on the parameter grid used.

To further our understanding of the relative sizes of the basins of attraction of different multi-year cycles and the effectiveness of using random initial conditions, we present a detailed basin of attraction plot in one case of multiple solution behaviour (Figure 2.12). This shows the complicated nature of each basin of attraction and indicates that using 500 simulations with random initial conditions is an appropriate method for calculating the relative proportions of each solution.

2.6 Different Values of K

It is natural to ask how the bifurcation diagrams match up as K varies and to see if the values of K picked for each type of unforced dynamics is a good representation of the forced dynamics for all K values with those unforced dynamics. We have already investigated how the period doubling curve PD2 changes for different values of K in Figure 2.9. Of special interest is whether Arnol'd tongues are possible in the oscillatory decay regime. For $K = 1$, the largest of these fold bifurcation curves is the three year fold curve around $r_0 = 3$. We investigated how this curve changes as K is decreased below 1 (Figure 2.13). The curve continues to exist below $K = K_2 = 0.9$: for $K = 0.85$ it lies entirely in the $\epsilon > 1$ region, and it continues to shrink as K is decreased further, disappearing entirely by $K = 0.83$, well above the switch to monotonic decay (Figure 2.1). Therefore, there are Arnol'd tongues in some part of the oscillatory decay parameter regime; however, our results suggest that such folds do not occur in the monotonic decay regime.

Further, we consider how the Neimark-Sacker bifurcation curve, NS1, changes as we vary K (Figure 2.14). This shows that as K decreases towards 0.9, the curve moves

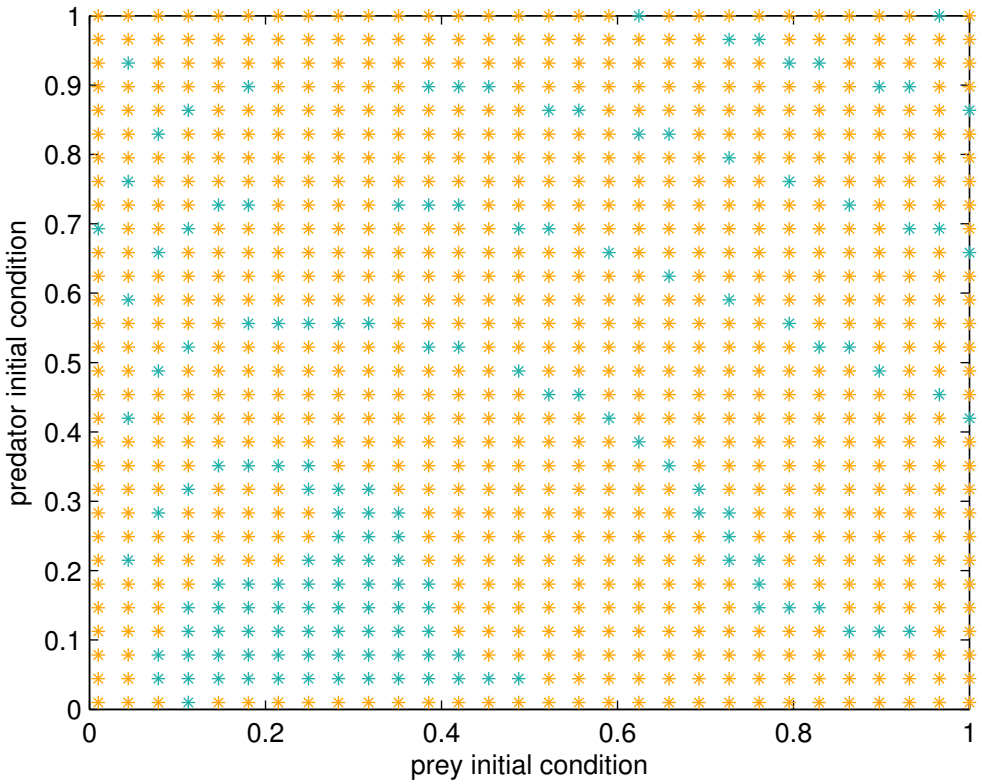

Figure 2.12: A basin of attraction plot for the point $(\epsilon, r_0) = (0.95, 3)$ when $K = 1$. A grid between 0 and 1 is used as initial conditions for both prey and predator; the period was then tested after 2,000 years. Orange crosses indicate 3 year solutions, dark green for 8 year solutions. All other details are as in Figure 2.11.

closer to the $\epsilon = 0$ axis. From Figure 2.1 it is clear that when $K = 0.9$ there is a Hopf bifurcation for all values of r. Thus the Neimark-Sacker bifurcation is approaching the Hopf bifurcation curve as we decrease K. Figures 2.13, 2.14 show that above $K = 0.9$ changes in K do not lead to drastic changes in the bifurcation diagrams but rather the curves vary smoothly with K. Thus we believe that our bifurcation diagram at $K = 1$ is a good representation of the bifurcation structure for all values of $K > 0.9$.

From Figures 2.9, 2.13 and 2.14 we see that the 2 year period-doubling curve, the 3 year fold curve and the Neimark-Sacker bifurcation curve have all disappeared for $K < 0.6$. This confirms the bifurcation work for $K = 0.35$ where only annual cycles were found. It would also indicate this is a good representation of the behaviour for all values of K up to $K = 0.6$.

2.7 Discussion

In this chapter we have investigated the dynamics of the predator-prey model (2.1) with forcing in the prey growth rate through the combined method of bifurcation dia-

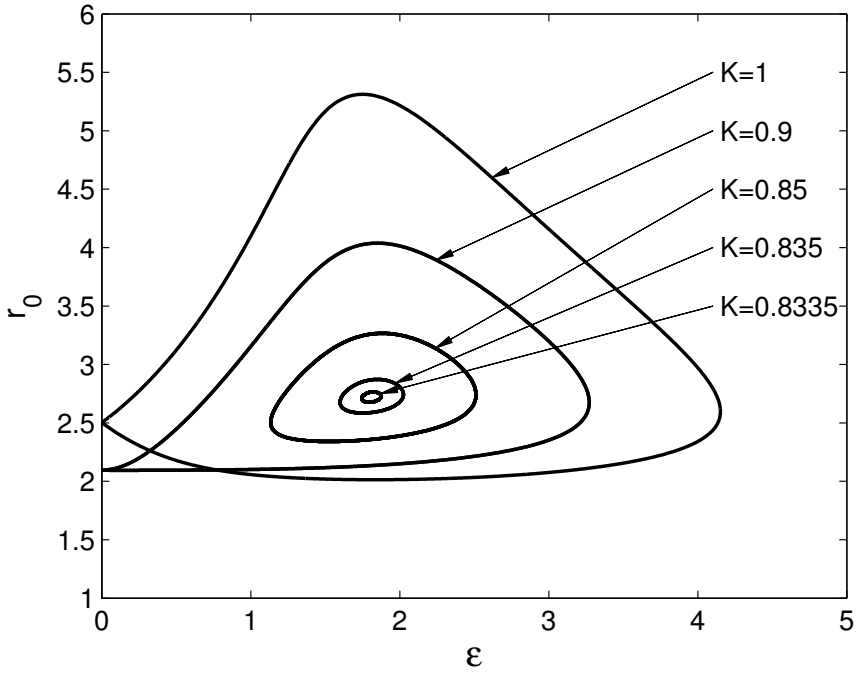

Figure 2.13: The three year fold curve, as seen in Figure 2.3(b), is drawn in $\epsilon - r_0$ space for different values of K. This shows the decay in the size of the tongue as K decreases past the Hopf bifurcation value ($K = 0.9$). Note that by $K = 0.85$ the fold curve only exists for $\epsilon > 1$.

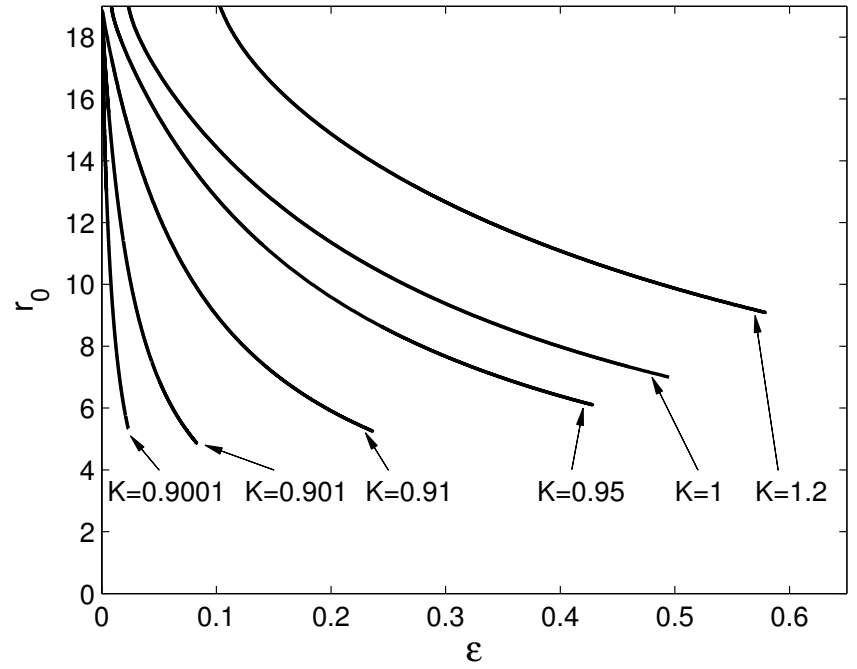

Figure 2.14: The Neimark-Sacker bifurcation curve, as seen in Figure 2.3(a), is drawn in $\epsilon - r_0$ space for different values of K. As K approaches $K_2 = 0.9$ the curve smoothly approaches the $\epsilon = 0$ axis.

grams and simulation. This has helped to explain why cycles are occurring in different parameter regions, providing a good representation of key population behaviour and the relative frequency with which different cycles occur. Through our use of simulation that directly corresponds to the bifurcation diagrams we have provided a further tool for understanding these diagrams.

Our choice of prey growth rate as the forced parameter has enabled us to separate the cases of oscillatory decay and limit cycles, in contrast with forcing parameters involved in the condition for a Hopf bifurcation in the unforced system (Rinaldi et al., 1993). This has led to a clear understanding of the dependence of cycles on the underlying oscillatory nature of the unforced model, highlighting the fact that the level of oscillation in the unforced system has a large effect on the range of possible behaviour. Specifically we have shown that when the unforced dynamics of the model exhibits monotonic decay or oscillatory decay, with low amplitude oscillations, to the coexistence steady state, the forced system will exhibit annual cycles which follow the forcing oscillation only. When the unforced system exhibits limit cycles or a sufficient level of oscillatory decay, multi-year cycles are induced due to seasonal forcing. However, the limit cycles case showed a much richer range of behaviour. This includes coexisting multi-year cycles, quasi-periodicity and chaos, particularly when the forcing strength is high. This is in keeping with the work of Rinaldi and co-workers (Rinaldi et al., 1993; Rinaldi and Muratori, 1993; Gragnani and Rinaldi, 1995). This does not rule out Arnol'd tongues occurring for the cases where multi-year cycles are induced in the oscillatory decay system: these do occur (Figure 2.13), and they are often seen in epidemiological models, which do not have limit cycles in the absence of forcing (Kuznetsov and Piccardi, 1994; Greenman et al., 2004; Childs and Boots, 2010). However, our results highlight the particular importance of studying systems under the influence of seasonal forcing which are intrinsically cyclic, as they may be able to exhibit a wider range of population behaviour.

For both the limit cycle and oscillatory decay case, the range of behaviour that we have found includes (for some parameters) coexisting multi-year cycles of different periods. However, the limit cycle case showed this more frequently than the oscillatory decay case, as well as having parameter regions where coexisting multi-year cycles of the same period occurred. In general, the limit cycle case exhibited more variety and a larger area of parameter space resulted in non-annual behaviour. We also found (in the limit cycle case) the unintuitive phenomenon of increasing forcing leading to more regular behaviour (Figure 2.3). This occurred when a higher forcing amplitude led to stability of the yearly cycle instead of the quasi-periodic cycle.

The onset of cycles, in terms of the forcing parameters r_0 and ϵ, was dependent on the unforced dynamics of the system. In the oscillatory decay case, a significant level of forcing was required in order to produce subharmonics. In the limit cycle case,

non-annual cycles occurred for low levels of forcing, such as the parameter region giving quasi-periodic solutions and the Arnol'd tongues which touch the $\epsilon = 0$ axis (Figure 2.3(b)). However, in reality most of the tongues are so thin near the axis that the solutions are hard to distinguish from quasi-periodic behaviour unless the amplitude of forcing is increased. Also of note is that in the oscillatory decay regime, multi-year cycles appear for higher values of r_0 compared to the limit cycle case. The robustness of this result to changes in other model parameters is a natural area for future work.

There are many examples where multi-year cycles occur in natural populations, especially in insect, plankton and small mammal systems (Kendall et al., 1999; Turchin, 2003). *Daphnia pulex* and its algal prey *Chlamydonomas reinhardii* is one system where the behaviour is cyclic (McCauley and Murdoch, 1987; McCauley et al., 1999; Nisbet et al., 1991) and where seasonal forcing has been implicated as an important driver of the dynamical behaviour (Scheffer et al., 1997). Moreover, this predator-prey interaction has been studied and parameterised in detail (Nisbet et al., 1991). Therefore it makes a natural test system for further study with the growth rate of the algae forced by changing light conditions in a similar manner to the fish-plankton model of Doveri et al. (1993). Many small mammal systems also show multi-year cycles (Turchin, 2003). A number of different mechanisms have been proposed as the cause of this cyclic behaviour, but for the well-studied case of Fennoscandian voles, predator-exclusion experiments have shown that the multi-year cycles in the northern areas depend fundamentally on predation (Korpimaki and Norrdahl, 1998; Hanski et al., 2001; Korpimaki et al., 2002). At these northern latitudes, which have a higher degree of seasonality in the environment, vole abundance fluctuates with period $3 - 5$ years (Hanski et al., 2001; Turchin, 2003). As one moves further south, there is a switch to annual fluctuations (Hanski et al., 2001) attributed to a change in predation from specialist predators (weasels) to generalist predators (e.g. birds, foxes) (Hanski et al., 1993; Turchin and Hanski, 1997). The methods described in this chapter are extended in Chapter 3 to consider the relative effects of specialist and generalist predation in conjunction with the impact of seasonality to determine the influence of changes in the degree of seasonality on vole population behaviour.

Many extensions of this work could be undertaken to enhance biological realism and to further our understanding of the effects of seasonal forcing, including forcing more than one parameter, in particular with different phases and forcing strengths (Rinaldi and Muratori, 1993; Greenman and Pasour, 2011). Moreover, adaptations could be made to the forcing term in order to add more realism into the model. Instead of a sinusoidal term, step functions have been used to represent a defined breeding season although this tends to yield similar results (Ireland et al., 2004). Other possibilities could be to alter the sinusoidal term to consider different breeding

season lengths or to consider chaotic forcing (Greenman and Norman, 2007; Colombo et al., 2008). Furthermore, this approach could be applied to a wide range of biological systems including tritrophic food chains (Kuznetsov et al., 2001), disease systems (Kuznetsov and Piccardi, 1994; Earn et al., 2000; Greenman et al., 2004) and invading populations (Webb and Sherratt, 2004; Greenman and Norman, 2007).

These, and other population systems, highlight the importance of studying seasonal forcing in systems with cyclic dynamics. Cyclic predator-prey systems in the real world require careful analysis to determine the origin of those cycles, and this analysis must recognise that these cycles could be highly dependent on the seasonality inherent in their environment.

Chapter 3

How Do Variations in Seasonality Affect Population Cycles?

This chapter forms the following publication:
Rachel A. Taylor, Andrew White, Jonathan A. Sherratt. How Do Variations in Seasonality Affect Population Cycles? *Proceedings of the Royal Society B: Biological Sciences*, 280 (1754):20122714, 2013.

3.1 Introduction

Seasonal forcing represents a pervasive source of environmental variability in natural systems, with many species exhibiting seasonal changes in their life history parameters (Turchin, 2003). This can affect both epidemiological and interacting population dynamics and has been proposed as a cause of multi-year cycles in these systems (Altizer et al., 2006; Keeling and Rohani, 2008). Considerable focus has been placed on the impact of seasonality in predator-prey systems, and theory has been developed both for general model frameworks (Kuznetsov et al., 1992; Rinaldi et al., 1993) and for specific wildlife populations (Hanski et al., 1993; Turchin and Hanski, 1997; Holt and Colvin, 1997). This has shown that seasonal forcing, alongside the nonlinear dynamics, can lead to complicated population dynamics including multi-year cycles, quasi-periodic solutions and chaos.

Many populations span large geographical areas over which the characteristic features of the seasonal fluctuations can vary considerably (Bjørnstad et al., 1995; Stenseth et al., 1996; Erb et al., 2000; Murray, 2000). This variation is, for instance, dependent on latitude, altitude, proximity to the coastline and prevailing weather patterns. There is also evidence that climate change has led to changes in seasonal patterns such as the earlier onset of breeding and increased variability in climatic conditions (Intergovernmental Panel On Climate Change, 2001). It is therefore important to extend the analysis of the effects of seasonality to assess the impact of changes in

the amplitude and functional form of seasonal forcing on the underlying population dynamics. In particular, to what extent do modifications in seasonal patterns lead to shifts in population dynamics?

While numerous examples of widespread populations exist in which seasonal forcing and predator-prey dynamics combine to produce cyclic population dynamics, in order to examine the impact of changes in seasonality we will focus on a well-known case study – namely the Fennoscandian vole system (Hansson and Henttonen, 1985, 1988; Hansen et al., 1999; Hanski et al., 2001; Inchausti and Ginzburg, 2009). This system spans a large geographical area and undergoes high amplitude seasonal forcing which varies with location (typically, the length of the breeding season decreases with latitude). The important features of this vole system are the large amplitude, multi-annual cycles north of 60°N, synchronous over large spatial scales with a period of $3-5$ years, with the 5 year cycles occurring furthest north. In comparison, the southern Fennoscandian region has low amplitude "non-cyclic" seasonal fluctuations, effectively an annual cycle. Therefore, period and amplitude decrease as one moves along a north – south gradient in Fennoscandia (Hansson and Henttonen, 1985, 1988; Bjørnstad et al., 1995; Korpimaki and Krebs, 1996).

It has been suggested that changes in generalist predation with latitude explain this gradient within Fennoscandia (Hanski et al., 1991, 2001; Norrdahl, 1995) and this is supported by theory (Hanski et al., 1993; Turchin and Hanski, 1997). However, the seasonal forcing term remains fixed in these models. This contrasts with the pronounced differences in the pattern of seasonality between the southern and northern parts of Fennoscandia and the effect of this on the predation hypothesis has received almost no attention (a notable exception being Dalkvist et al. (2011) who consider three different breeding season lengths). In southern Fennoscandia, the breeding season can be over 7 months long, whereas in northern areas it is usually $3-4$ months (Nelson et al., 1991; Hansen et al., 1999; Dalkvist et al., 2011). Furthermore there is evidence to suggest that the vole cycles have been reducing in period length because of climate change (Hornfeldt et al., 2005; Ims et al., 2008). The vole system can be used to see if geographical variations in seasonal forcing can help explain the gradient in cyclicity which is currently found in Fennoscandia, as well as how changes in the pattern of seasonality will alter the population dynamics. To capture the changing seasonality we will vary breeding season length. By using the vole system as a case study, we will highlight the wide range of complex population dynamics which can arise due to seasonal forcing and indicate how variation in seasonality can generate shifts in population dynamics.

3.2 Model

A wide range of intrinsic and extrinsic factors have been proposed to explain the geographical gradient in cyclicity found in Fennoscandian voles but the most widely supported is the predation hypothesis, first formulated by Hanski et al. (1991) and further discussed in Korpimaki and Krebs (1996); Turchin and Hanski (1997); Hanski et al. (2001). This states that the northern cycles are caused by specialist predation, usually by the least weasel. As the weasels have little alternative prey, they have delayed reactions in their reproduction in response to changes in vole numbers, generating the cycles (although food limitation may play a role in determining the size of the prey peak (Hansson, 2002)). Both the protective layer of snow cover, which hinders predators unable to tunnel under the snow, and the low diversity of prey in these northerly locations mean that there are few generalist predators. In the south there are numerous generalist predators, such as birds, badgers and foxes. In fact, 80% of rodent mortality by predation in the south is by generalists (Hansson and Henttonen, 1988). Since generalist predators exhibit rapid prey switching when vole numbers drop, this type of predation has a stabilising effect on the vole population. The predation hypothesis effectively states that specialist predators induce cycles while the generalist predators in the south act to dampen these fluctuations. This is backed up by predator exclusion experiments (Korpimaki and Norrdahl, 1998; Korpimaki et al., 2002) as well as through analysis of many of the proposed reasons for the cycles (such as the predation hypothesis, landscape fragmentation, maternal effects) using statistical methods to assess the extent of their agreement with the vole data collected (Bjørnstad et al., 1995; Norrdahl, 1995; Turchin and Hanski, 2001).

3.2.1 Model Details

Our work is based on the model of Turchin and Hanski (1997) which incorporates both specialist and generalist predation. Importantly, we introduce seasonal forcing to the growth rates and implicitly also the carrying capacities of both prey and predator through a seasonal term $S(t)$, which includes breeding season length (see below for details). When suitably non-dimensionalised (see Appendix B) the model is

$$\frac{dx}{dt} = rS(t)x - rx^2 - \frac{gx^2}{x^2+h^2} - \frac{axy}{x+d} \tag{3.1a}$$

$$\frac{dy}{dt} = sS(t)y - s\frac{y^2}{x}. \tag{3.1b}$$

Here, $x(t)$ and $y(t)$ are the densities of prey and specialist predator at time t respectively. The prey undergo logistic growth. They are affected by two predation terms, the first due to generalist, the second specialist predation. Generalist predation is a

Holling Type III functional form because generalists will switch to other prey items when vole numbers are low. The specialist predation is the Holling Type II functional form which incorporates handling time of prey (Holling, 1959a,b). The predators have a logistic growth with growth rate s and a carrying capacity which is determined by the density of prey. We use the parameter values of Turchin and Hanski (1997) namely $r = 6$, $s = 1.25$, $d = 0.04$, $a = 15$, and $h = 0.1$. These values were chosen based on a combination of field data, previous literature and time series analysis. The parameter g represents the level of generalist predation, which changes along a north-south gradient. We vary g between 0 and 1 because Turchin and Hanski (1997) estimate the value of g to be in the range 0.933 to 0.066 at four vole localities, ranging from Revinge, Sweden at 56°N to Kilpisjärvi, Finland at 69°N. Note that small g indicates less generalist predation, corresponding to a more northerly location.

The main aim of this chapter is to consider how geographical changes in seasonal forcing affect the population dynamics and we do this by varying the breeding season length. We introduce a parameter l as part of the seasonal term $S(t)$ which is given by the following equation (see Appendix B):

$$S(t) = 2(\tfrac{1}{2}(1 + \epsilon \sin(2\pi t)))^l. \tag{3.2}$$

The parameter l determines the length of the breeding season, defined as when the forced growth term is above its unforced value: for the prey this is when $rS(t) > 6$. Figure 3.1 shows how our forcing term changes depending on the value of l. As l increases then the breeding season length decreases. Although we vary l from $0 - 5$, the most biologically relevant part of the range is $0.5 - 3.9$, which gives a breeding season between 3 and 8 months long; the data discussed above shows that this is the appropriate variation across Fennoscandia.

In addition, Figure 3.1 shows that as l increases, the mean value of the growth rate decreases. This reflects the fact that voles produce more litters if the breeding season is longer, and that female young from the first 1 or 2 litters are also able to breed if the breeding season is long enough for them to have matured (Dyczkowski and Yalden, 1998). Turchin and Ostfeld (1997) suggest 14 as a maximum value for the growth rate and our values are below this limit. However, this does mean our results are based on both breeding season length and mean value of the growth rate varying as we vary l, and we do not determine how each component affects the results separately.

3.2.2 Model Analysis

We studied the model using two different methods - a bifurcation and a simulation approach, following the procedure in Chapter 2. The bifurcation results were calcu-

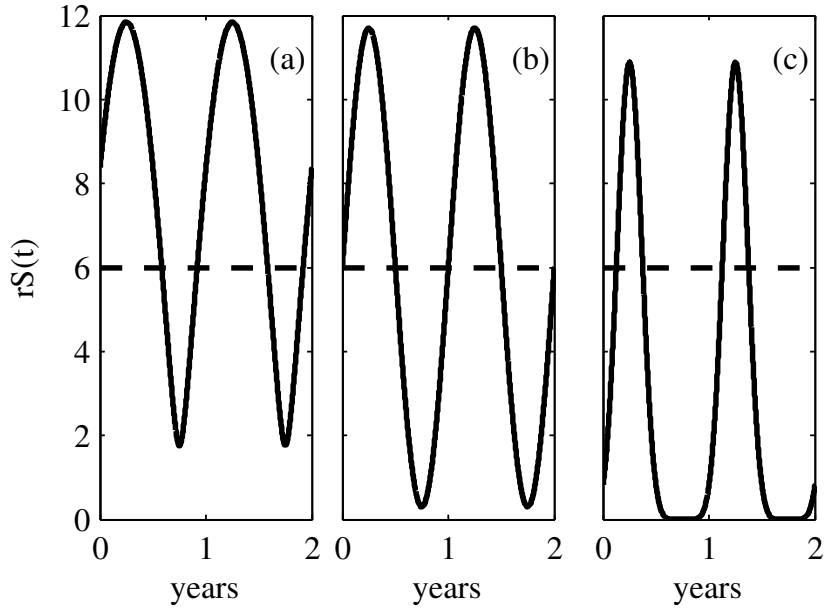

Figure 3.1: The forcing function for different values of l, producing different lengths of breeding season. The values of l are (a) 0.52 (b) 1 (c) 3.87 and $\epsilon = 0.95$. The breeding season is designated as when the growth rate (black curve) is above the unforced growth rate (dotted line). This leads to breeding season lengths of 2/3, 1/2, 1/3 year respectively.

lated using essentially standard numerical continuation techniques implemented via the software AUTO (Doedel, 1981). This method determines parameter ranges in which different multi-year cycles exist, and when they are stable. The simulation results were produced by solving the model equations (3.1) using Matlab (`ode15s`) for 2000 years and the solutions were tested to determine whether there existed a periodic solution of $1-9$ years; if not, the solution was labelled as quasi-periodic, meaning that the solution was approximately periodic but does not have a finite period. We also used fast Fourier transforms to determine the period most closely reflected in the solution ("dominant period"); this was especially helpful when the cycle was quasi-periodic. We performed our simulations over a grid of points in parameter space, with 50 simulations at each point to illustrate the relative sizes of the basins of attraction of the different solutions. See Appendix B for further details.

3.3 Results

Hanski et al. (1993) and Turchin and Hanski (1997) focussed on the case where breeding season is exactly 6 months long ($l = 1$) and considered the effects of varying the extent of generalist predation (g). This revealed a change from annual to multi-annual cycles (period $3-4$ years) as the level of generalist predation is reduced. We illustrate this in Figure 3.2 which shows simulations for $l = 1$ and various values of g, for two

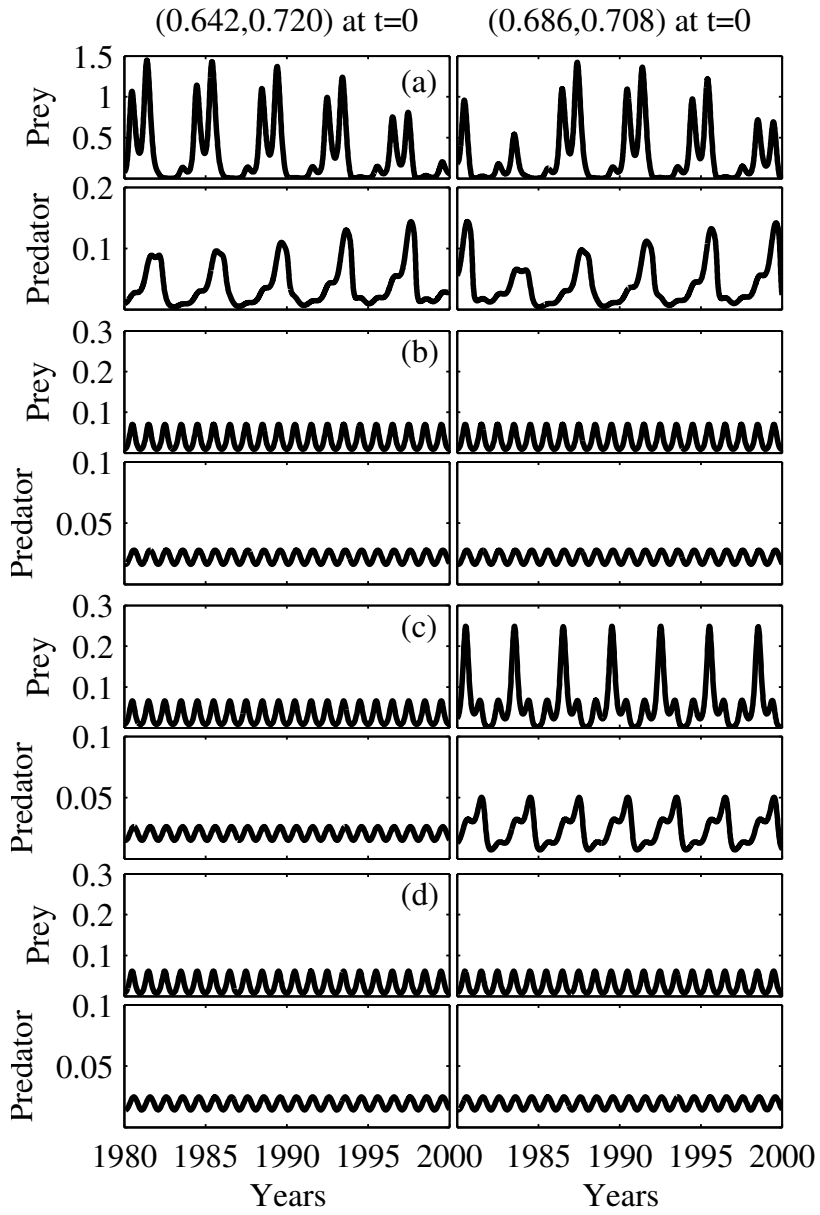

Figure 3.2: Solution plots when the breeding season is 6 months long ($l = 1$), for different levels of generalist predation g: (a) $g = 0.25$, (b) $g = 0.4$, (c) $g = 0.5$, (d) $g = 0.6$. The two columns show results for two different initial conditions namely $(x(0), y(0)) = (0.642, 0.720)$ and $(0.686, 0.708)$. For each value of g we plot both the prey and predator solution for the two sets of initial conditions. For (a), (b) and (d) the two sets of initial conditions produce the same results, quasi-periodicity and then annual cycles. Although the quasi-periodic solutions plotted in (a) are different, fast Fourier transforms give 3.75 as the dominant period in both cases. However, in (c) one set of initial conditions produced an annual cycle whereas the other set of initial conditions produced a 3 year cycle. The solutions are solved for 2000 years and the results are shown after the initial transient dynamics have dissipated. Other parameter values are $r = 6$, $s = 1.25$, $d = 0.04$, $a = 15$, $h = 0.1$, $\epsilon = 0.95$.

sets of initial conditions. Note that for $g = 0.5$, 3 year cycles occur for one set of initial conditions and annual cycles for the other. These results highlight the existence

of multiple solutions, with strong sensitivity to initial conditions. Clearly bifurcation analysis and/or extensive simulation are necessary to reveal the full range of model predictions.

We used the bifurcation method to investigate potential dynamics as both season length l and generalist predation level g are varied (Figure 3.3(a)). This divides the $l-g$ parameter plane into different regions denoting the different possible dynamics. This shows that for moderate or high l and g values only annual cycles are possible, with multi-year and quasi-periodic solutions for lower l and g. Figure 3.3(a) therefore shows that when the breeding season is longer there is a larger range of generalist predation levels giving multi-year cycles. However, this figure does not show the period of the cycles as a function of parameters.

To examine the solutions in more detail we show parameter regions giving both existence and stability for 2, 3, 4 and 5 year cycles (Figure 3.4). For cycles with higher period ($6-9$ years) the results are similar to Figure 3.4(d), although the regions tend to get smaller with increasing period. The cycles exist inside the boundary curves, with stability/instability shown by the thick black/thin grey lines respectively. The coloured curves represent different types of bifurcation: period-doubling bifurcation (blue), fold (a.k.a. saddle-node or tangent; red) and Neimark-Sacker (green); a Neimark-Sacker bifurcation is a discrete version of a Hopf bifurcation. (More details and a full bifurcation diagram are provided in Appendix C.)

Each of the regions in Figure 3.4 has a complicated form; in particular for the 3 and 4 year cycles there are two separate regions of stability. From these diagrams we can see that cycles of longer period occur only for lower values of g. There are many areas where the cycles are unstable and here we expect either quasi-periodic or annual solutions to be stable. The cyclic regions also intersect (see Figure C.2) and so there are parameter regions that give rise to coexisting stable multi-year cycles. Therefore it is important to consider which cycles actually occur for different values of l and g.

Simulation results displaying the population dynamical outcome in parameter space (Figure 3.3(b)) provide a clearer view of how the multi-year solutions overlap and indicate the relative sizes of the basins of attraction when multiple solutions coexist. The results compare favourably with the bifurcation picture in Figure 3.3(a), with a relatively clear split between the yearly and quasi-periodic solutions interspersed with multi-year solutions. Due to the large regions of instability within the multi-year cycle regions shown in Figure 3.4, there were not many regions in Figure 3.3(b) where two multi-year cycles coexisted and were both stable. Thus there were hardly any pie charts which showed multiple multi-year stable solutions, although in one case both 4 and 9 year cycles occur (where $l=1.5$, $g=0.2$). However, for a number of parameter pairs multi-year solutions coexist with annual or quasi-periodic solutions.

Figure 3.3(a) shows that when the breeding season is longer there is a larger range

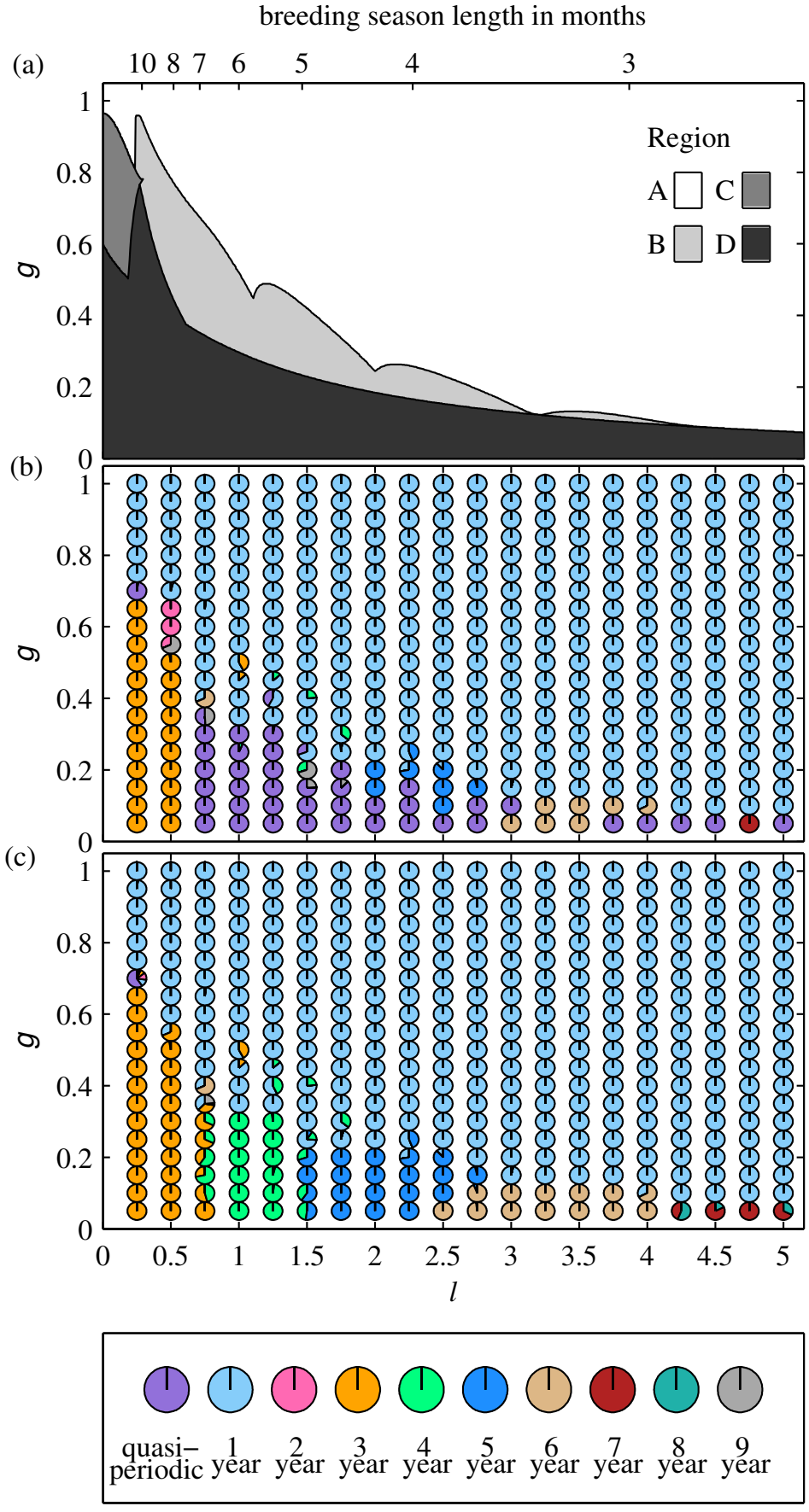

Figure 3.3: Legend on next page.

Figure 3.3: Potential dynamics when season length parameter (l) and extent of generalist predation (g) are varied. (a) The bifurcation diagram split into 4 regions: A - annual cycles, B - annual and multi-year cycles, C - annual, multi-year and quasi-periodic cycles, D - multi-year and quasi-periodic cycles. (b) A simulation diagram with a grid of pie charts showing what proportion of the 50 simulations had a particular period, indicated by the legend. Each simulation was run with random initial conditions (between 0 and 1 for prey and predator) and the period was tested after 2000 years. (c) The same simulations tested using fast Fourier transforms to determine the dominant period of the solutions. The remaining purple solutions indicate the dominant period was larger than 9. Other parameter values are $r = 6$, $s = 1.25$, $d = 0.04$, $a = 15$, $h = 0.1$, $\epsilon = 0.95$.

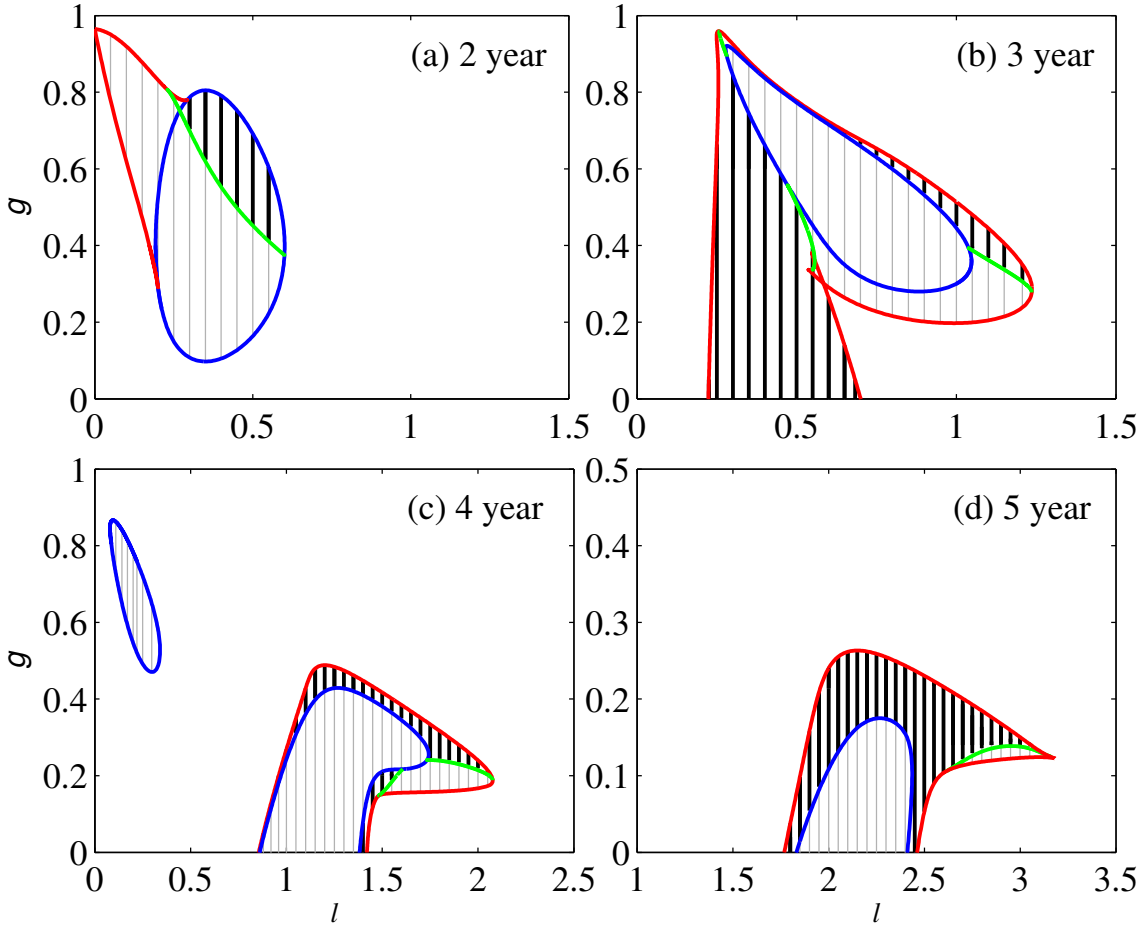

Figure 3.4: The regions for existence and stability of (a) 2 year, (b) 3 year, (c) 4 year and (d) 5 year cycles in $l - g$ parameter space. The coloured curves denote different bifurcation curves representing period-doubling - blue, fold - red, Neimark-Sacker bifurcation - green. Stability/instability is shown by the thick black/thin grey lines respectively. Other parameter values are $r = 6$, $s = 1.25$, $d = 0.04$, $a = 15$, $h = 0.1$, $\epsilon = 0.95$.

of generalist predation levels giving multi-year cycles. But the multi-year cyclic dynamics in Fennoscandia occur in the areas where the breeding season is shorter. To produce further detail on the nature of the population dynamics in regions where

quasi-periodicity is predicted we use fast Fourier transforms to analyse each simulation, revealing the dominant cycle period (Figure 3.3(c)). As l is increased for low g, i.e. as the breeding season length is reduced, the periodicity of the solutions increases. This concurs with the gradient of periodicity that has been found in Fennoscandia where in mid Fennoscandia there are 3 year cycles and further north (with shorter season lengths) there are 5 year cycles (Hansson and Henttonen, 1988; Ims et al., 2008).

3.4 Discussion

The basic conclusion from previous modelling of the predation hypothesis for Fennoscandian vole cycles is that cycle period increases as the generalist predation level decreases. Our work shows that this is an over-simplification. Even with fixed breeding season length, the existence of multiple stable solutions implies that switches between, say, annual and three year cycles are possible. When variations in both season length and generalist predation level are considered, there is a rich variety of potential dynamics, with coexisting multi-year solutions and numerous possible cycle periods. This includes parameter values showing both 4 and 9 year cycles, an interesting phenomenon considering that short-term and long-term cycles are often seen as either-or dynamics, rather than both being possible for the same system (Korpimaki and Krebs, 1996).

Empirical support for the dependence of vole cycle period on breeding season length is provided by the work by Strann et al. (2002) on voles in Kirkesdalen, Norway. Here the population undergoes cycles with a period of three years, which contrasts with the five year cycles at other sites with a similar latitude. Strann et al. (2002) attributed this difference to climatic differences, due to Kirkesdalen's proximity to the coast. A key implication of this climatic difference might be a longer breeding season; our model predicts that this would indeed cause lower period cycles.

The variation in vole breeding season length in Fennoscandia is considerable: from as little as 3 months in the most northern locations to 8 months in the south (Nelson et al., 1991; Hansen et al., 1999). This wide range is important for our conclusions. In particular, if one restricts attention to breeding season lengths of $6-8$ months, the results in Figure 3.3 predict little variation in the dynamics. This is consistent with the results of Dalkvist et al. (2011). They study data on Fennoscandian voles with breeding season lengths of 6, 7 and 8 months, and found that the difference between these season lengths was not a statistically significant factor in differences in cyclicity.

To illustrate our results, we have plotted parameter planes in which the generalist predation level varies on one axis, with the breeding season length on the other. The north-south gradient in Fennoscandia corresponds to a curve in this parameter plane.

There is currently insufficient data to enable a detailed formulation of this curve, but it is likely to be nonlinear, especially when factors such as landscape fragmentation (Huitu et al., 2003; Strohm and Tyson, 2009; Dalkvist et al., 2011) are taken into account. Our results suggest that more information on the form of this nonlinear curve would be a key step in understanding the complexities in vole dynamics, such as the sudden change from annual to multi-year cycles that occurs in mid-Fennoscandia (Turchin and Hanski, 1997).

In the model we forced both the prey and predator growth rates with the same forcing term. Although weasels are able to breed throughout the whole year, this only happens in peak years of vole populations (King, 1989). Therefore, including a weasel breeding season is valid but it is unclear whether this should follow the same pattern as the vole breeding season, on which the forcing term was based. In order to understand the effects of different forcing in the predator growth rate, we considered the scenario of no forcing for the weasels (see Appendix D). This yielded similar results, showing the complexity of moving on a north-south gradient, the change to annual cycles as generalist levels increase, and the possibility of switching between different multi-year cycles. However, the pattern of decreasing breeding season length leading to increased period was less clearly defined.

Significant changes in vole population dynamics have been observed in recent years in Fennoscandia, with the boundary between annual and multi-year cycles moving further north, and very few locations still showing five year cycles (Hornfeldt et al., 2005). These changes are widely attributed to climate change. This is affecting the Fennoscandia system in many different ways and the implications for vole dynamics are consequently complex. However, two effects of climate change are increases in both breeding season length and generalist predation level (Hersteinsson and MacDonald, 1992; Ims and Fuglei, 2005). Our results (Figure 3.3) predict that these two effects could together cause decreases in cycle length and a northerly movement of the location of the switch between annual and multi-year cycles. Since annual cycles typically have a much lower amplitude than multi-year solutions (Figure 3.2), and since voles are a keystone species in Fennoscandia (Ims and Fuglei, 2005), a switch to annual cycles is highly significant for the whole ecosystem.

Fennoscandia is not the only region in which there are established geographical variations in vole cyclicity. For example, vole cycles occur over large regions in central Europe (Tkadlec and Stenseth, 2001) and in Hokkaido, Japan (Stenseth et al., 1996). Notably, Stenseth et al. (1996) showed the importance of season length in driving the gradient of cyclicity in Hokkaido. In central Europe both the period and amplitude of vole cycles increase from north to south (Tkadlec and Stenseth, 2001); this is in the opposite direction to the trend in Fennoscandia. Data on breeding season length and level of generalist predation is currently very limited for this region, and our work

argues for the importance of such data in understanding this trend.

Large-scale geographical variations in population dynamics also occur in other populations: Canadian muskrats are another classic example (Erb et al., 2000). Our results argue for a detailed appraisal of the role of breeding season variability on the population dynamics in such cases. Although we expect similar trends to those found in the present study, they may be quenched by the effects of seasonality in parameters other than simply the birth rate; specific case studies are essential.

Seasonality varies geographically due to a multitude of factors including latitude, altitude, proximity to a coastline and general weather patterns. Our work argues that this cannot be ignored as variations in seasonality can be an important driver of the observed population dynamics.

Chapter 4

Seasonal Forcing in a Host-Macroparasite System

The majority of this chapter has been submitted for publication in *Journal of Theoretical Biology* as: Rachel A. Taylor, Andrew White, Jonathan A. Sherratt. Seasonal Forcing in a Host-Macroparasite System.

4.1 Introduction

Seasonal forcing is a ubiquitous force in nature affecting species through their life-history parameters, with an annual pulse of births in spring and summer seen as perhaps its most pervasive manifestation (Turchin, 2003). Seasonal forcing has been shown to be important in generating the cycles observed in many ecological and epidemiological systems. For example, by including seasonal forcing to represent changes in transmission during the school year, modelling results have been shown to be consistent with observations of measles case reports (Finkenstadt and Grenfell, 2000; Earn et al., 2000; Altizer et al., 2006). Numerous other examples exist in which seasonal forcing has been shown to be a driver of fluctuations: including outbreaks of influenza (Dushoff et al., 2004), plankton-fish dynamics (Doveri et al., 1993) and vole population cycles (Smith et al., 2008; Taylor et al., 2013b). Thus, within the field of interacting populations and host-microparasite systems, the importance of seasonal forcing is both well-established and well-studied (Altizer et al., 2006; Sherratt and Smith, 2008).

Seasonal forcing within host-macroparasite systems is less well identified and studied. In part, this may be because seasonality is associated with its ability to produce cyclic dynamics and these are less frequently reported in macroparasite compared to microparasite systems (Gulland, 1995; White et al., 1996). However, there are significant examples where macroparasites are thought to be influential in driving population cycles. Red grouse fluctuate irregularly across England and Scotland (Haydon

et al., 2002; Cattadori et al., 2005b) and the role of nematode parasites, alongside territorial dynamics, in driving these cycles has been strongly argued (Dobson and Hudson, 1992; Hudson et al., 1998; Redpath et al., 2006). Soay sheep have population crashes every 3 to 4 years, which have been attributed to nematode parasites in combination with harsh winters and malnutrition (Gulland and Fox, 1992; Gulland, 1992; Coulson et al., 2001). There is considerable evidence to indicate that seasonal forcing alters many aspects of both these systems, such as the host birth rate, the maturation of parasite larvae in the environment, and arrested development of larvae within the host (Anderson, 2000), which could impact on the dynamics. However, no detailed analysis has been attempted to elucidate the effect of seasonal forcing alongside parasitism for these systems.

Theoretical studies of seasonal forcing in general host-macroparasite systems have been of two types. Roberts and Grenfell (1991, 1992) explored system-specific model frameworks to understand the effect of a periodic pulse on the level of acquired host immunity and how environmental forcing on maturation of the nematode larvae affects the epidemiological dynamics of farmed ruminants. This work has been extended to consider wildlife systems, focussing on how host immunity and the relationship between host age and parasite intensity changes over one season within the host (Cattadori et al., 2005a; Cornell et al., 2008). These studies found that the host immune response was affected by both seasonal changes in larvae transmission and the month of host birth; therefore different host age – parasite intensity curves exist for different birth cohorts. General host-macroparasite models have examined the role of seasonality on population dynamics by representing annual reproduction as a step-function (White et al., 1996) and a pulse of births (White and Grenfell, 1997). When free-living stages are considered explicitly, seasonality can increase the period and amplitude of population cycles and there is evidence of multiple population attractors (White et al., 1996), although there has not been a detailed investigation of these findings. Therefore a detailed examination of the role of seasonality on host-macroparasite dynamics is lacking and could utilize the recent developments in computational bifurcation theory and resonance-based analysis (Greenman et al., 2004; Choisy et al., 2006; Bolzoni et al., 2008; Taylor et al., 2013a) that have been applied to understand population cycles in microparasite and interacting systems.

Experimental and theoretical studies highlight the need to explore seasonal effects in host-macroparasite systems. In this chapter we propose to undertake a comprehensive analysis of the role of seasonality on host-macroparasite population dynamics that utilizes the new developments in the study of forced coupled systems (Taylor et al., 2013a). We will undertake this analysis in a system that explicitly represents free-living stages of the parasite, since White et al. (1996) indicated that seasonality could have a marked effect in such systems. This allows us to understand the wide

range of outcomes occurring from seasonal forcing in general host-macroparasite systems. In particular, we will show the importance of the unforced dynamics on the seasonally forced system and the possibility of multiple solution behaviour, multi-year cycles and period-doubling to chaos. Furthermore, such model formulations without seasonal forcing have been parameterised to represent the red grouse - *Trichostrongylus tenuis* system (Dobson and Hudson, 1992) and therefore our results will provide important insight into the influence of seasonality on the population dynamics in a specific ecological system.

4.2 Methods

Macroparasites (helminths) differ from microparasites (viruses, bacteria, protozoa) in that they reproduce by releasing free-living infective stages, which mature in the environment or a secondary host before being transmitted to the definitive host. They usually have a relatively long life span and are persistent in the host with multiple re-infections being typical (Anderson and May, 1992). This added complexity in the life cycle of the macroparasite leads to the necessity of modelling the parasite burden within each host explicitly. A pattern seen across a wide range of different host and parasite species is that a minority of hosts within the population harbour the majority of parasites (Anderson and May, 1978; Wilson et al., 2002); regularly more than 80% of parasites are contained within 20% of the hosts (Anderson and May, 1992). Macroparasites can cause a reduction in breeding capabilities of the host, by modifying host behaviour or lowering the average brood size. Reduced survival is also possible indirectly, by making the host more susceptible to predation, and when hosts contain large numbers of parasites, this can become a direct cause of death (Anderson and May, 1978, 1992; Hudson et al., 1992; Gulland, 1995).

Numerous models have been used to represent host-macroparasite systems, with different frameworks for including aggregation, the effect of immunity, arrested development and larval dynamics (Anderson and May, 1978; May and Anderson, 1978; Diekmann and Kretzschmar, 1991; White et al., 1996; White and Grenfell, 1997; Rosà and Pugliese, 2002). In this study we use a general model formulation which includes the larval stage explicitly, and the aggregation of parasite spread throughout hosts is represented by the commonly used negative binomial distribution (Anderson and May, 1978; Diekmann and Kretzschmar, 1991; Rosà and Pugliese, 2002). We rescale the model to reduce the number of parameters (for further details on the model, see

Appendix E) leading to the following system of equations:

$$\frac{dh}{dt} = (a-1)h - (1+\delta)p \tag{4.1a}$$

$$\frac{dp}{dt} = \beta lh - (\mu+1)p - \frac{p^2}{h}\left(\frac{k+1}{k}\right) \tag{4.1b}$$

$$\frac{dl}{dt} = p - \gamma l - lh, \tag{4.1c}$$

where $h(t)$ and $l(t)$ are the host and larvae species respectively at time t and $p(t)$ is the adult parasite population spread among the hosts at time t. The host species undergoes exponential birth (a) and death, as well as parasite-induced death and reduced fecundity caused by the parasite (δ). We restrict δ to small values to prevent the host birth rate becoming negative (see Figure 4.4 for clarification). The term βlh denotes the transmission of larvae to hosts leading to adult parasites. Parasites are lost due to natural mortality, natural death of the host and parasite induced death of the host. However, the loss of parasites due to host death requires knowledge of the expected number of parasites within each host, and we assume a negative binomial distribution for the parasites with aggregation parameter k (which leads to the form of (4.1b)). Finally, the larvae are produced by adult parasites laying eggs and lost due to natural death (γ).

Our work is not specifically focussed on red grouse; rather we use this example to elucidate our results for the effects of introducing a seasonally forced birth rate into host-macroparasite systems. Red grouse (*Lagopus lagopus scoticus*) are a common case study for macroparasites due to the relative simplicity of the parasite dynamics, the interesting cyclic dynamics seen across England and Scotland and the availability of data from hunting records. The adult nematode *Trichostrongylus tenuis* lives in the caeca of the grouse, passing eggs out of the host through the caecal faeces. The larvae mature in the environment (if conditions are suitable) and then migrate to the tips of heather. The grouse ingest these larvae by eating the heather, their main food plant (Hudson et al., 1992; Anderson, 2000). Experimental studies have shown that the nematode *Trichostrongylus tenuis* reduces reproduction in red grouse populations through lower clutch sizes, egg mortality and chick loss (Hudson et al., 1992), thus Dobson and Hudson (1992) emphasised the reduced fecundity term, δ. The above model (4.1) has previously been parameterised for the red grouse system (Dobson and Hudson, 1992). For consistency we use these parameter values, which after rescaling become: $a = 1.7$, $\beta = 10/1.05$, $\mu = 1.0003/1.05$, $k = 1$ and $\gamma = 10/1.05$. Dobson and Hudson (1992) let $\delta = 1.667$, which combined with the other parameter values leads to diverging cycles driving the hosts and parasites to extinction. Dobson and Hudson

(1992) chose to counteract this by adding host regulation through logistic growth. We instead keep the model formulation as in (4.1) but will vary the value of δ and analyse the effect of this on the dynamics.

We introduce seasonal forcing into the birth rate of the host, using a sinusoidal form, a common method for representing seasonal changes (Dietz, 1976; Rinaldi et al., 1993; Choisy et al., 2006). The birth rate becomes

$$a(t) = a(1 + \epsilon \sin(2\pi t)) \tag{4.2}$$

where a is the mean value of the forced birth rate (the same value as in the unforced case, $a = 1.7$) and ϵ is the amplitude of the forcing.

4.2.1 Unforced Dynamics

In order to understand the effect of seasonal forcing, we first need to consider the unforced dynamics. The system (4.1) undergoes a Hopf bifurcation when δ is varied, with a stable equilibrium for $\delta < 0.78$ and stable limit cycles for δ above this value. Explicit inclusion of the larval stage is somewhat akin to the addition of a time delay and this is fundamental in causing the cycles. In Figure 4.1 the period and amplitude of these limit cycles are plotted as a function of δ.

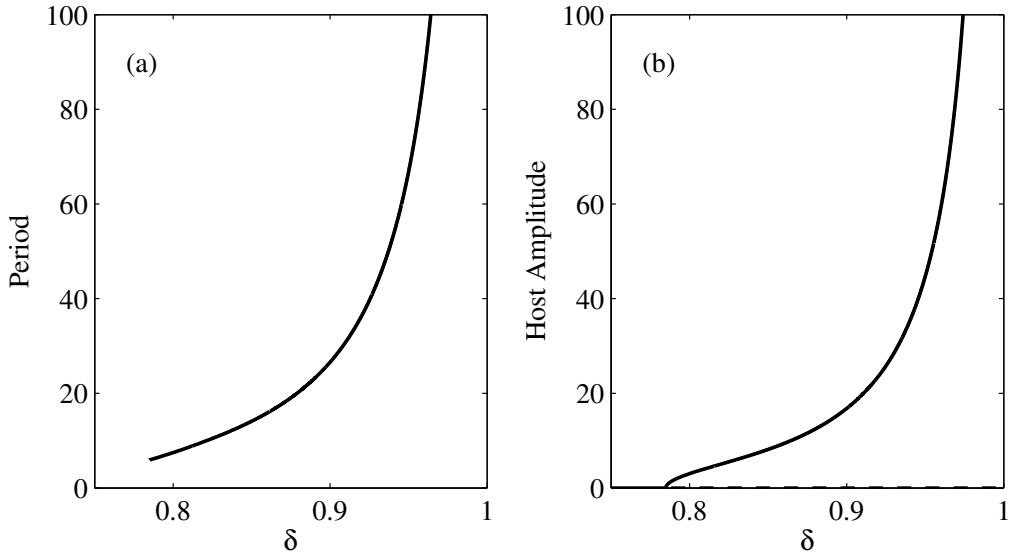

Figure 4.1: In (a) the period of the limit cycles is plotted as δ is varied. In (b) the amplitudes of the steady state and the limit cycles are plotted as δ is varied. Stability and instability are indicated by the solid and dashed lines respectively. All other parameter values are kept constant with the following values: $a = 1.7$, $\beta = \gamma = 10/1.05$, $\mu = 1.0003/1.05$ and $k = 1$.

As shown in Figure 4.1, the period of the limit cycles starts at 5.9 years and increases rapidly as δ increases. Previous studies (Rinaldi et al., 1993; Greenman et al., 2004; Taylor et al., 2013a) have shown how yearly forcing can resonate with the unforced period at integer values to produce multi-year cycles of that integer period or multiples thereof. Thus, we do not expect to be able to find multi-year solutions which have period less than 6 (since that is the smallest integer period that can be exhibited in the model for our parameter choice). The amplitude plot in Figure 4.1(b) shows the amplitude of the limit cycles also increasing rapidly as δ increases (and explains why divergent cycles leading to extinction occur for $\delta = 1.667$ in Dobson and Hudson (1992)).

4.2.2 Bifurcation Method

We will investigate the effects of seasonal forcing in this example by varying both δ and ϵ and show the multi-year dynamics and multiple solution behaviour that occur using a two-dimensional bifurcation diagram. We will then move on to a more general framework to understand seasonal forcing within host-macroparasite systems in greater detail. We begin with a brief overview of the necessary bifurcation theory; for more information please see §2.3. There are three main bifurcation curves namely, period-doubling bifurcation curves, fold bifurcation curves and Neimark-Sacker bifurcation curves. The standard procedure for locating bifurcations uses the Poincaré (or stroboscopic) map that transforms the continuous system into a discrete one by sampling the solution once in each forcing period; once per year in our case. Note that the stable/unstable annual cycles become stable/unstable fixed points of the Poincaré map. Discrete bifurcation theory reveals that this fixed point is unstable if one of the eigenvalues of its linearisation has modulus larger than 1. Changes in stability are of three possible types. If the eigenvalue is equal to -1, it is a period-doubling (flip) bifurcation; if the eigenvalue is equal to $+1$ it is a fold (saddle-node, tangent) bifurcation; and if there is a pair of complex conjugate eigenvalues with modulus 1, it is a Neimark-Sacker (torus) bifurcation.

At a period-doubling bifurcation curve, which we denote by PDk, a stable cycle of period k loses stability and a stable cycle of period $2k$ arises. On one side of a fold bifurcation curve denoted by FDk there is no solution but on the other side there are both stable and unstable solution branches of a cycle of period k, which meet at a fold at the bifurcation point. A Neimark-Sacker bifurcation is often described as a discrete version of a Hopf bifurcation because for a standard supercritical bifurcation, the fixed point on the Poincaré section becomes unstable and a stable closed invariant curve arises around the point. Typically, each iteration of the Poincaré map brings the solution back to a different point on the closed invariant curve. Therefore, in the continuous setting when crossing a Neimark-Sacker bifurcation curve, denoted by

NSk, a cycle of period k loses stability and a quasi-periodic solution arises. That is, the solution may superficially appear periodic but in fact it has no finite period. Thus, there are different Neimark-Sacker bifurcation curves and separate regions of quasi-periodicity related to each of the different periodic solutions.

We use AUTO bifurcation software (Doedel, 1981) to produce the bifurcation diagrams and Matlab (`ode15s`) to produce numerical simulations. The simulations were run for 7000 years, with initial conditions randomly chosen; arbitrarily we use a uniform distribution between 0 and 1. We then tested whether they had an exact period of between 1 and 16 years. If the simulations did not have an exact period within this range, they were labelled as quasi-periodic. Note that we also log-transformed the equations to speed up computational time as the solutions spend a large proportion of each cycle very close to zero and it takes a long time for the transient dynamics to die out (see Appendix E). Log-transforming the equations significantly improves both computational time in Matlab and accuracy in AUTO. However, we reverse this log-transformation before presenting results.

4.3 Results

We consider first the host-macroparasite system with the red grouse parameters. This highlights key properties of seasonal forcing in host-macroparasites systems, such as a wide range of multi-year cycles of different periods, multiple solution behaviour and the possibility for increases in the amplitude of seasonal forcing alone to significantly change the dynamics. We then vary the model parameters, which has the effect of changing the unforced dynamics of the system and allows us to explore the effect of seasonal forcing on host-macroparasite dynamics more generally.

4.3.1 The Red Grouse Dynamics

In Figure 4.2, a two-dimensional bifurcation diagram is plotted for parameters representing the red grouse system showing the fold bifurcation curves and the Neimark-Sacker bifurcation curve. The Neimark-Sacker bifurcation curve (NS1) hits the $\epsilon = 0$ axis where the unforced system has a Hopf bifurcation. Below this curve there are stable yearly cycles – the effect of annual forcing on a stable equilibrium. Above the Neimark-Sacker bifurcation quasi-periodicity exists, caused by the annual forcing on the stable limit cycles. There are also regions of periodicity due to the resonance between the annual forcing and limit cycles with integer period, leading to the fold bifurcation curves. These curves originate from the $\epsilon = 0$ axis and diverge as ϵ increases with periodic behaviour possible within the fold boundaries. Note, however, that the curves indicate the existence of multi-year cycles but not their stability, which we will

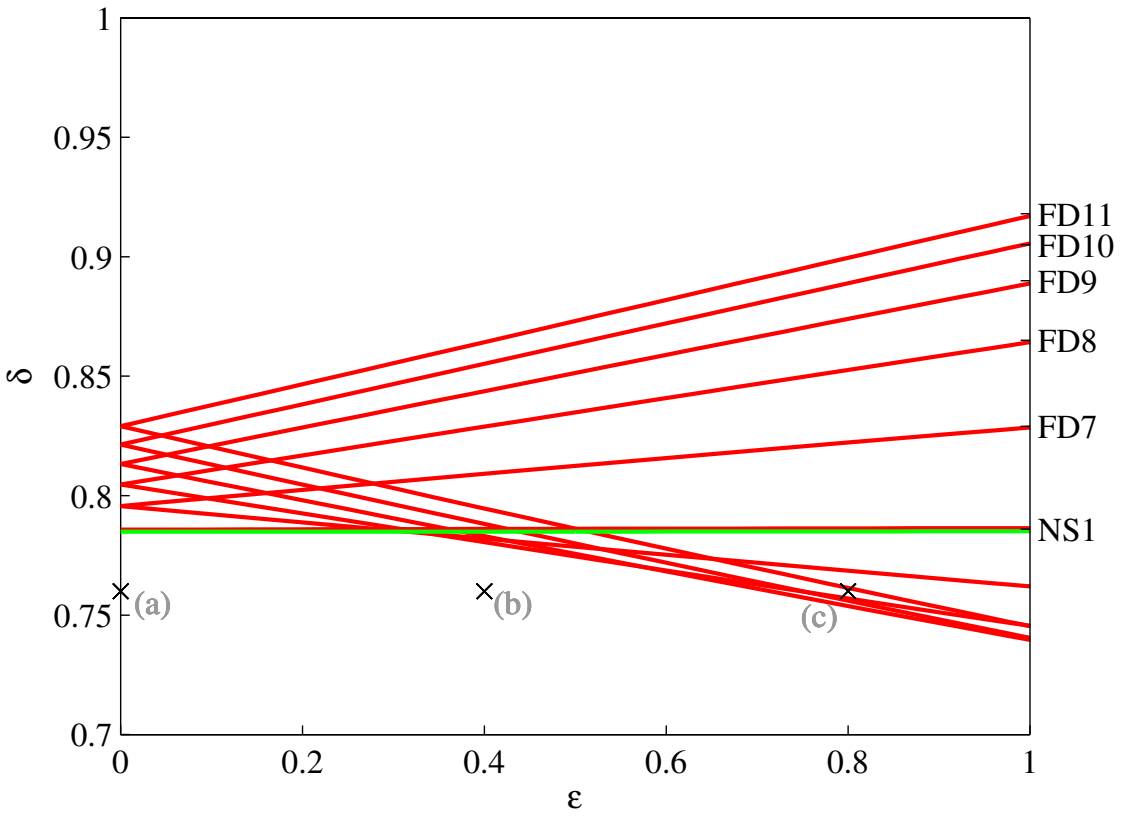

Figure 4.2: A two-dimensional bifurcation diagram in δ and ϵ. The Neimark-Sacker bifurcation curve is green, the fold curves are red. The FD6 curve lies almost on top of the NS1 curve. More fold curves exist with period higher than 11 but these are omitted to avoid over-complication. There is no period-doubling bifurcation of the annual cycles. Only existence and not stability of the multi-year solutions is shown, outlined by the fold curves. The points labelled (a), (b) and (c) refer to the corresponding simulations in Figure 4.3. All other parameters values are kept constant with the following values: $a = 1.7$, $\beta = \gamma = 10/1.05$, $\mu = 1.0003/1.05$ and $k = 1$.

discuss later. The fold curves start at period 6 (FD6) which is the first integer greater than the lowest possible period in the unforced system (which is 5.9). The fold regions get larger as the period increases from period 6 to period 11 (FD6 is very narrow and FD11 is significantly wider). The fold regions decrease in size for periods greater than period 11 (not shown in Figure 4.2 but see Figure 4.6). No period-doubling of the yearly cycle occurs thus we do not find solutions with periods between $2 - 5$ years inclusive.

The fold curves hit the axis at the value of δ at which the unforced limit cycles have the corresponding period, and the regions widen as ϵ increases from 0. The rapid increase of the unforced period with δ, as seen in Figure 4.1, leads to an overlap of the fold curves and indicates that there is potential for multiple solution behaviour. Moreover, some of the fold curves extend below the Neimark-Sacker bifurcation curve for larger values of ϵ. Thus, increasing the amplitude of seasonal forcing from 0 to 1

can change the system from a stable equilibrium to a yearly cycle to multi-year cycles, with no change in any other parameter (Figure 4.3). The multi-year cycles also have a significant increase in amplitude in comparison to the yearly cycle. Therefore, the inclusion of seasonal forcing can have a dramatic effect on the dynamics of the host and parasite for parameters corresponding to the red grouse system.

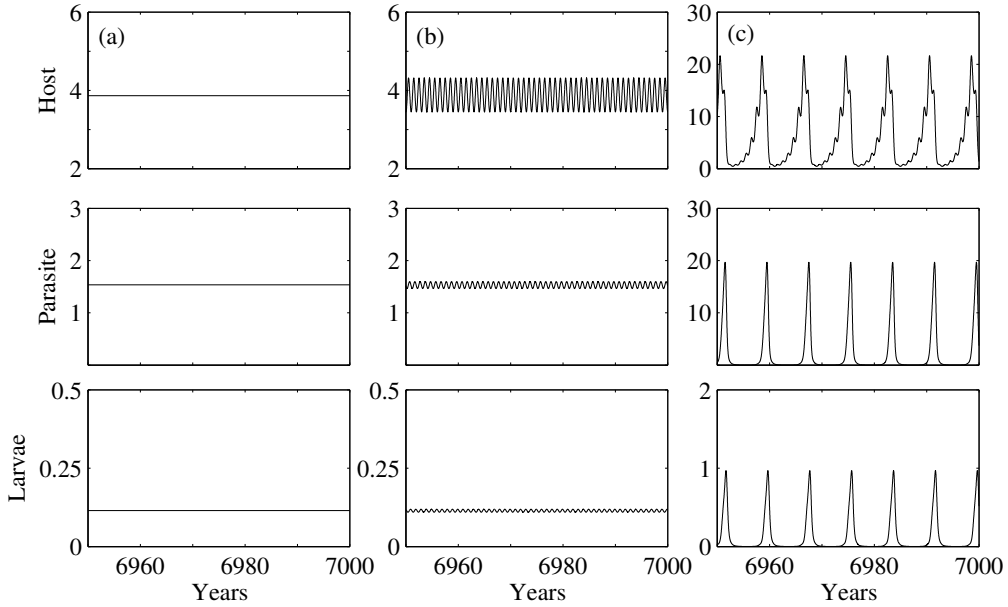

Figure 4.3: Simulations showing the effect of increasing the amplitude of forcing while all other parameters are kept constant. (a) $\epsilon = 0$; a stable equilibrium. (b) $\epsilon = 0.4$; a stable yearly cycle. (c) $\epsilon = 0.8$; a stable 8 year cycle (corresponding to the points labelled in Figure 4.2). The initial conditions are the same for all three simulations. $\delta = 0.76$ and all other details are as in Figure 4.2.

4.3.2 General Host-Macroparasite Dynamics

We wish to investigate further the effect of the unforced dynamics on the resulting multi-year cycles when forcing is introduced into the system. When the red grouse parameters are used, the model does not exhibit any multi-year cycles with period less than 6 (and the 6 year cycles occur only for a very narrow range of δ-values). In comparison, interacting population and epidemiological systems frequently exhibit cycles with periods of $3 - 4$ years (Korpimaki and Krebs, 1996; Earn et al., 2000). Are these higher period cycles observed purely because of the parameter values that are relevant for red grouse dynamics, or are they representative of our general host-macroparasite system?

To answer this question we consider the unforced dynamics in more detail and investigate the period at the Hopf bifurcation. As mentioned previously, the forcing only resonates with integer periods expressed in the unforced limit cycles. Thus, we investigated whether it is possible to reduce the initial period arising at the Hopf bifurcation so that the system will be able to resonate with lower period limit cycles. We varied the parameters in pairs, in order to stay on the Hopf bifurcation, and calculated the initial period at the Hopf bifurcation. We found that the host birth rate parameter a was the key driver of the period in the unforced system (regardless of the other parameter that was varied concurrently). See Appendix F for plots of all the parameter pair combinations.

In Figure 4.4, we show how changing a affects the period at the Hopf bifurcation, and the corresponding changes in δ that are required in order to stay on the Hopf bifurcation. For $a < 1$ only the trivial steady state exists (where the host and parasite are absent). As a increases from 1 the period at the Hopf bifurcation decreases with a minimum period of 2.3 years for $a = 5.9$. As a increases further the period increases and there is a rapid increase in period for $a > 8$ as δ approaches 1. For $\delta > 1$, there are diverging cycles that drive the host and parasite to extinction (Dobson and Hudson, 1992). For larger a the parasites are unable to regulate the host population

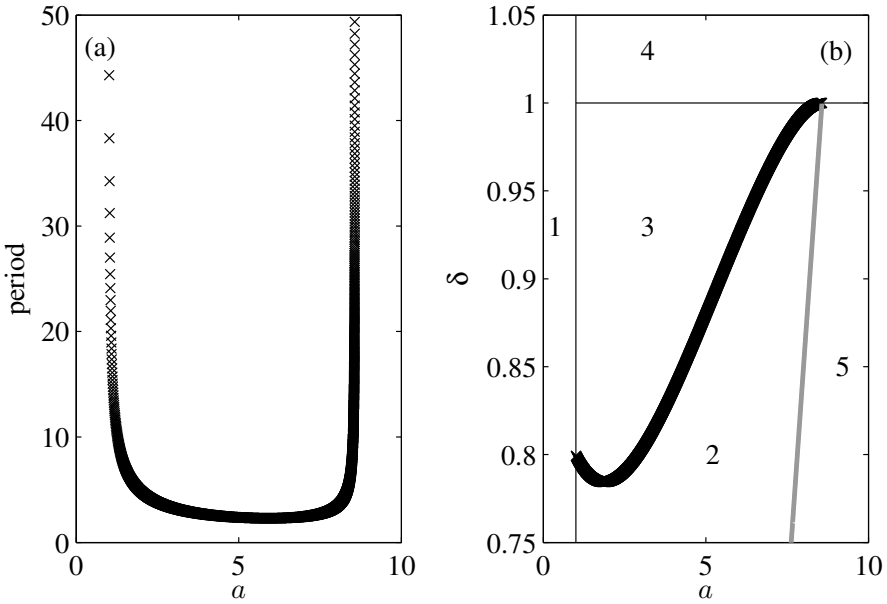

Figure 4.4: The Hopf bifurcation in the unforced system in more detail. In (a) the period at the Hopf bifurcation of the unforced system is plotted as a (and implicitly also δ) is varied. (b) The bifurcation diagram of the unforced system in a and δ. The thick black line is the Hopf bifurcation while the thick grey line indicates where the equilibrium is replaced by exponential growth. Dynamics by region: 1 - trivial equilibrium; 2 - stable equilibrium; 3 - stable limit cycles; 4 - diverging cycles driving host and parasite to extinction; 5 - exponential growth. All other details are as in Figure 4.1.

and since there is no host self-regulation in (4.1), the steady state increases in value. The host and parasite populations experience exponential growth for parameter values in region 5 in Figure 4.4. The limit cycles are bounded by a homoclinic curve, the Hopf bifurcation curve and a fold bifurcation curve (due to subcriticality of the Hopf bifurcation). In Figure 4.5 we plot as much of these boundary curves as possible but experienced problems in AUTO hence the curves are incomplete. We intuitively believe the homoclinic curve stretches to connect the two ends of the Hopf bifurcation.

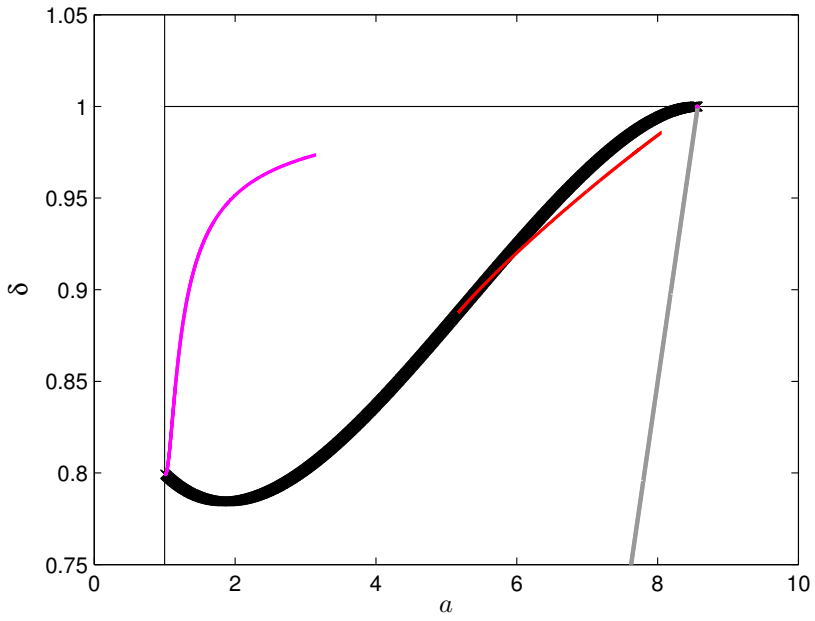

Figure 4.5: The bifurcation diagram of the unforced system in a and δ exploring the limit cycles in more detail. The thick black line is the Hopf bifurcation while the thick grey line indicates where the equilibrium is replaced by exponential growth. The homoclinic curve is purple; the red curve indicates a fold in the limit cycles. All other details are as in Figure 4.4.

Importantly, Figure 4.4 shows that there is potential for lower period cycles in this model system. To understand how seasonal forcing interacts with the underlying period of the unforced system, we produce bifurcation diagrams in δ and ϵ for different values of a (Figure 4.6).

In Figure 4.6 the fold regions (red lines) for the different periods are plotted separately for each value of a. For lower values of a there are empty plots in the upper region of Figure 4.6 since here the cycle period is less than the initial period of the unforced dynamics (Figure 4.4). The fold regions are small if the period is close to the initial period. For example, suppose that the initial period at the Hopf bifurcation is either 5.2 or 5.9. The lowest possible period for multi-year cycles will

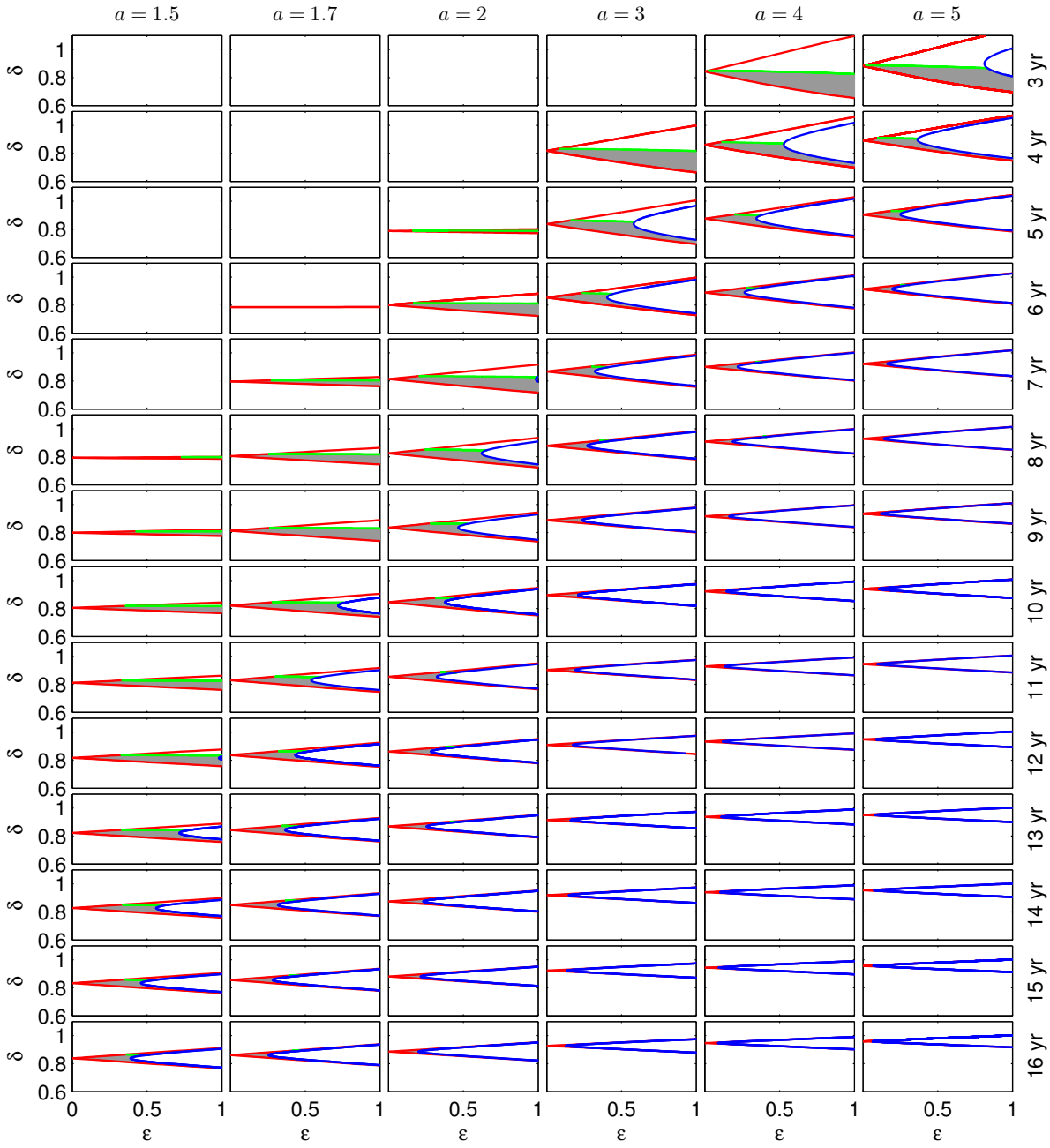

Figure 4.6: Bifurcation diagrams in δ and ϵ for different values of a. Each fold curve, outlining the different periodic regions, is plotted on a separate graph. The shaded regions indicate where each of the multi-year cycles are stable. Fold curves are red, period-doubling curves are blue and Neimark-Sacker bifurcation curves are green. Only those curves relevant to each particular multi-year cycle are plotted within each figure. For each value of a there is also a Neimark-Sacker bifurcation curve (NS1) indicating loss of stability of the yearly cycles but these aren't included. The 15 and 16 year fold curves for $a = 5$ stop before $\epsilon = 1$ due to continuation problems in AUTO (although not shown due to overlap of the period-doubling curves). All other details as in Figure 4.2.

be 6 year in both cases, but the 6 year fold region will be much smaller for the latter case. The fold regions start to decrease in size once the period is much larger than the initial period expressed in the unforced system. In general, there is a pattern of the largest fold regions occurring across a diagonal from top-right to bottom-left in Figure 4.6.

There is a significant difference between existence and stability of multi-year cycles in terms of the resulting dynamics of the system, and thus it is important to consider the region of stability of the multi-year cycles within each of the fold curves (i.e. the shaded regions in Figure 4.6). The presence of Neimark-Sacker bifurcation curves and period-doubling curves inside the fold curves leads to loss of stability of the multi-year cycles. For example, if we focus on the 3 year fold region for $a = 5$ (i.e. the top right plot in Figure 4.6), the 3 year cycles are stable in the shaded region, but crossing the Neimark-Sacker bifurcation curve for larger δ results in quasi-periodicity while crossing the period-doubling curve through increasing ϵ produces stable 6 year cycles. The size of the regions of stability follows a similar pattern to the fold regions: it decreases as the period increases for each value of a, mostly due to the period-doubling region inside the fold curves increasing in size. Notably, many of the fold curves contain only very small regions of stability, especially for the higher period cycles.

To investigate the potential for multiple solutions we superimpose the stable regions of the different multi-year solutions in Figure 4.6 for each value of a (Figure 4.7). The yearly Neimark-Sacker bifurcation curve (NS1) is shown but the fold, period-doubling and Neimark-Sacker curves for each of the multi-year cycles are omitted for clarity. There is considerable overlap of different stable multi-year regions implying that multiple solutions are possible for a fixed set of parameters. Figure 4.7 highlights the large effect that varying a has on the stability of multi-year cycles. This is further emphasised by noting that the stability regions shown in Figure 4.7(a) predominantly correspond to $10 - 14$ year cycles whereas those in (f) have periods of $3 - 5$ years, as seen in Figure 4.6.

To examine the likelihood of multiple solutions we ran simulations of our model system for four different parameter sets (indicated by the crosses in Figure 4.7) for 200 sets of initial conditions selected at random. Figure 4.8 indicates that multiple solution behaviour was observed. Both of the points which lie above the Neimark-Sacker bifurcation curves in Figure 4.7 (Figure 4.8(a),(c)) exhibit quasi-periodic dynamics while the two points below the curves (Figure 4.8(b),(d)) show yearly cycles as well as the multi-year cycles. Figure 4.8 also shows typical host population solutions for the four parameter sets, indicating that a range of annual, multi-year and quasi-periodic behaviour can be exhibited. A wide range of amplitude is seen across the 12 simulations. This varies with cycle period, and with the values of ϵ, δ and a. For the

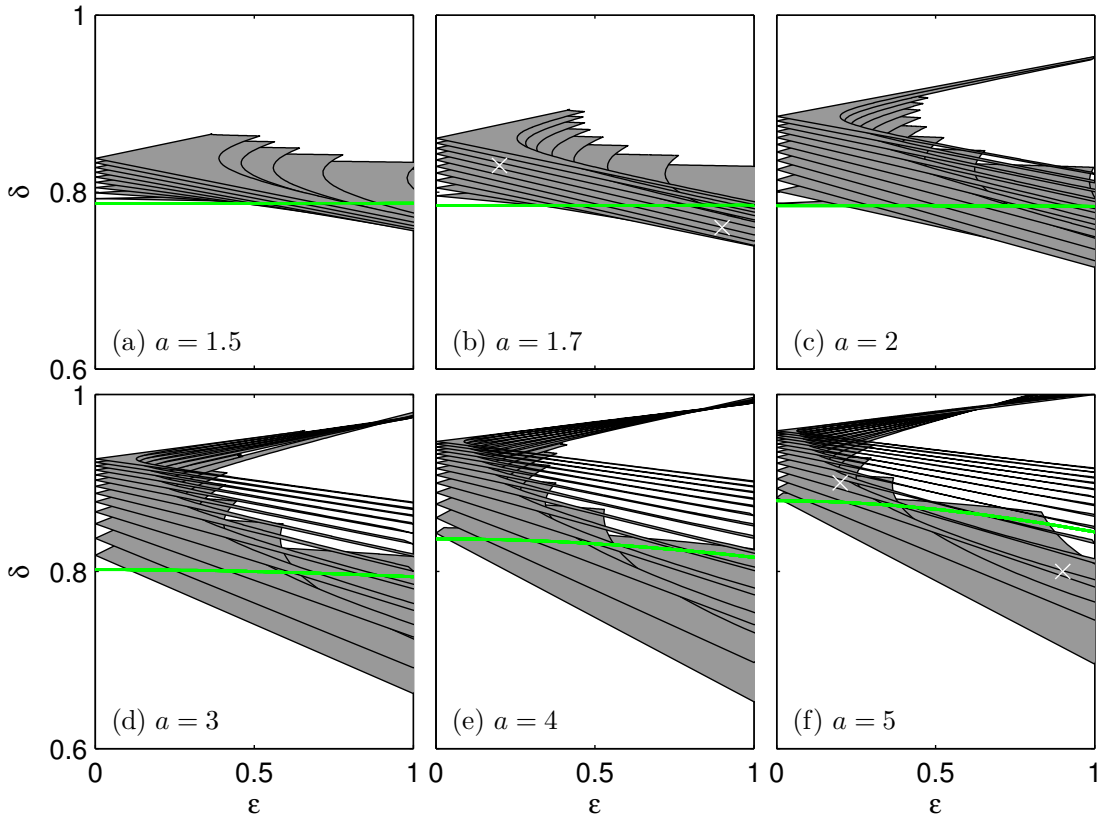

Figure 4.7: Two-dimensional bifurcation diagrams in δ and ϵ for each value of a showing only the stability regions (shaded) of the multi-year solutions. The Neimark-Sacker bifurcation curves (green) indicate the change in stability of the yearly cycle, with yearly cycles stable below the line. The four crosses in (b) and (f) indicate the points that we used for testing multiple solution behaviour, as shown in Figure 4.8. All other details are the same as in Figure 4.2.

case $a = 5$, it would be expected that there would mainly be low period cycles due to their larger regions of stability but there are some 16 year cycles. These 16 year cycles have peaks every 4 years, which suggests that they have arisen due to period-doubling (we examine this below). In comparison, a 16 year cycle that has arisen through the 16 year fold curve would usually have only one peak in the 16 year period.

In this more general framework of the host-macroparasite model we have shown that changing a has an important impact on the periodic solutions possible, with a greater likelihood of lower period multi-year cycles for higher values of a. The overlap of stable regions for these multi-year cycles has been highlighted, and we have confirmed that multiple solution behaviour is possible, involving a wide range of cycle periods and amplitudes. We now move on to some of the more complicated aspects of these bifurcation diagrams for different values of a, such as the period-doubling bifurcations in Figure 4.6 and the overall effect of increasing the forcing amplitude ϵ.

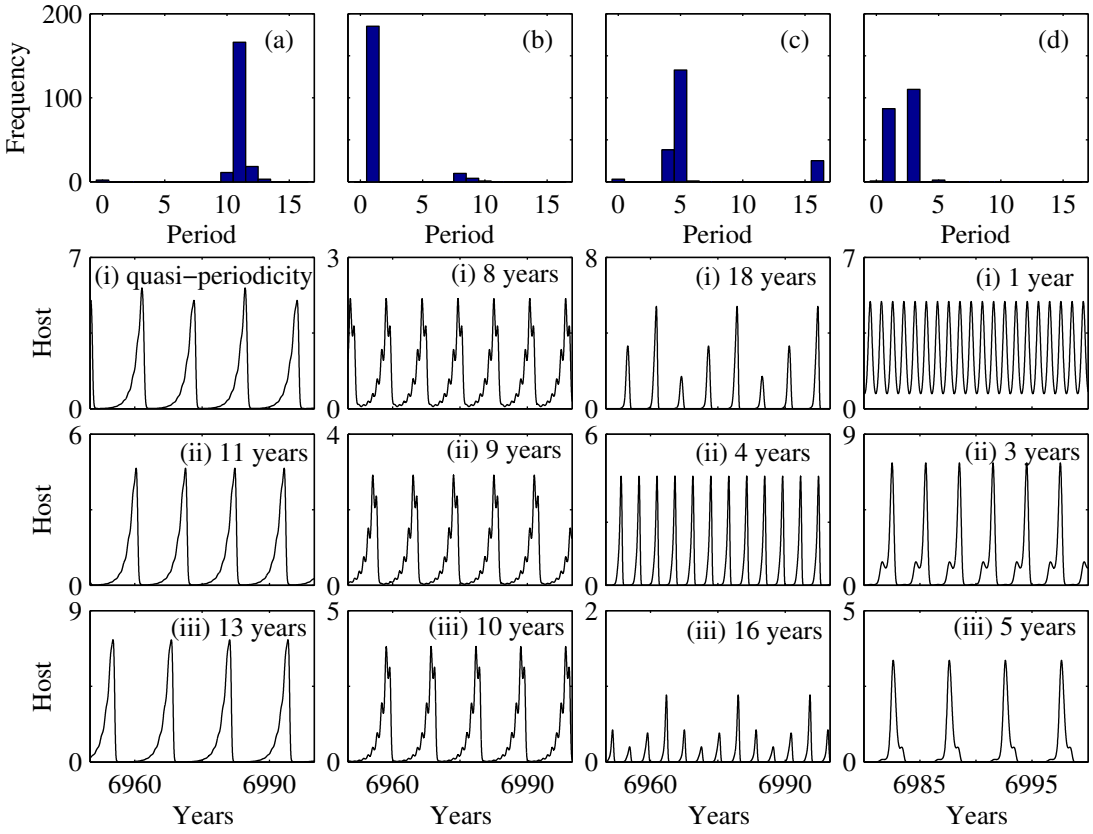

Figure 4.8: Investigating the potential for multiple solution behaviour. In $(a) - (d)$ histograms show the results of 200 simulations for 4 different points (indicated on Figure 4.7). (a) $a = 1.7$, $\epsilon = 0.2$ and $\delta = 0.83$; (b) $a = 1.7$, $\epsilon = 0.9$ and $\delta = 0.76$; (c) $a = 5$, $\epsilon = 0.2$ and $\delta = 0.9$; and (d) $a = 5$, $\epsilon = 0.9$ and $\delta = 0.8$. Quasi-periodicity is represented by period 0 years. Three simulations of host populations are plotted for each histogram (in the same column), showing that different multi-year cycles are possible for that point. The period of the multi-year cycles are as indicated. In (c)(i) the solution was calculated to be quasi-periodic but is actually an 18 year cycle (since we only test the simulations for periodicity of 16 years or lower). The simulations are not to scale; specifically (c)(i) $\times 10^5$, (c)(ii) $\times 10^3$, (c)(iii) $\times 10^4$, (d)(ii) $\times 10^2$, (d)(iii) $\times 10^4$ and the rest of the simulations are all $\times 10$. All other details are the same as in Figure 4.2.

4.3.3 Period-Doubling and Chaos

One aspect of Figure 4.6 which requires further attention is period-doubling inside the fold loci. Nearly all of the fold regions in Figure 4.6 contain period-doubling curves which indicate not only the loss of stability of the cycles generated at the folds but also the generation of stable higher period cycles. Trying to show all this information on one plot, such as Figure 4.6, is rather complicated and thus we highlight one case (the 4 year cycles for $a = 4$) to show the full range of dynamics that can occur due to period-doubling (Figure 4.9).

In Figure 4.9 there are three fold regions plotted, the largest being the 4 year fold region (FD4) in which the 4 year cycles lose stability as ϵ increases through a period-

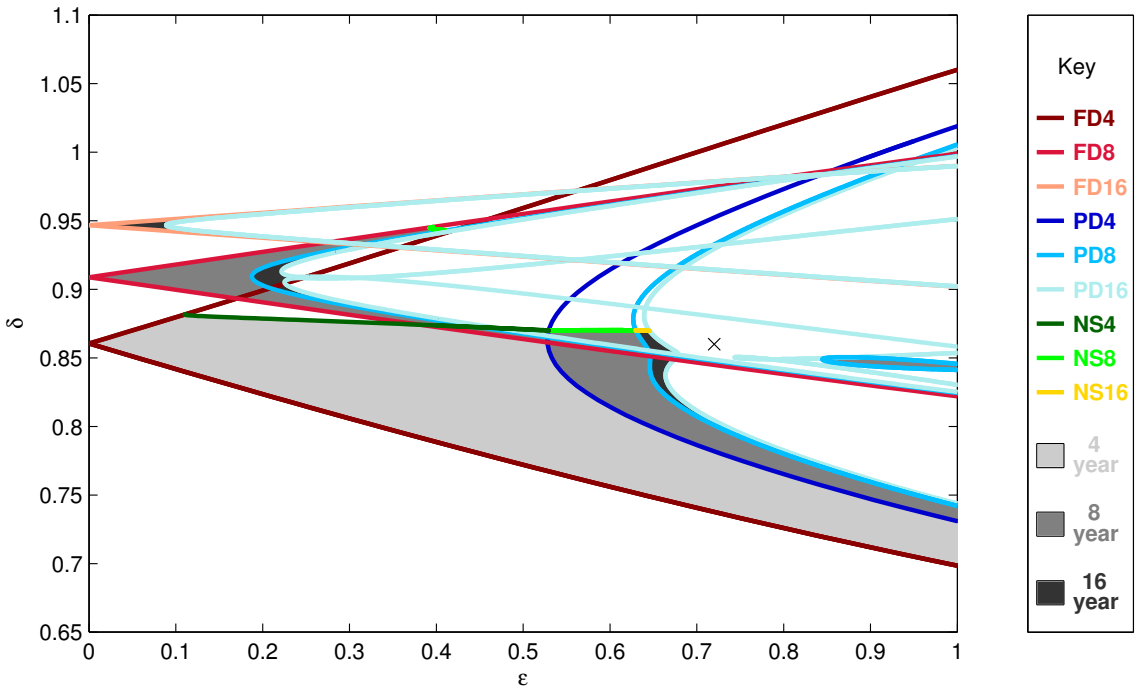

Figure 4.9: A bifurcation diagram in δ and ϵ showing only the 4, 8 and 16 year fold regions with their subsequent period-doubling bifurcations for the case $a = 4$. Both type and period of each curve is represented by the different colours. Stability of the different periodic solutions is shown by the shaded regions as indicated. The cross at $\epsilon = 0.72$, $\delta = 0.86$ corresponds to the simulation in Figure 4.11. All other details are as in Figure 4.2.

doubling bifurcation (PD4) leading to stable 8 year cycles. These 8 year cycles also undergo period-doubling (PD8) leading to stable 16 year cycles. Also shown is the 8 year fold region (FD8), in which the 8 year cycles lose stability through a period-doubling bifurcation (PD8) leading to stable 16 year cycles. And lastly, there is the 16 year fold region (FD16) which also indicates a region of stable 16 year cycles. All 3 of these stable 16 year regions lose stability through more period-doubling bifurcations (PD16). Moreover, period-halving occurs for large ϵ in the 4 year fold region, leading to more regions of stable 8 and 16 year cycles (although the additional 16 year stable region is very small and not visible at this scale). This highlights that there are several routes that can lead to 16 year population cycles. It is interesting to note that the region of stability for the 16 year cycles resulting from two successive period-doublings of the 4 year cycles is larger than that for the 16 year fold curve, so that these period-doubling bifurcations are of key importance in providing information on the stable dynamics of the system. Also, the form of the period 16 cycles resulting from period-doubling and from the 16 year fold curve are very different, with only one peak every 16 years for the fold curve compared to a peak every 4 years for the period-doubled solution (Figure 4.10). There is also a significant difference in amplitude, which is

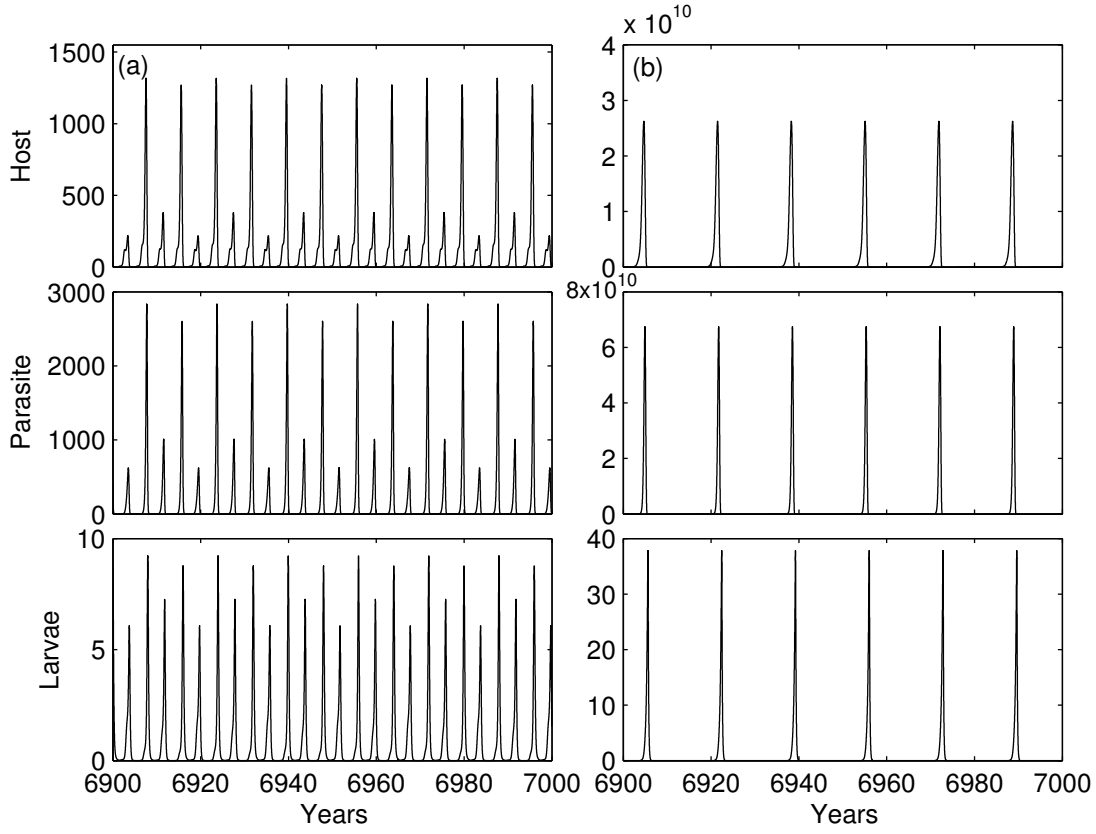

Figure 4.10: Simulations of two different 16 year solutions. (a) A 16 year cycle stable from two successive period-doublings of the 4 year cycle. Parameter values are $a = 4$, $\delta = 0.85$ and $\epsilon = 0.67$. (b) A 16 year cycle stable within the 16 year fold. Parameter values are $a = 4$, $\delta = 0.9404$ and $\epsilon = 0.15$. All other details as in Figure 4.2.

much larger for the fold curve solution.

Figure 4.9 raises the possibility of chaos in this system through a period-doubling cascade. Within the 4 year fold curve there is a region after the 16 year cycles have lost stability before the period-halving begins, in which there is the suggestion of period-doubling to chaos. Simulation results have shown solutions which appear chaotic (Figure 4.11), although we have not tested this in detail.

Figure 4.9 is useful for exhibiting the complexities of the host-macroparasite model with seasonal forcing, especially when it is remembered that there are many other multi-year fold curves omitted from this figure, all with period-doubling regions which might lead to chaos. One common factor of all the multi-year cycles, as seen in Figures 4.6, 4.7 and 4.9 is that they lose stability as ϵ increases. Thus, an increase in seasonal forcing, with no changes in any other parameters, can change the dynamics dramatically from multi-year limit cycles, to multi-year cycles of potentially different period due to the multiple solution behaviour and period-doubling, to quasi-periodicity and chaos. This again highlights the substantial impact of increasing the strength of the seasonal forcing on the dynamics. Overall, the host-macroparasite model when subject to seasonal forcing is a complicated system with a wide range

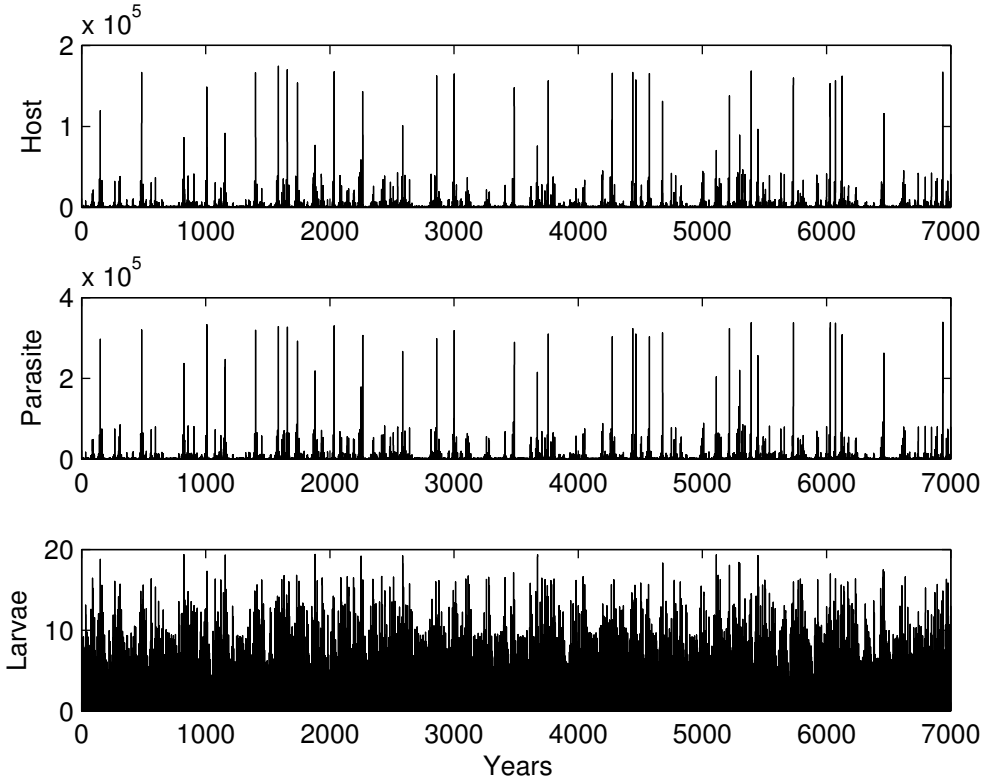

Figure 4.11: A simulation of an apparently chaotic solution. The fast Fourier transform method indicates a period of 70 years. Parameter values are $a = 4$, $\delta = 0.86$ and $\epsilon = 0.72$, indicated by a cross in Figure 4.9. All other details as in Figure 4.2.

of possible dynamics depending on parameter values, the amplitude of the seasonal forcing and the initial conditions.

4.3.4 Results Summary

We have considered a general host-macroparasite model with reduced fecundity and explicit inclusion of a larval stage and explored the effects of introducing seasonal forcing through the host birth rate. When seasonal forcing is introduced into this host-macroparasite model it leads to stability of multi-year cycles, multiple stable solutions, period-doubling to higher period cycles, quasi-periodicity and apparently chaotic behaviour. We studied this for different values of the host birth rate, parameter a in (4.1), as this leads to changes in the initial period of the unforced system at the Hopf bifurcation. For all values of a the unforced period increases rapidly from the initial period at the Hopf bifurcation, and this results in the different period fold curves on the $\epsilon = 0$ axis lying very close together (as seen in Figure 4.6). This leads to an overlap of fold curves of many different periods and to multiple solution behaviour possible, as shown for two values of a in Figure 4.8. Furthermore, in all cases the effect of increasing ϵ (the strength of the seasonal forcing) is substantial when the

parameter choice gives rise to both a stable equilibrium and stable limit cycles in the unforced system.

Whilst there are many similarities in the bifurcation diagrams for the different values of a, variation in the initial period of the unforced system has important consequences for the different dynamics possible in the forced system, specifically the range of stable periodic solutions. Lower period cycles are only possible when a is larger. Apart from this difference in period, the bifurcation diagrams change more generally, as seen in Figure 4.7, where the Neimark-Sacker bifurcation curve for the yearly cycles (NS1) moves up in δ as a increases. In the $a = 5$ case, the Neimark-Sacker curve also becomes less straight so that it is possible to move from a stable equilibrium to quasi-periodicity and chaos by increasing ϵ and keeping all other parameters constant. The fold regions are also much wider for $a = 5$ indicating that seasonal forcing has an effect for a wider range of δ values in this case. From Figures 4.6 and 4.7, it is clear that there is a considerable difference in the dynamics between low values of a, say $a = 1.5$ or 1.7 which are in the range given for the red grouse system, compared to $a = 5$, with the inference that seasonal forcing has more of an impact for higher values of a.

The largest fold and stability regions for $a = 4$ and $a = 5$ are much larger than those for lower values of a (as seen in Figure 4.6). This raises an interesting question: is this occurring because lower period cycles resonate more, creating more stability for the multi-year cycles of lower period, in comparison to those of higher period? This could be because the 3 and 4 year cycles are closer in period to the forcing (1 year). Or are the regions larger because the initial amplitude of the limit cycles in the unforced system is higher, causing more resonance when forcing is introduced? Or is it the fact that a is now much larger: since a is the parameter being annually forced this could lead to greater resonance and hence larger fold regions? One approach to gain some insight into this would be to produce a similar figure to Figure 4.6 with the same range of a values, but with a different parameter being seasonally forced. This is a natural area for future study.

4.4 Discussion

Seasonal forcing has been well studied in both interacting population and microparasite systems (Rinaldi et al., 1993; Kuznetsov and Piccardi, 1994; Greenman et al., 2004; Choisy et al., 2006). As in this host-macroparasite study, these have all shown that seasonal forcing can lead to multi-year cycles, quasi-periodicity, chaos and multiple solution behaviour. Other similarities include the increased amplitude in population abundance of the multi-year cycle solutions compared to the yearly cycle and the significant impact on the dynamics observed through increasing the amplitude of

forcing. The similarities are particularly true for systems in which there is a Hopf bifurcation present in the unforced dynamics, since this is the determining factor for the existence of quasi-periodicity and is influential in the production of the fold curves (although these can occur when non-cyclic systems are forced (Kuznetsov and Piccardi, 1994; Taylor et al., 2013a)).

However, seasonal forcing within this host-macroparasite system shows some important differences to ecological and microparasite systems. One of the most noticeable aspects of this host-macroparasite system is the existence of a wide range of different period solutions, with sizable regions of stability for 3 to 16 year cycles as well as an 18 year cycle found by simulation and the numerous period-doubling bifurcations to higher period cycles. This indicates that host-macroparasite interactions, including the red grouse system, are able to experience many different periodic solutions. In contrast, data for predator-prey systems often show a smaller range of cycles such as $3-5$ years for Fennoscandian voles (Bjørnstad et al., 1995) or $8-11$ years for the snowshoe hare and lynx cycles (Murray, 2000). Also, in the measles literature, cycles of $1-3$ years are most common, although there is the possibility of cycles with periods of up to 8 years (Earn et al., 2000). In the host-macroparasite system the wide range of cyclic dynamics occurs due to the rapid increase of the limit cycle period from the Hopf bifurcation in the unforced system.[1] Thus the bifurcation diagram shows that the fold curves overlap to a much greater extent than is typical for interacting population and microparasite systems (Rinaldi et al., 1993; Kuznetsov and Piccardi, 1994). Not only does this rapid increase in the unforced period lead to the wide range of different period cycles but most importantly, it leads to an increased chance of multiple solution behaviour. While multiple solutions do occur in interacting population and microparasite systems, it is often for a small number of parameter sets and is usually restricted to 2 or 3 different solution possibilities (Earn et al., 2000; Taylor et al., 2013b). In contrast, Figure 4.7 shows that multiple solution behaviour is possible for a wide range of δ and ϵ values for all values of a tested, and in Figure 4.8 the points tested have at least 5 different solutions possible. Furthermore, the wide range of periodic dynamics and the multiple solution behaviour combine so that both higher and lower period cycles can be found in the resulting dynamics for the same parameter values. For example, in Figure 4.8(c) both 4 and 18 year cycles occur in simulations for the same parameter values but different initial conditions.

There are other aspects of the bifurcation diagrams shown here for host-macroparasite systems which differ from seasonal models of interacting population and microparasite systems. Our results indicate several regions of (apparently) chaotic behaviour, due to the many period-doubling bifurcation curves which can give rise

[1]Comparison of rapidity of the increase is based upon observing the relative width of the fold curves in comparison to the distance between the cusp of each fold curve on the axis.

to period-doubling cascades (Aron and Schwartz, 1984). This multitude of period-doubling cascades is not readily observed in other seasonal systems (Rinaldi et al., 1993; O'Regan et al., 2013). Our study also shows that period-halving can occur, which has not been reported in previous studies of seasonally forced models. This highlights the importance of the period-doubling bifurcations on the resultant population dynamics.

The overlap of stable multi-year regions and the abundance of multiple solution behaviour indicate that the system may be sensitive to small perturbations in parameters or to noise. Small perturbations in the strength of the seasonal forcing or other parameters can lead to significantly different dynamics through a change of period and amplitude, or to quasi-periodic or chaotic solutions. This is in contrast to the unforced model, where a small change in parameter values would lead to a relatively small change in the period of the limit cycles (unless the parameters are very close to the Hopf bifurcation, in which case switches between a stable equilibrium and limit cycles could occur). In Figure 4.12, a simulation shows the effect of a perturbation in the host population abundance (but no change of any parameters), which leads to a change in cycle period and amplitude. A similar perturbation in the corresponding unforced case would always settle back to the stable equilibrium as there are no multiple solutions. This sensitivity to perturbations leads to difficulties in determining the factors that are the key drivers of population cycles and in explaining the causes of shifts in population behaviour. Furthermore, since multiple solutions can exist for a single parameter set it is not possible at the outset to predict the resulting population dynamics.

The literature on red grouse documents a very wide range of periods of population cycles in England and Scotland, with reported periods varying between $4-8$ years (Hudson et al., 1998), $3-13$ years (Cattadori et al., 2005b) or $2-15$ years (Haydon et al., 2002). The driver of red grouse cycles is subject to debate, with infection from the nematode macroparasites and territorial behaviour seen as the most likely causative factors (Dobson and Hudson, 1992; Hudson et al., 1998; Redpath et al., 2006). It has also been shown that there is no strong latitudinal variation in periodicity but rather a plethora of intermixing periods across the whole of England and Scotland (Haydon et al., 2002). Both these aspects are consistent with our results. With parameter values corresponding to red grouse populations across England and Scotland, the host-macroparasite model showed a wide range of periodic cycles and multiple solution behaviour was found (Figures 4.6, 4.8). In the model it is possible for two geographically close populations of red grouse to have very similar life-history parameters and yet show exceedingly different dynamics such as low period and high period cycles with different amplitudes. Furthermore, the sensitivity to perturbations may explain the difficulty in determining cyclicity and the presence of only weakly

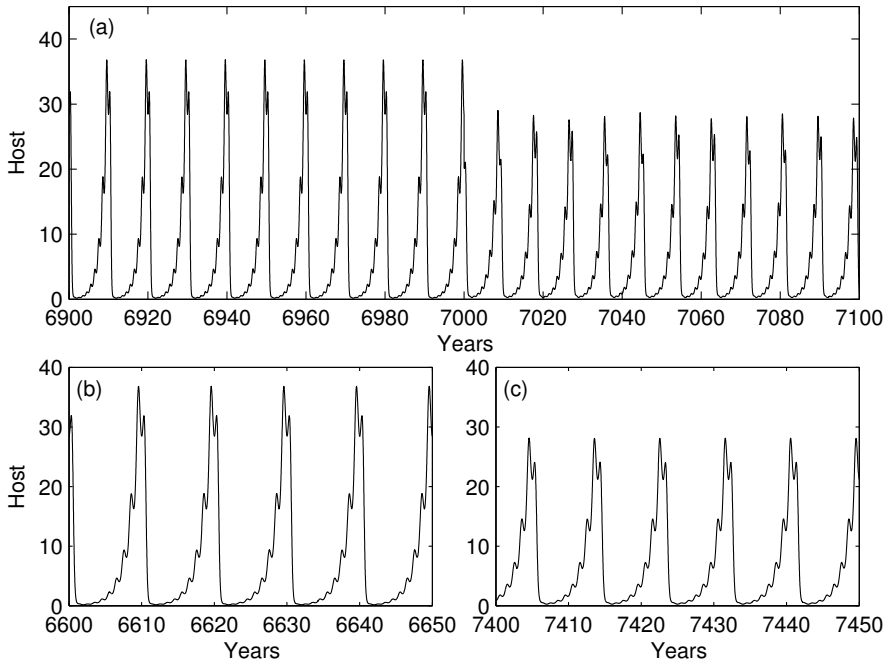

Figure 4.12: A simulation showing the effect of perturbations. A 10 year cycle is perturbed at 7000 years by changing the host population by 10%. It switches to a 9 year cycle. The transition in shown in (a) and the 10 and 9 year cycles are shown in more detail in (b) and (c) respectively for the host population. Parameter values are $a = 1.7$, $\delta = 0.77$, $\epsilon = 0.8$ and all other details are as in Figure 4.2.

cyclic time-series data (Haydon et al., 2002). This suggests that seasonal forcing may be an important factor in producing the wide range of cyclic periods observed in red grouse population dynamics and can have a significant impact on the dynamics of host-macroparasite system in general.

Chapter 5

Discussion

This thesis has studied the influence of seasonal forcing on the population dynamics of different ecological systems, with a specific focus on predator-prey and host-macroparasite interactions. In this discussion we highlight the overarching conclusions which can be drawn from all three sections of work. We remind the reader that more detailed discussions about each individual topic are included within Chapters 2 - 4.

5.1 Conclusions

A major aim of this thesis has been to understand in detail the influence of the unforced dynamics when forcing is applied to the system. To do this, we considered the effect of seasonal forcing when there was oscillatory decay to the coexistence steady state, monotonic decay and limit cycles in the unforced system in Chapter 2. This allowed comparisons to be made between each regime. The resultant dynamics are heavily dependent on the unforced dynamics, with no multi-year cycles present for the monotonic decay case; some multi-year cycles but no quasi-periodic dynamics for the oscillatory decay case; and a broad range of possible dynamics for the limit cycle case, with quasi-periodicity, multi-year cycles with a wide range of periods and chaos. The strength of the oscillations in the unforced system determines the amount of resonance that occurs between these oscillations and the forcing period, and leads to significant differences in the dynamics that are exhibited. A key focus of previous studies of seasonal forcing has been the impact of seasonality in microparasite models. These models do not exhibit limit cycles in the unforced dynamics but our work highlights the importance of studying the effect of seasonal forcing in systems which are inherently cyclic.

In Chapter 4, we considered the effect of changing the unforced dynamics by decreasing the period of limit cycles and asked whether this significantly alters the forced dynamics. Only multi-year cycles exist which have periods expressed in the

unforced limit cycles. Thus, as the initial period of the limit cycles is decreased, lower multi-year cycle periods can be induced by seasonal forcing. However, other changes in the bifurcation diagrams can be observed as the period of the limit cycles is reduced. In Figure 4.7, the width of the Arnol'd tongues changes such that the largest tongues occur when the period of the limit cycles is lowest. Also, it was only possible to move from a stable equilibrium to quasi-periodicity as forcing was increased when the initial period of the limit cycles was lower. However, it is unclear whether these are caused by the lower period or the change in parameter values required to decrease the period of the limit cycles. It would be interesting to investigate this in more detail. However, in general, the effect of the seasonal forcing was more pronounced when the limit cycle period was lower.

An additional aspect of the unforced dynamics which impacts on the system when seasonal forcing is applied is the rapidity of the increase in period of the limit cycles. This discovery is facilitated by contrasting the bifurcation diagrams of the predator-prey systems (in Chapter 2 and Appendix C) and the host-macroparasite system (in Chapter 4). Due to the rapid increase in period in the host-macroparasite system compared to the predator-prey system, there is a wider range of periods of multi-year cycles and more overlap of the Arnol'd tongues. This leads to more multiple solution behaviour and an increased likelihood for these multiple solutions to have very different periods. In Gragnani and Rinaldi (1995), the chemostat and the Rosenzweig-MacArthur models produce topologically equivalent bifurcation diagrams. But this is clearly not the case for the predator-prey and host-macroparasite models, even though they have similar unforced dynamics, and when forced the range of dynamics for both includes multi-year cycles, quasi-periodicity and chaos as well as the potential for multiple solution behaviour. The configuration of the unforced dynamics has an important role in determining the bifurcation structure of the forced system.

Therefore, we have shown three ways in which the unforced dynamics can impact on the seasonally forced dynamics – through the presence/absence of limit cycles, the initial period of these limit cycles and the rapidity of the increase in period of these limit cycles.

A further idea which we wished to explore is that of a "universal" bifurcation diagram, in which all the bifurcation diagrams of a model are topologically equivalent regardless of which parameter is forced. In Rinaldi et al. (1993), six different combinations of parameters (either a single parameter or a pair) were forced in the Rosenzweig-MacArthur predator-prey model and the bifurcation diagrams produced for each of these combinations were topologically equivalent. However, they did not force the prey growth rate on its own, as we do in Chapter 2, but instead forced it alongside the prey carrying capacity. The bifurcation diagram produced in our scenario is not topologically equivalent to those produced by Rinaldi et al. (1993) since

the Neimark-Sacker bifurcation curve does not touch the $\epsilon = 0$ axis (see Figure 2.3). Hence, there are stipulations on this equivalence. In this case, the lack of equivalence arises because the prey growth rate is not involved in the condition for a Hopf bifurcation in the unforced system. However, there could be other factors which would prevent topological equivalence in different models.

In Chapter 3, the seasonal forcing term was adapted to represent changes in breeding season length. We found the trend that decreasing the length of the breeding season led to longer period cycles, when the level of generalist predation was low. This method of representing changes in season length (whether it is a breeding season or otherwise) is vital to the understanding of the effect of seasonal forcing. This is especially true when the aim is to understand the potential effects of climate change, as it can lead to such seasonal adaptations. Furthermore, we broadened the scope of the bifurcation diagrams in this chapter by using the level of generalist predation and the season length as the parameters that were varied rather than the mean value and the amplitude of the forced parameter. The main consideration was no longer how the forced parameter impacted on the system but how a forced system will respond when other aspects of the system are varied. This affected the Arnol'd tongues, with no cusp on the $\epsilon = 0$ axis and a bent-over shape (see Figure C.2). It was also harder to distinguish the influence of the unforced dynamics on the forced system.

5.2 Further Work

In this thesis, we have analysed predator-prey and host-macroparasite systems with seasonality. In general, seasonally forced interacting populations and microparasite systems have been well studied (Altizer et al., 2006; Sherratt and Smith, 2008). We draw attention to the need to consider free-living host-pathogen systems subject to seasonal forcing. In these models, the pathogen kills the host releasing free-living infective stages into the environment (Anderson and May, 1981). These systems have been used to explain the high period population cycles seen in forest insect systems. Therefore, in some respects, these are very similar to host-macroparasite systems and often exhibit high period cycles in which population density can reach low levels following a disease outbreak. By studying the unforced system, specifically the period of the limit cycles, it could be possible to predict whether the forced system will be more similar to the predator-prey or the host-macroparasite systems studied here, based on our comparisons above. The high period cycles would indicate that perhaps the free-living host-pathogen system would be more akin to the host-macroparasite system.

An interesting area involving further study concerns the relative sizes of the basins of attraction. In Greenman et al. (2004), it is suggested that the lowest existing multi-

year cycle (i.e. lowest period higher than annual cycles) will have the largest basin of attraction when there are multiple solutions. However, in Figure 3.3(b), a basin of attraction exists which contains more 9 year cycles than 4 year cycles. Clearly, more work is needed in order to understand which solutions are more likely when multiple solutions exist. A more thorough method for calculating the relative sizes of the basins of attraction is perhaps necessary. As seen in Figure 2.12 and in Earn et al. (2000); Choisy et al. (2006), the basins of attractions can be well intermixed making predictions harder about the likelihood of each solution and the potential for jumping between attractors.

More work is still desirable to understand which parameters to force and which type of forcing function to use. As mentioned above, forcing different parameters of the model can lead to very dissimilar results or to topologically equivalent bifurcation diagrams. Investigation into why this is the case could help in determining which are the important parameters to focus on to gain a full understanding of the system when any parameter is forced. Similarly, the effects of forcing more than one parameter in or out of phase have shown that multi-year cycles and chaos can be dependent on the phase difference (Rinaldi and Muratori, 1993; Greenman and Pasour, 2011). Thus, if it is feasible to alter the timing of one of the forcing terms (for example, if one of the forcing terms is pulse vaccination) then it could be possible to control the amplitude or periodicity of the solutions. However, the effect of this phase difference is still not completely understood. Finally, the use of sinusoidal or step functions to represent the seasonal forcing is debated, with some saying a step function is necessary to produce results consistent with data while others stating that the differences are not significant (Earn et al., 2000; Ireland et al., 2004; Altizer et al., 2006; Keeling and Rohani, 2008). More detailed comparisons are necessary.

In summary we have shown how seasonality can play a critical role in determining the population dynamics. The influence of seasonal forcing is likely to become of increased importance as climate and environmental change is expected to alter the pattern of seasonality, with the potential to dramatically affect the population dynamics of natural systems.

Bibliography

S. Altizer, A. P. Dobson, P. Hosseini, P. J. Hudson, M. Pascual, and P. Rohani. Seasonality and the Dynamics of Infectious Diseases. *Ecology Letters*, 9:467–484, 2006. doi: 10.1111/j.1461-0248.2005.00879.x.

R. C. Anderson. *Nematode Parasites of Vertebrates: Their Development and Transmission*. Cabi Wallingford, UK, 2000.

R. M. Anderson and R. M. May. Regulation and Stability of Host-Parasite Population Interactions: I. Regulatory Processes. *Journal of Animal Ecology*, pages 219–247, 1978. doi: 10.2307/3933.

R. M. Anderson and R. M. May. The Population Dynamics of Microparasites and Their Invertebrate Hosts. *Philosophical Transactions of the Royal Society B: Biological Sciences*, pages 451–524, 1981.

R. M. Anderson and R. M. May. *Infectious Diseases of Humans: Dynamics and Control*. Oxford University Press, Oxford, UK, 1992.

J. L. Aron and I. B. Schwartz. Seasonality and Period-Doubling Bifurcations in an Epidemic Model. *Journal of Theoretical Biology*, 110(4):665–679, 1984. doi: 10.1016/S0022-5193(84)80150-2.

W. Baltensweiler, U. M. Weber, and P. Cherubini. Tracing the Influence of Larch-Bud-Moth Insect Outbreaks and Weather Conditions on Larch Tree-Ring Growth in Engadine (Switzerland). *Oikos*, 117(2):161–172, 2008. doi: 10.1111/j.2007.0030-1299.16117.x.

O. N. Bjørnstad, W. Falck, and N. C. Stenseth. A Geographic Gradient in Small Rodent Density Fluctuations: A Statistical Modelling Approach. *Proceedings of the Royal Society B: Biological Sciences*, 262:127–133, 1995. doi: 10.1098/rspb.1995.0186.

L. Bolzoni, A. P. Dobson, M. Gatto, and G. A. De Leo. Allometric Scaling and Seasonality in the Epidemics of Wildlife Diseases. *The American Naturalist*, 172:818–828, 2008. doi: 10.1086/593000.

I. M. Cattadori, B. Boag, O. N. Bjørnstad, S. J. Cornell, and P. J. Hudson. Peak Shift and Epidemiology in a Seasonal Host–Nematode System. *Proceedings of the Royal Society B: Biological Sciences*, 272(1568):1163–1169, 2005a. doi: 10.1098/rspb.2004.3050.

I. M. Cattadori, D. T. Haydon, and P. J. Hudson. Parasites and Climate Synchronize Red Grouse Populations. *Nature*, 433(7027):737–741, 2005b. doi: 10.1038/nature03276.

D. Z. Childs and M. Boots. The Interaction of Seasonal Forcing and Immunity and the Resonance Dynamics of Malaria. *Journal of the Royal Society, Interface*, 7: 309–319, 2010.

M. Choisy, J. F. Guegan, and P. Rohani. Dynamics of Infectious Diseases and Pulse Vaccination: Teasing Apart the Embedded Resonance Effects. *Physica D: Nonlinear Phenomena*, 223:26–35, 2006. doi: 10.1016/j.physd.2006.08.006.

A. Colombo, F. Dercole, and S. Rinaldi. Remarks on Metacommunity Synchronization with Application to Prey-Predator Systems. *The American Naturalist*, 171:430–442, 2008. doi: 10.1086/528959.

S. J. Cornell, O. N. Bjørnstad, I. M. Cattadori, B. Boag, and P. J. Hudson. Seasonality, Cohort-Dependence and the Development of Immunity in a Natural Host–Nematode System. *Proceedings of the Royal Society B: Biological Sciences*, 275 (1634):511–518, 2008. doi: 10.1098/rspb.2007.1415.

T. Coulson, E. A. Catchpole, S. D. Albon, B. J. T. Morgan, J. M. Pemberton, T. H. Clutton-Brock, M. J. Crawley, and B. T. Grenfell. Age, Sex, Density, Winter Weather, and Population Crashes in Soay Sheep. *Science*, 292(5521):1528–1531, 2001. doi: 10.1126/science.292.5521.1528.

V. Dakos, E. H. van Nes, and M. Scheffer. Flickering as an Early Warning Signal. *Theoretical Ecology*, 6(3):309–317, 2013. doi: 10.1007/s12080-013-0186-4.

T. Dalkvist, R. M. Sibly, and C. J. Topping. How Predation and Landscape Fragmentation Affect Vole Population Dynamics. *PLoS ONE*, 6(7):e22834, 2011. doi: 10.1371/journal.pone.0022834.

A. Dhooge, W. Govaerts, and Y. A. Kuznetsov. MatCont: a MATLAB Package for Numerical Bifurcation Analysis of ODEs. *ACM Transactions on Mathematical Software (TOMS)*, 29(2):141–164, 2003. URL `http://www.matcont.ugent.be/`.

O. Diekmann and M. Kretzschmar. Patterns in the Effects of Infectious Diseases on Population Growth. *Journal of Mathematical Biology*, 29(6):539–570, 1991. doi: 10.1007/BF00164051.

K. Dietz. The Incidence of Infectious Disease Under the Influence of Seasonal Fluctuations. In J. Berger, W. Buhler, R. Repger, and P. Tautu, editors, *Lecture Notes in Biomathematics: Mathematical Models in Medicine*, pages 1–15. Springer-Verlag, Berlin, Germany, 1976.

A. P. Dobson and P. J. Hudson. Regulation and Stability of a Free-Living Host-Parasite System: *Trichostrongylus tenuis* in Red Grouse. II. Population Models. *Journal of Animal Ecology*, 61(2):487–498, 1992. doi: 10.2307/5339.

E. J. Doedel. AUTO, A Program for the Automatic Bifurcation Analysis of Autonomous Systems. *Congressus Numerantium*, 30:265–384, 1981.

E. J. Doedel and B. E. Oldeman. *AUTO-07P : Continuation and Bifurcation Software for Ordinary Differential Equations*. Manual, 2009. URL `http://indy.cs.concordia.ca/auto`.

E. J. Doedel, H. B. Keller, and J. P. Kernevez. Numerical Analysis and Control of Bifurcation Problems: (I) Bifurcation in Finite Dimensions. *International Journal of Bifurcation and Chaos*, 1:493–520, 1991.

E. J. Doedel, W. Govaerts, Y. A. Kuznetsov, and A. Dhooge. Numerical Continuation of Branch Points of Equilibria and Periodic Orbits. In E. J. Doedel, G. Domokos, and I. G. Kevrekidis, editors, *Modelling and Computations in Dynamical Systems*, pages 145–164. World Scientific, Singapore, 2006.

F. Doveri, M. Scheffer, S. Rinaldi, S. Muratori, and Y. A. Kuznetsov. Seasonality and Chaos in a Plankton-Fish Model. *Theoretical Population Biology*, 43:159–183, 1993. doi: 10.1006/tpbi.1993.1008.

J. Dushoff, J. B. Plotkin, S. A. Levin, and D. J. D. Earn. Dynamical Resonance Can Account for Seasonality of Influenza Epidemics. *Proceedings of the National Academy of Sciences USA*, 101:16915–16916, 2004. doi: 10.1073/pnas.0407293101.

J. Dyczkowski and D. W. Yalden. An Estimate of the Impact of Predators on the British Field Vole *Microtus agrestis* Population. *Mammal Review*, 4:165–184, 1998. doi: 10.1046/j.1365-2907.1998.00032.x.

D. J. D. Earn, P. Rohani, B. M. Bolker, and B. T. Grenfell. A Simple Model for Complex Dynamical Transitions in Epidemics. *Science*, 287:667–670, 2000. doi: 10.1126/science.287.5453.667.

J. Erb, N. C. Stenseth, and M. S. Boyce. Geographic Variation in Population Cycles of Canadian Muskrats *(Ondatra zibethicus). Canadian Journal of Zoology*, 78:1009–1016, 2000. doi: 10.1139/cjz-78-6-1009.

B. Ermentrout. XPPAUT. In *Computational Systems Neurobiology*, pages 519–531. Springer, 2012. URL `http://www.math.pitt.edu/~bard/xpp/xpp.html`.

B. F. Finkenstadt and B. T. Grenfell. Time Series Modelling of Childhood Diseases: A Dynamical Systems Approach. *Journal of the Royal Statistical Society: Series C (Applied Statistics)*, 49:187–205, 2000. doi: 10.1111/1467-9876.00187.

L. Gammaitoni, P. Hänggi, P. Jung, and F. Marchesoni. Stochastic Resonance. *Reviews of Modern Physics*, 70(1):223, 1998. doi: 10.1103/RevModPhys.70.223.

P. Giesl. *Construction of Global Lyapunov Functions Using Radial Basis Functions*. Springer-Verlag, Berlin, Germany, 2007.

A. Gragnani and S. Rinaldi. A Universal Bifurcation Diagram for Seasonally Perturbed Predator-Prey Models. *Bulletin of Mathematical Biology*, 57:701–712, 1995. doi: 10.1007/BF02461847.

J. V. Greenman and T. G. Benton. Large Amplification in Stage-Structured Models: Arnol'd Tongues Revisited. *Journal of Mathematical Biology*, 48:647–671, 2004.

J. V. Greenman and R. A. Norman. Environmental Forcing, Invasion and Control of Ecological and Epidemiological Systems. *Journal of Theoretical Biology*, 247: 492–506, 2007. doi: 10.1016/j.jtbi.2007.03.031.

J. V. Greenman and V. B. Pasour. Phase Control of Resonant Systems: Interference, Chaos and High Periodicity. *Journal of Theoretical Biology*, 278:74–86, 2011. doi: 10.1016/j.jtbi.2011.03.002.

J. V. Greenman, M. Kamo, and M. Boots. External Forcing of Ecological and Epidemiological Systems: A Resonance Approach. *Physica D: Nonlinear Phenomena*, 190:135–151, 2004. doi: 10.1016/j.physd.2003.08.008.

J. Guckenheimer and P. Holmes. *Nonlinear Oscillations, Dynamical Systems and Bifurcations of Vector Fields*. Springer-Verlag, Berlin, Germany, 1983.

F. M. D. Gulland. The Role of Nematode Parasites in Soay Sheep (*Ovis aries L.*) Mortality During a Population Crash. *Parasitology*, 105(3):493–503, 1992. doi: 10.1017/S0031182000074679.

F. M. D. Gulland. The Impact of Infectious Diseases on Wild Animal Populations - A Review. In B. T. Grenfell and A. P. Dobson, editors, *Ecology of Infectious Diseases in Natural Populations*, pages 20–51. Cambridge University Press, Cambridge, UK, 1995. doi: 10.1017/CBO9780511629396.002.

F. M. D. Gulland and M. Fox. Epidemiology of Nematode Infections of Soay Sheep (*Ovis aries L.*) on St Kilda. *Parasitology*, 105(3):481–492, 1992. doi: 10.1017/S0031182000074667.

T. F. Hansen, N. C. Stenseth, and H. Henttonen. Multiannual Vole Cycles and Population Regulation During Long Winters: An Analysis of Seasonal Density Dependence. *The American Naturalist*, 154:129–139, 1999. doi: 10.1086/303229.

I. Hanski, L. Hansson, and H. Henttonen. Specialist Predators, Generalist Predators and the Microtine Rodent Cycle. *Journal of Animal Ecology*, 60:353–367, 1991. doi: 10.2307/5465.

I. Hanski, P. Turchin, E. Korpimaki, and H. Henttonen. Population Oscillations of Boreal Rodents: Regulation by Mustelid Predators Leads to Chaos. *Nature*, 364: 232–235, 1993. doi: 10.1038/364232a0.

I. Hanski, H. Henttonen, E. Korpimaki, L. Oksanen, and P. Turchin. Small-Rodent Dynamics and Predation. *Ecology*, 82:1505–1520, 2001. doi: 10.1890/0012-9658(2001)082[1505:SRDAP]2.0.CO;2.

L. Hansson. Dynamics and Trophic Interaction of Small-Rodents: Landscape or Regional Effects on Spatial Variation. *Oecologia*, 130:259–266, 2002. doi: 10.1007/s004420100802.

L. Hansson and H. Henttonen. Gradients in Density Variations of Small Rodents: The Importance of Latitude and Snow Cover. *Oecologia*, 67:394–402, 1985. doi: 10.1007/BF00384946.

L. Hansson and H. Henttonen. Rodent Dynamics as Community Processes. *Trends in Ecology and Evolution*, 3:195–200, 1988. doi: 10.1016/0169-5347(88)90006-7.

D. T. Haydon, D. J. Shaw, I. M. Cattadori, P. J. Hudson, and S. J. Thirgood. Analysing Noisy Time–Series: Describing Regional Variation in the Cyclic Dynamics of Red Grouse. *Proceedings of the Royal Society B: Biological Sciences*, 269 (1500):1609–1617, 2002. doi: 10.1098/rspb.2002.2053.

D. He and D. J. D. Earn. Epidemiological Effects of Seasonal Oscillations in Birth Rates. *Theoretical Population Biology*, 72:274–291, 2007. doi: 10.1016/j.tpb.2007.04.004.

P. Hersteinsson and D. MacDonald. Interspecific Competition and the Geographical Distribution of Red and Arctic Foxes *Vulpes vulpes* and *Alopex lagopus*. *Oikos*, 64: 505–515, 1992.

C. S. Holling. The Components of Predation as Revealed by a Study of Small-Mammal Predation of the European Pine Sawfly. *The Canadian Entomologist*, 91(05):293–320, 1959a.

C. S. Holling. Some Characteristics of Simple Types of Predation and Parasitism. *The Canadian Entomologist*, 91(07):385–398, 1959b.

J. Holt and J. Colvin. A Differential Equation Model of the Interaction Between the Migration of the Senegalese Grasshopper, *Oedaleus senegalensis*, its Predators, and a Seasonal Habitat. *Ecological Modelling*, 101:185–193, 1997. doi: 10.1016/S0304.3800(97)01981-9.

B. Hornfeldt, T. Hipkiss, and U. Eklund. Fading Out of Vole and Predator Cycles? *Proceedings of the Royal Society B: Biological Sciences*, 272:2045–2049, 2005. doi: 10.1098/rspb.2005.3141.

P. J. Hudson, D. Newborn, and A. P. Dobson. Regulation and Stability of a Free-Living Host-Parasite System: *Trichostrongylus tenuis* in Red Grouse. I. Monitoring and Parasite Reduction Experiments. *Journal of Animal Ecology*, 61:477–486, 1992. doi: 10.2307/5338.

P. J. Hudson, A. P. Dobson, and D. Newborn. Prevention of Population Cycles by Parasite Removal. *Science*, 282(5397):2256–2258, 1998. doi: 10.1126/science.282.5397.2256.

O. Huitu, K. Norrdahl, and E. Korpimaki. Landscape Effects on Temporal and Spatial Properties of Vole Population Fluctuations. *Oecologia*, 135:209–220, 2003. doi: 10.1007/s00442-002-1171-6.

R. A. Ims and E. Fuglei. Trophic Interaction Cycles in Tundra Ecosystems and the Impact of Climate Change. *BioScience*, 55:311–322, 2005. doi: 10.1641/0006-3568(2005)055[0311:TICITE]2.0.CO;2.

R. A. Ims, J. Henden, and S. T. Killengreen. Collapsing Population Cycles. *Trends in Ecology and Evolution*, 23:79–86, 2008. doi: 10.1016/j.tree.2007.10.010.

P. Inchausti and L. R. Ginzburg. Maternal Effects Mechanism of Population Cycling: A Formidable Competitor to the Traditional Predator-Prey View. *Philosophical Transactions of the Royal Society B: Biological Sciences*, 364:1117–1124, 2009. doi: 10.1098/rstb.2008.0292.

I. P. C. C. Intergovernmental Panel On Climate Change. *Climate Change 2001: Impacts, Adaptation and Vulnerability. Contribution of Working Group II to the Third*

Assessment Report of the Intergovernmental Panel on Climate Change. Cambridge University Press, Cambridge, UK, 2001.

J. M. Ireland, R. A. Norman, and J. V. Greenman. The Effect of Seasonal Host Birth Rates on Population Dynamics: The Importance of Resonance. *Journal of Theoretical Biology*, 231:229–238, 2004. doi: 10.1016/j.jtbi.2004.06.017.

M. J. Keeling and P. Rohani. *Modelling Infectious Diseases in Humans and Animals*. Princeton University Press, Princeton, NJ, 2008.

B. E. Kendall, J. Prendergast, and O. N. Bjørnstad. The Macroecology of Population Dynamics: Taxonomic and Biogeographic Patterns in Population Cycles. *Ecology Letters*, 1(3):160–164, 1998. doi: 10.1046/j.1461-0248.1998.00037.x.

B. E. Kendall, C. J. Briggs, W. W. Murdoch, P. Turchin, S. P. Ellner, E. McCauley, R. Nisbet, and S. N. Wood. Why Do Populations Cycle? A Synthesis of Statistical and Mechanistic Modelling Approaches. *Ecology*, 80:1789–1805, 1999. doi: 10.1890/0012-9658(1999)080%5B1789:WDPCAS%5D2.0.CO;2.

A. I. Khibnik, Y. A. Kuznetsov, V. V. Levitin, and E. V. Nikolaev. *Interactive LOCal BIFurcation Analyzer Version 2*, 1992.

A. A. King and W. M. Schaffer. The Rainbow Bridge: Hamitonian Limits and Resonance in Predator-Prey Dynamics. *Journal of Mathematical Biology*, 39:439–469, 1999. doi: 10.1007/s002850050174.

A. A. King and W. M. Schaffer. The Geometry of a Population Cycle: A Mechanistic Model of Snowshoe Hare Demography. *Ecology*, 82:814–830, 2001. doi: 10.1890/0012-9658(2001)082%5B0814:TGOAPC%5D2.0.CO;2.

C. King. *The Natural History of Weasels and Stoats*. Christopher Helm, Bromley, Kent, 1989.

E. Korpimaki and C. J. Krebs. Predation and Population Cycles of Small Mammals: A Reassessment of the Predation Hypothesis. *BioScience*, 46:754–764, 1996.

E. Korpimaki and K. Norrdahl. Experimental Reduction of Predators Reverses the Crash Phase of Small-Rodent Cycles. *Ecology*, 79:24482455, 1998. doi: 10.1890/0012-9658(1998)079[2448:EROPRT]2.0.CO;2.

E. Korpimaki, K. Norrdahl, T. Klemola, T. Pettersen, and N. C. Stenseth. Dynamic Effects of Predators on Cyclic Voles: Field Experimentation and Model Extrapolation. *Proceedings of the Royal Society B: Biological Sciences*, 269:991–997, 2002. doi: 10.1098/rspb.2002.1972.

C. J. Krebs, R. Boonstra, S. Boutin, and A. R. E. Sinclair. What Drives the 10-year Cycle of Snowshoe Hares? *BioScience*, 51(1):25–35, 2001. doi: 10.1641/0006-3568(2001)051%5B0025:WDTYCO%5D2.0.CO;2.

M. Krkošek, R. Hilborn, R. M. Peterman, and T. P. Quinn. Cycles, Stochasticity and Density Dependence in Pink Salmon Population Dynamics. *Proceedings of the Royal Society B: Biological Sciences*, 278(1714):2060–2068, 2011. doi: 10.1098/rspb.2010.2335.

R. Kuske, L. F. Gordillo, and P. Greenwood. Sustained Oscillations via Coherence Resonance in SIR. *Journal of Theoretical Biology*, 245(3):459–469, 2007. doi: 10.1016/j.jtbi.2006.10.029.

Y. A. Kutznetsov and V. V. Levitin. Content: a Multiplatform Environment for Continuation and Bifurcation Analysis of Dynamical Systems. *Centrum voor Wiskunde en Informatica, Amsterdam*, 1997. URL `http://www.staff.science.uu.nl/~kouzn101/CONTENT/`.

Y. A. Kuznetsov. *Elements of Applied Bifurcation Theory.* Springer-Verlag, New York, NY, 1995.

Y. A. Kuznetsov and C. Piccardi. Bifurcation Analysis of Periodic SEIR and SIR Epidemic Models. *Journal of Mathematical Biology*, 32:109–121, 1994. doi: 10.1007/BF00163027.

Y. A. Kuznetsov, S. Muratori, and S. Rinaldi. Bifurcations and Chaos in a Periodic Predator-Prey Model. *International Journal of Bifurcation and Chaos*, 2:117–128, 1992. doi: 10.1142/S0218127492000112.

Y. A. Kuznetsov, O. De Feo, and S. Rinaldi. Belyakov Homoclinic Bifurcations in a Tritrophic Food Chain Model. *SIAM Journal on Applied Mathematics*, 62:462–487, 2001. doi: 10.1137/S0036139900378542.

A. J. Lotka. Undamped Oscillations Derived from the Law of Mass Action. *Journal of the American Chemical Society*, 42(8):1595–1599, 1920.

G. Mabille, S. Descamps, and D. Berteaux. Predation as a Probable Mechanism Relating Winter Weather to Population Dynamics in a North American Porcupine Population. *Population Ecology*, 52:537–546, 2010. doi: 10.1007/s10144-010-0198-5.

E. Mancusi, L. Russo, G. Continillo, and S. Crescitelli. Computation of Frequency Locking Regions for a Discontinuous Periodically Forced Reactor. *Computers & Chemical Engineering*, 28:187–194, 2004. doi: 10.1016/S0098-1354(03)00186-8.

R. M. May and R. M. Anderson. Regulation and Stability of Host-Parasite Population Interactions: II. Destabilizing Processes. *Journal of Animal Ecology*, pages 249–267, 1978. doi: 10.2307/3934.

E. McCauley and W. W. Murdoch. Cyclic and Stable Populations: Plankton as Paradigm. *The American Naturalist*, 129:97–121, 1987. doi: 10.1086/284624.

E. McCauley, R. M. Nisbet, W. W. Murdoch, A. M. de Roos, and W. Gurney. Large-Amplitude Cycles of Daphnia and its Algal Prey in Enriched Environments. *Nature*, 402:653–656, 1999.

D. L. Murray. A Geographic Analysis of Snowshoe Hare Population Demography. *Canadian Journal of Zoology*, 78:1207 – 1217, 2000. doi: 10.1139/z00-025.

J. Nelson, J. Agrell, S. Erlinge, and M. Sandell. Reproduction of Different Female Age Categories and Dynamics in a Non-Cyclic Field Vole, *Microtus agrestis*, Population. *Oikos*, 61:73–78, 1991. doi: 10.2307/3545408.

R. M. Nisbet and W. S. C. Gurney. *Modelling Fluctuating Populations*. Wiley, New York, NY, 1982.

R. M. Nisbet, E. McCauley, A. M. de Roos, W. W. Murdoch, and W. S. C. Gurney. Population Dynamics and Element Recycling in an Aquatic Plant-Herbivore System. *Theoretical Population Biology*, 40:125–147, 1991. doi: 10.1016/0040-5809(91)90050-P.

K. Norrdahl. Population Cycles in Northern Small Mammals. *Biological Reviews*, 70: 621–637, 1995. doi: 10.1111/j.1469-185X.1995.tb01654.x.

R. Olinky, A. Huppert, and L. Stone. Seasonal Dynamics and Thresholds Governing Recurrent Epidemics. *Journal of Mathematical Biology*, 56:827–839, 2008. doi: 10.1007/s00285-007-0140-4.

T. Oraby, O. Vasilyeva, D. Krewski, and F. Lutscher. Modeling Seasonal Behavior Changes and Disease Transmission with Application to Chronic Wasting Disease. *Journal of Theoretical Biology*, 340:50–59, 2014. doi: 10.1016/j.jtbi.2013.09.003.

S. M. O'Regan, T. C. Kelly, A. Korobeinikov, M. J. A. O'Callaghan, A. V. Pokrovskii, and D. Rachinskii. Chaos in a Seasonally Perturbed SIR Model: Avian Influenza in a Seabird Colony as a Paradigm. *Journal of Mathematical Biology*, 67(2):293–327, 2013. doi: 10.1007/s00285-012-0550-9.

S. M. Redpath, F. Mougeot, F. M. Leckie, D. A. Elston, and P. J. Hudson. Testing the Role of Parasites in Driving the Cyclic Population Dynamics of a Gamebird. *Ecology Letters*, 9(4):410–418, 2006. doi: 10.1111/j.1461-0248.2006.00895.x.

S. Rinaldi and S. Muratori. Conditioned Chaos in Seasonally Perturbed Predator-Prey Models. *Ecological Modelling*, 69:79–97, 1993. doi: 10.1016/0304-3800(93)90050-3.

S. Rinaldi, S. Muratori, and Y. A. Kuznetsov. Multiple Attractors, Catastrophes and Chaos in Seasonally Perturbed Predator-Prey Communities. *Bulletin of Mathematical Biology*, 55:15–35, 1993. doi: 10.1007/BF02460293.

M. G. Roberts and B. T. Grenfell. The Population Dynamics of Nematode Infections of Ruminants: Periodic Perturbations as a Model for Management. *Mathematical Medicine and Biology*, 8(2):83–93, 1991. doi: 10.1093/imammb/8.2.83.

M. G. Roberts and B. T. Grenfell. The Population Dynamics of Nematode Infections of Ruminants: The Effect of Seasonality in the Free-Living Stages. *Mathematical Medicine and Biology*, 9(1):29–41, 1992. doi: 10.1093/imammb/9.1.29.

R. Rosà and A. Pugliese. Aggregation, Stability, and Oscillations in Different Models for Host-Macroparasite Interactions. *Theoretical Population Biology*, 61(3):319–334, 2002. doi: 10.1006/tpbi.2002.1575.

M. L. Rosenzweig and R. H. MacArthur. Graphical Representation and Stability Conditions of Predator-Prey Interactions. *The American Naturalist*, 97:209–223, 1963. doi: 10.1086/282272.

W. M. Schaffer, B. S. Pederson, B. K. Moore, O. Sharpaas, A. A. King, and T. V. Bronnikova. Sub-Harmonic Resonance and Multi-Annual Oscillations in Northern Mammals: A Non-Linear Dynamical Systems Perspective. *Chaos, Solitons & Fractals*, 12:251–264, 2001. doi: 10.1016/S0960-0779(00)00062-X.

M. Scheffer, S. Rinaldi, Y. A. Kuznetsov, and E. H. van Nes. Seasonal Dynamics of Daphnia and Algae Explained as a Periodically Forced Predator-Prey System. *Oikos*, 80:519–532, 1997. doi: 10.2307/3546625.

R. Seydel. *Practical Bifurcation and Stability Analysis (2nd Edition)*. Springer-Verlag, New York, NY, 1994.

J. A. Sherratt and M. J. Smith. Periodic Travelling Waves in Cyclic Populations: Field Studies and Reaction–Diffusion Models. *Journal of the Royal Society, Interface*, 5(22):483–505, 2008. doi: 10.1098/rsif.2007.1327.

M. J. Smith, A. White, J. A. Sherratt, S. Telfer, M. Begon, and X. Lambin. Disease Effects on Reproduction can Cause Population Cycles in Seasonal Environments. *Journal of Animal Ecology*, 77:378–389, 2008. doi: 10.1111/j.1365-2656.2007.01328.x.

N. C. Stenseth, O. N. Bjørnstad, and T. Saitoh. A Gradient from Stable to Cyclic Populations of *Clethrionomys rufocanus* in Hokkaido, Japan. *Proceedings of the Royal Society B: Biological Sciences*, 263:1117–1126, 1996. doi: 10.1098/rspb.1996.0164.

N. C. Stenseth, O. N. Bjørnstad, and T. Saitoh. Seasonal Forcing on the Dynamics of *Clethrionomys rufocanus*: Modeling Geographic Gradients in Population Dynamics. *Researches on Population Ecology*, 40:85–95, 1998.

L. Stone, R. Olinky, and A. Huppert. Seasonal Dynamics of Recurrent Epidemics. *Nature*, 446(7135):533–536, 2007. doi: 10.1038/nature05638.

K. Strann, N. G. Yoccoz, and R. A. Ims. Is the Heart of Fennoscandian Rodent Cycle Still Beating? A 14-Year Study of Small Mammals and Tengmalm's Owls in Northern Norway. *Ecography*, 25:81–87, 2002. doi: 10.1034/j.1600-0587.2002.250109.x.

S. Strohm and R. Tyson. The Effect of Habitat Fragmentation on Cyclic Population Dynamics: A Numerical Study. *Bulletin of Mathematical Biology*, 71:1323 – 1348, 2009. doi: 10.1007/s11538-009-9403-0.

B. Sultan, K. Labadi, J. Guégan, and S. Janicot. Climate Drives the Meningitis Epidemics Onset in West Africa. *PLoS Medicine*, 2(1):e6, 2005. doi: 10.1371/journal.pmed.0020006.

R. A. Taylor, J. A. Sherratt, and A. White. Seasonal Forcing and Multi-Year Cycles in Interacting Populations: Lessons from a Predator-Prey Model. *Journal of Mathematical Biology*, 67(6-7):1741–1764, 2013a. doi: 10.1007/s00285-012-0612-z.

R. A. Taylor, A. White, and J. A. Sherratt. How do Variations in Seasonality Affect Population Cycles? *Proceedings of the Royal Society B: Biological Sciences*, 280 (1754):20122714, 2013b. doi: 10.1098/rspb.2012.2714.

E. Tkadlec and N. C. Stenseth. A New Geographical Gradient in Vole Population Dynamics. *Proceedings of the Royal Society B: Biological Sciences*, 268:1547–1552, 2001. doi: 10.1098/rspb.2001.1694.

P. Turchin. *Complex Population Dynamics*. Princeton University Press, Princeton, NJ, 2003.

P. Turchin and I. Hanski. An Empirically Based Model for Latitudinal Gradient in Vole Population Dynamics. *The American Naturalist*, 149:842–874, 1997. doi: 10.1086/286027.

P. Turchin and I. Hanski. Contrasting Alternative Hypotheses About Rodent Cycles by Translating Them into Parameterized Models. *Ecology Letters*, 4:267–276, 2001. doi: 10.1046/j.1461-0248.2001.00204.x.

P. Turchin and R. S. Ostfeld. Effects of Density and Season on the Population Rate of Change in the Meadow Vole. *Oikos*, 78:355–361, 1997. doi: 10.2307/3546303.

V. Volterra. Variations and Fluctuations of the Number of Individuals in Animal Species Living Together. *ICES Journal of Marine Science*, 3(1):3–51, 1928. doi: 10.1093/icesjms/3.1.3.

D. M. Watts, D. A. Burke, B. A. Harrison, R. E. Whitmire, and A. Nisalak. Effect of Temperature on the Vector Efficiency of *Aedes aegypti* for Dengue 2 Virus. *The American Journal of Tropical Medicine and Hygiene (USA)*, 1987.

S. D. Webb and J. A. Sherratt. Oscillatory Reaction-Diffusion Equations with Temporally Varying Parameters. *Mathematical and Computer Modelling*, 39:45–60, 2004. doi: 10.1016/S0895-7177(04)90505-5.

K. A. J. White and B. T. Grenfell. Regulation of Complex Host Dynamics by a Macroparasite. *Journal of Theoretical Biology*, 186(1):81–91, 1997. doi: 10.1006/jtbi.1996.0344.

K. A. J. White, B. T. Grenfell, R. J. Hendry, O. Lejeune, and J. D. Murray. Effect of Seasonal Host Reproduction on Host-Macroparasite Dynamics. *Mathematical Biosciences*, 137(2):79–99, 1996. doi: 10.1016/S0025-5564(96)00061-2.

K. Wilson, O. N. Bjørnstad, A. P. Dobson, S. Merler, G. Poglayen, S. E. Randolph, A. F. Read, and A. Skorping. Heterogeneities in Macroparasite Infections : Patterns and Processes. In P. J. Hudson, A. Rizzoli, B. T. Grenfell, H. Heesterbeek, and A. P. Dobson, editors, *The Ecology of Wildlife Diseases*, pages 6–44. Oxford University Press, Oxford, UK, 2002.

Appendix A

AUTO Code

In this Appendix, we include code from each of the models in Chapters 2 - 4 which was used to compute the bifurcation diagrams in AUTO, and examples of the necessary constants files.

A.1 The Equations Files

We show code for the forced system in Chapters 2 and 3. The code for the unforced and forced models in Chapter 4 are included as it highlights the differences required to input forcing into the system.

A.1.1 The Forced Predator-Prey Model

```
C---------------------------------------------------------
C---------------------------------------------------------
C   ppb : A periodically forced predator prey system
C---------------------------------------------------------
C---------------------------------------------------------
C
      SUBROUTINE FUNC(NDIM,U,ICP,PAR,IJAC,F,DFDU,DFDP)
C     ---------- ----
C
      IMPLICIT REAL*8 (A-H,O-Z)
      DIMENSION U(NDIM),PAR(*),F(NDIM)
C
C      Definition of parameters
       A = PAR(1)
       B = PAR(2)
       C = PAR(3)
```

```
       D = PAR(4)
       R = PAR(5)
       EPS = PAR(6)

C
       U1=U(1)
       U2=U(2)
       X=U(3)
       Y=U(4)
C
C      Defining some shorthand functions and 2pi
       SS = X**2 + Y**2
       H = R*(1 + EPS*X)
       G = A/(B+U1)
       TPI=8*DATAN(1.0D0)
C
C      The differential equations including the forced oscillator equations
C      in X and Y
       F(1)= U1*H*(1-(U1/C)) - U1*U2*G
       F(2)= U2*(G*U1 - D)
       F(3) =  X + TPI*Y - X*SS
       F(4) = -TPI*X + Y - Y*SS
C
      RETURN
      END
C
      SUBROUTINE STPNT(NDIM,U,PAR,T)
C     ---------- -----
C
      IMPLICIT REAL*8(A-H,O-Z)
      DIMENSION U(NDIM),PAR(*)
C
C      Parameter initial values including the initial period
       TPI=8*DATAN(1.0D0)
       PAR(1)=2*TPI
       PAR(2)=0.3
       PAR(3)=1
       PAR(4)=TPI
       PAR(5)=TPI
```

```
       PAR(6)=0
       PAR(11)=1
C
C      Initial conditions
       U(1)=0.3
       U(2)=0.21
       U(3)=DSIN(TPI*T)
       U(4)=DCOS(TPI*T)
C
      RETURN
      END
C
      SUBROUTINE BCND
      RETURN
      END
C
      SUBROUTINE ICND
      RETURN
      END
C
      SUBROUTINE FOPT
      RETURN
      END
C
      SUBROUTINE PVLS
      RETURN
      END
```

A.1.2 The Forced Vole Model

```
C---------------------------------------------------------
C---------------------------------------------------------
C   vole :      A periodically forced vole system
C---------------------------------------------------------
C---------------------------------------------------------
C
      SUBROUTINE FUNC(NDIM,U,ICP,PAR,IJAC,F,DFDU,DFDP)
C     ---------- ----
C
      IMPLICIT REAL*8 (A-H,O-Z)
```

```
      DIMENSION U(NDIM),PAR(*),F(NDIM)
C
C      Definition of parameters
       A = PAR(1)
       D = PAR(2)
       H = PAR(3)
       S = PAR(4)
       R = PAR(5)
       EPS = PAR(6)
       P = PAR(7)
       G = PAR(8)

C
       U1=U(1)
       U2=U(2)
       X=U(3)
       Y=U(4)
C
C  Defining some functions including the new forced function Q
       SS = X**2 + Y**2
       Q = (0.5*(1 + EPS*X))**P
       B = A/(D+U1)
       TPI=8*DATAN(1.0D0)
C
C      The differential equations including the forced oscillator equations
C      in X and Y
       F(1)= 2*R*Q*U1 - R*(U1**2) - U1*U2*B - G*(U1**2)/(U1**2 + H**2)
       F(2)= 2*S*Q*U2 - (S*(U2**2))/U1
       F(3) =  X + TPI*Y - X*SS
       F(4) = -TPI*X + Y - Y*SS
C
      RETURN
      END
C
      SUBROUTINE STPNT(NDIM,U,PAR,T)
C     ---------- -----
C
      IMPLICIT REAL*8(A-H,O-Z)
      DIMENSION U(NDIM),PAR(*)
```

```
C
C      Parameter initial values including the initial period
       TPI=8*DATAN(1.0D0)
       PAR(1)=15
       PAR(2)=0.04
       PAR(3)=0.1
       PAR(4)=1.25
       PAR(5)=6
       PAR(6)=0.95
       PAR(7)=0.0D0
       PAR(8)=0.8
       PAR(11)=1
C
C      Initial conditions
       U(1)=0.0208
       U(2)=0.0417
       U(3)=DSIN(TPI*T)
       U(4)=DCOS(TPI*T)
C
      RETURN
      END
C
      SUBROUTINE BCND
      RETURN
      END
C
      SUBROUTINE ICND
      RETURN
      END
C
      SUBROUTINE FOPT
      RETURN
      END
C
      SUBROUTINE PVLS
      RETURN
      END
```

A.1.3 The Unforced Macroparasite Model

This equations file also shows the use of the subroutine PVLS to enable AUTO to output the minimum of two of the variables.

```
C---------------------------------------------------------
C---------------------------------------------------------
C   AM :     Anderson & May macroparasite model
C               with reduced fecundity
C---------------------------------------------------------
C---------------------------------------------------------
C
      SUBROUTINE FUNC(NDIM,U,ICP,PAR,IJAC,F,DFDU,DFDP)
C     ---------- ----
C
      IMPLICIT REAL*8 (A-H,O-Z)
      DIMENSION U(NDIM),PAR(*),F(NDIM)
C
C
       A = PAR(1)
       RMU = PAR(2)
       BETA = PAR(3)
       RK = PAR(4)
       GAM = PAR(5)
       DEL = PAR(6)
C
       U1=U(1)
       U2=U(2)
       U3=U(3)
       RKSTAR = (RK+1)/RK
C
C      The log-transformed differential equations with no forced oscillator
       F(1)= (A-1) - (1+DEL)*EXP(U2-U1)
       F(2)= BETA*EXP(U1+U3-U2) - (1 + RMU) - RKSTAR*EXP(U2-U1)
       F(3)= EXP(U2-U3) - GAM - EXP(U1)
C
      RETURN
      END
C
      SUBROUTINE STPNT(NDIM,U,PAR,T)
```

```
C     ---------- -----
C
      IMPLICIT REAL*8(A-H,O-Z)
      DIMENSION U(NDIM),PAR(*)
C
C      Initial parameter values
       TPI=8*DATAN(1.0D0)
       PAR(1)=1.7
       PAR(2)=1.0003/1.05
       PAR(3)=10/1.05
       PAR(4)=1.00
       PAR(5)=10/1.05
       PAR(6)=0.5
C
C      Initial conditions
       U(1)=1.420884374
       U(2)=0.658744133
       U(3)=-1.956063715
C
      RETURN
      END
C
      SUBROUTINE BCND
      RETURN
      END
C
      SUBROUTINE ICND
      RETURN
      END
C
      SUBROUTINE FOPT
      RETURN
      END
C
      SUBROUTINE PVLS(NDIM,U,PAR)

      IMPLICIT NONE
      INTEGER, INTENT(IN) :: NDIM
      DOUBLE PRECISION, INTENT(IN) :: U(NDIM)
```

```
      DOUBLE PRECISION, INTENT(INOUT) :: PAR(*)

      DOUBLE PRECISION, EXTERNAL :: GETP,GETU2
      INTEGER NDX,NCOL,NTST

C     The minimum of H, the hosts, and L, the larvae, are calculated
      PAR(7)=GETP('MIN',1,U)
      PAR(8)=GETP('MIN',3,U)

      RETURN
      END
```

A.1.4 The Forced Macroparasite Model

This code shows the situation of starting on a higher period cycle obtained from simulation. The initial conditions are omitted from the code but parameter 11 must have the same period as the simulation data. Numerical data of a whole period of the simulation is inputted into a separate data file (with name ".dat") and converted into AUTO format following the procedure in Doedel and Oldeman (2009, §14.4)

```
C-----------------------------------------------------------------
C-----------------------------------------------------------------
C   SPAR :  Anderson & May macroparasite model with reduced
C                   fecundity and seaonal forcing
C-----------------------------------------------------------------
C-----------------------------------------------------------------
C
      SUBROUTINE FUNC(NDIM,U,ICP,PAR,IJAC,F,DFDU,DFDP)
C     ---------- ----
C
      IMPLICIT REAL*8 (A-H,O-Z)
      DIMENSION U(NDIM),PAR(*),F(NDIM)
C
       A = PAR(1)
       RMU = PAR(2)
       BETA = PAR(3)
       RK = PAR(4)
       GAM = PAR(5)
       DEL = PAR(6)
       EPS = PAR(7)
```

```
C
       U1=U(1)
       U2=U(2)
       U3=U(3)
       X=U(4)
       Y=U(5)
       SS = X**2 + Y**2
       FORCE = A*(1+EPS*X)
       RKSTAR = (RK+1)/RK
       TPI=8*DATAN(1.0D0)
C
C      The log-transformed differential equations with forced oscillator
       F(1)= (FORCE-1) - (1+DEL)*EXP(U2-U1)
       F(2)= BETA*EXP(U1+U3-U2) - (1 + RMU) - RKSTAR*EXP(U2-U1)
       F(3)= EXP(U2-U3) - GAM - EXP(U1)
       F(4) =  X + TPI*Y - X*SS
       F(5) = -TPI*X + Y - Y*SS
C
      RETURN
      END
C
      SUBROUTINE STPNT(NDIM,U,PAR,T)
C     ---------- -----
C
      IMPLICIT REAL*8(A-H,O-Z)
      DIMENSION U(NDIM),PAR(*)
C
C      The initial parameter values. Par 11 indicates a 4 year cycle
       TPI=8*DATAN(1.0D0)
       PAR(1)=5
       PAR(2)=1.0003/1.05
       PAR(3)=10/1.05
       PAR(4)=1.00
       PAR(5)=10/1.05
       PAR(6)=0.89351
       PAR(7)=0.05
       PAR(11)=4
C
C     No initial conditions are given for the variables
```

```
C
      RETURN
      END
C
      SUBROUTINE BCND
      RETURN
      END
C
      SUBROUTINE ICND
      RETURN
      END
C
      SUBROUTINE FOPT
      RETURN
      END
C
      SUBROUTINE PVLS
      RETURN
      END
```

A.2 Constants Files

We provide some sample constants files from the macroparasite work in Chapter 4 to show how some of the constants change for different scenarios. The constants file has different formats due to the different versions of AUTO; we show here the older format, which also works in the newest version of AUTO. The main constants of note are IPS, IRS, ICP, NMX, ISW and DS. Respectively, these are the constants indicating periodic solutions, the starting label (if 0 then AUTO will use the initial conditions in the equations file), the free parameters, the number of points, branch switching to other solutions or types of curves and the initial step size (if negative then it traces in the opposite direction). More details and information on the other parameters can be found in Doedel and Oldeman (2009).

Starting from an equilibrium in the unforced system

```
3 1 0 1                        NDIM,IPS,IRS,ILP
1   6                       NICP,(ICP(I),I=1,NICP)
100 4 3 2 1 7 0 0              NTST,NCOL,IAD,ISP,ISW,IPLT,NBC,NINT
1000  0.00 10.00  0.0 1.e6      NMX,RL0,RL1,A0,A1
100 5 2 8 7 3 0                NPR,MXBF,IID,ITMX,ITNW,NWTN,JAC
```

```
1.e-7 1.e-7 1.e-4             EPSL,EPSU,EPSS
0.001 1.e-10 0.005  1           DS,DSMIN,DSMAX,IADS
0                             NTHL,(/,I,THL(I)),I=1,NTHL)
0                             NTHU,(/,I,THU(I)),I=1,NTHU)
0                            NUZR,(/,I,PAR(I)),I=1,NUZR)
```

IPS = 1 indicating that AUTO is on a stationary solution. NDIM = 3 showing that the system has 3 variables.

Starting from an equilibrium in the forced system

```
5 2 0 1                       NDIM,IPS,IRS,ILP
2   7 11                    NICP,(ICP(I),I=1,NICP)
100 4 3 2 1 11 0 0              NTST,NCOL,IAD,ISP,ISW,IPLT,NBC,NINT
300  0.00 10.00  0.0 1.e6     NMX,RL0,RL1,A0,A1
50 5 2 8 7 3 0                NPR,MXBF,IID,ITMX,ITNW,NWTN,JAC
1.e-7 1.e-7 1.e-4             EPSL,EPSU,EPSS
0.01 1.e-8 0.5  1           DS,DSMIN,DSMAX,IADS
0                             NTHL,(/,I,THL(I)),I=1,NTHL)
0                             NTHU,(/,I,THU(I)),I=1,NTHU)
0                            NUZR,(/,I,PAR(I)),I=1,NUZR)
```

NDIM = 5 due to the additional 2 forced oscillator equations. IPS = 2 for tracing periodic solutions and 11 (the period) is now a free parameter.

Tracing a bifurcation curve

```
5 2 9 1                       NDIM,IPS,IRS,ILP
3   7 6 11                      NICP,(ICP(I),I=1,NICP)
300 4 3 2 2 11 0 0              NTST,NCOL,IAD,ISP,ISW,IPLT,NBC,NINT
5000  0.00 10.00  0.0 1.e6      NMX,RL0,RL1,A0,A1
1000 5 2 8 7 3 0                NPR,MXBF,IID,ITMX,ITNW,NWTN,JAC
1.e-7 1.e-7 1.e-4             EPSL,EPSU,EPSS
0.0001 1.e-8 0.05  1           DS,DSMIN,DSMAX,IADS
1                             NTHL,(/,I,THL(I)),I=1,NTHL)
 11 0.0
0                             NTHU,(/,I,THU(I)),I=1,NTHU)
0                             NUZR,(/,I,PAR(I)),I=1,NUZR)
```

Again this is the periodic setting since IPS = 2. ISW = 2 indicates that we are tracing a locus of bifurcation points, which start from label IRS = 9. To do this, we require 3 free parameters.

Appendix B

Vole Model: Further Details

B.1 Model Details

We use the model of Turchin and Hanski (1997):

$$\frac{dN}{d\tau} = r\left(1 - \frac{N}{K}\right)N - \frac{GN^2}{N^2 + H^2} - \frac{CNP}{N + D} \tag{B.1a}$$

$$\frac{dP}{d\tau} = s\left(1 - Q\frac{P}{N}\right)P, \tag{B.1b}$$

where $N(\tau)$ and $P(\tau)$ are the densities of prey and specialist predator at time τ respectively. The prey undergo logistic growth with growth rate r and carrying capacity K. They are affected by two predation terms, representing generalist and specialist predation. Generalist predation is a Holling Type III functional form because generalists will switch to other prey items when prey numbers are low. The specialist predation is the Holling Type II functional form which incorporates handling time of prey. The predators have logistic growth with growth rate s and a carrying capacity determined by the number of prey.

We non-dimensionalise the model using the following scalings: $x = \frac{N}{K}$, $y = \frac{PQ}{K}$, $t = \tau$ and new parameters: $g = \frac{G}{K}$, $h = \frac{H}{K}$, $d = \frac{D}{K}$ and $a = \frac{C}{Q}$. The model is shown in dimensionless form in (B.2), which includes seasonal forcing in the growth rates and implicitly also in the carrying capacities through the term $S(t)$:

$$\frac{dx}{dt} = rS(t)x - rx^2 - \frac{gx^2}{x^2 + h^2} - \frac{axy}{x + d} \tag{B.2a}$$

$$\frac{dy}{dt} = sS(t)y - s\frac{y^2}{x}. \tag{B.2b}$$

There is a long history of using a sinusoidal function for the seasonal term as

follows:

$$S(t) = 1 + \epsilon \sin(2\pi t) \tag{B.3}$$

(Dietz, 1976; Rinaldi et al., 1993; Turchin and Hanski, 1997). However, as we wish to consider how changes in breeding season length affect population dynamics, we adapt the forcing term as follows:

$$S(t) = 2(\tfrac{1}{2}(1 + \epsilon \sin(2\pi t)))^l. \tag{B.4}$$

The new parameter l determines the length of the breeding season, which we define as when the forced growth term is above the unforced value of the parameter, i.e. when $S(t) > 1$. When $l = 1$, the breeding season length is half a year and the forcing term (B.4) reduces to (B.3). As l is increased the breeding season length decreases and vice versa. We wish the amplitude of the seasonal term to be large to represent strong seasonal forcing; nevertheless we require $\epsilon \leq 1$ so that the forcing term is not negative. We choose $\epsilon = 0.95$ to avoid the numerical problems that occur for $\epsilon = 1$ when l is small. Although we vary l from $0 - 5$, the range $0.5 < l < 3.9$ is most relevant for Fennoscandian voles, since this leads to a breeding season between 3 months and 8 months long, which corresponds to the variation observed in field data (Nelson et al., 1991; Hansen et al., 1999; Dalkvist et al., 2011).

B.2 Method Details

In order to study the predator-prey system (B.2) we employed both bifurcation and simulation methods, following the procedure in Chapter 2. The bifurcation diagrams were created using essentially standard numerical continuation techniques via the software AUTO (Doedel, 1981). The simulation results were produced in Matlab (`ode15s`), solving equations (B.2) for 2000 years. Once the solutions had settled to their dynamic attractor, a test to determine whether there existed a periodic solution of $1 - 9$ years was performed; if not, the solution was labelled as quasi-periodic. The choice of 9 years as a maximum test period is arbitrary; there could in principle be solutions with any finite integer period, but an upper limit is required for numerical study. To test whether a solution had a period of, for example, four years, we recorded the prey density for 20 time points at intervals of 4 years, after an initial time interval of sufficient length that transients had decayed. If the difference between the maximum and minimum of these numbers was less than 2.5% of their mean value, then it was classified as a four year solution. Tests of some difficult cases near bifurcation curves or within multiple solution regions led to the choices of 2000 years run time, 20 test points and 2.5% variation; these enabled periodic and quasi-periodic solutions to be distinguished. We considered the parameter region $0 < l < 5$, $0 < g < 1$. For each

set of parameter values, solutions were replicated 50 times using different (random) initial conditions between 0 and 1, independently chosen for both prey and predator. However, for parameter pairs lying in region B of Figure 3.3 we used 500 simulations to gain increased accuracy of the relative sizes of the basins of attractions because of the possibility of multiple solution behaviour in this region. Furthermore, fast Fourier transforms were used to determine the period most closely reflected in the solution ("dominant period"). In order to plot these results in a similar manner to the exact cycle method, all the dominant periods were rounded to the nearest integer. If a dominant period was higher than 9.5 then the solution was classified as quasi-periodic. The fast Fourier transform method is not as accurate for calculating stability of the solutions, for example, see Figure 3.3(b) and (c) at $(l, g) = (0.5, 0.6)$ where (b) shows that 2 year cycles are stable while the dominant period in (c) is given as 1 year. However, it is very useful for calculating approximate periods of the quasi-periodic solutions.

Appendix C

Vole Model: Further Results

C.1 Bifurcation Definitions

Definitions of period-doubling, fold and Neimark-Sacker bifurcation curves are included here to aid understanding of the bifurcation diagrams shown in Figures 3.4, C.1, C.2, D.1 and D.3. More detailed bifurcation theory can be found in §2.3.

The standard procedure for locating bifurcations of periodically forced systems uses the Poincaré (or stroboscopic) map that transforms the continuous system into a discrete one by sampling the solution once in each forcing period; one year in our case. Note that the stable/unstable annual cycles become stable/unstable fixed points of the Poincaré map. Discrete bifurcation theory reveals that this fixed point is unstable if one of the eigenvalues of its linearisation has modulus larger than 1. Changes in stability are of three possible types. If the eigenvalue is equal to -1, it is a *period-doubling (flip) bifurcation*; if the eigenvalue is equal to $+1$ it is a *fold (saddle-node, tangent) bifurcation*; and if there is a pair of complex conjugate eigenvalues with modulus 1, it is a *Neimark-Sacker (torus) bifurcation.*

At a period-doubling bifurcation curve (shown in blue), which we denote by PDk, a stable cycle of period k loses stability and a stable cycle of period $2k$ arises.

On one side of a fold bifurcation curve denoted by FDk there is no solution but on the other side there are both stable and unstable solution branches of a cycle of period k, which have a fold at the bifurcation point. These are shown in red.

A Neimark-Sacker bifurcation is often described as a discrete version of a Hopf bifurcation because for a standard supercritical bifurcation, the fixed point on the Poincaré section becomes unstable and a stable closed invariant curve arises around the point. Each iteration of the Poincaré map brings the solution back to a different point on the closed invariant curve. Therefore, in the continuous setting when crossing a Neimark-Sacker bifurcation curve, denoted by NSk, a cycle of period k loses stability and a quasi-periodic solution arises. That is, the solution may superficially appear periodic but in fact it has no finite period. Neimark-Sacker bifurcation curves are

shown in green.

C.2 Bifurcation Results

Figure 3.3(a) is based on a bifurcation diagram produced in AUTO which shows the full range of potential behaviour. In Figure C.1 we show this bifurcation diagram for annual, quasi-periodic and 2 year cycles, as well as dynamics resulting from period-doubling of the 2 year cycle. The whole bifurcation diagram (Figure C.2) is quite complicated, with a number of different curves overlapping, so it is helpful to consider first the partial bifurcation diagram in Figure C.1. In region 0 there are stable annual cycles but then as g is decreased one crosses the Neimark-Sacker bifurcation curve, NS1, leading to loss of stability of the annual cycles and a gain of stability of quasi-periodic cycles in region 1. The rest of the region is bounded within the fold curve FD2 and the period-doubling curve PD1. As one crosses the period-doubling curve

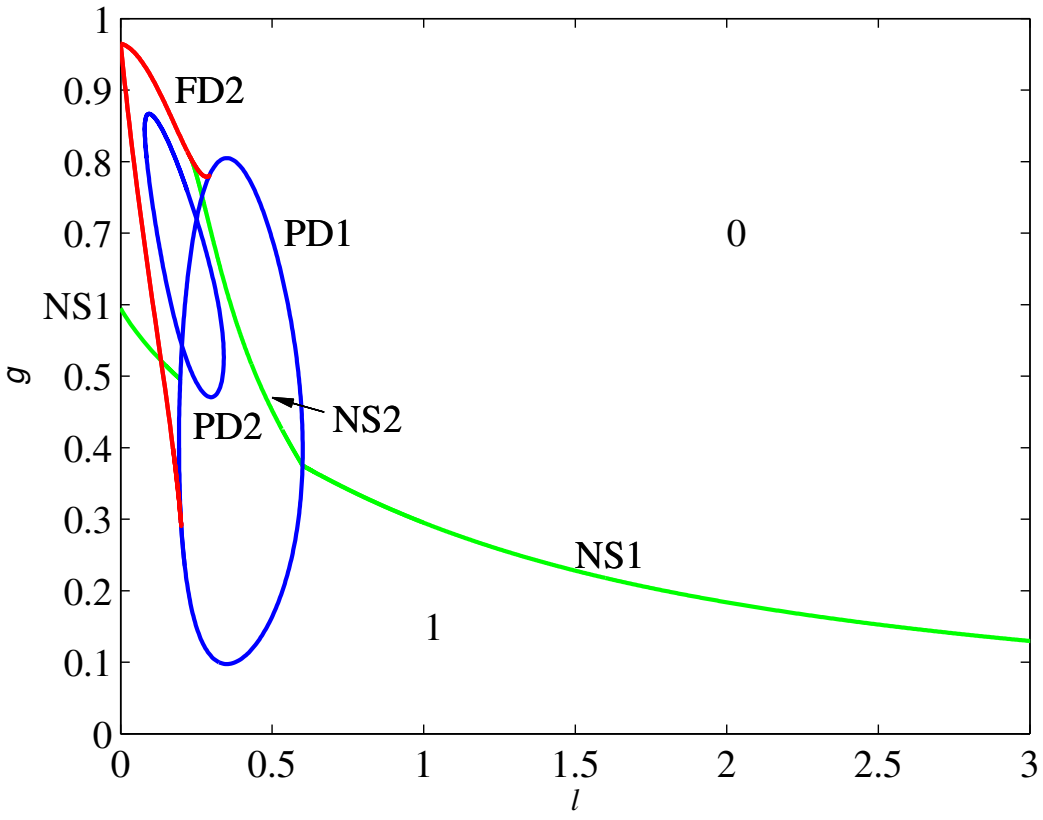

Figure C.1: Partial bifurcation diagram in season length parameter (l) and extent of generalist predation (g). Only the bifurcations resulting from the annual cycle are shown. The different bifurcation curves shown by colour: blue: period-doubling, red: fold, green: Neimark-Sacker bifurcation. In region 0 (bounded below by the NS1 and PD1 curves) there are annual cycles; in region 1 (bounded above by the NS1, NS2 and FD2 curves) there are quasi-periodic cycles.

one loses stability of the yearly cycles and gains two year cycles, which also exist outside the period-doubling region due to the fold curve. In fact, we can see the existence and stability of these two year cycles in greater detail in Figure 3.4(a). The Neimark-Sacker bifurcation curve, NS2, within this region leads to instability of all the 2 year cycles below the green line. There is also a period-doubling curve within the 2 year cycles region denoting the existence of four year cycles, as can be seen in Figure 3.4(c).

We also note that the point where the continuation of the first Neimark-Sacker bifurcation (NS1), hits the $l = 0$ axis is where the unforced system undergoes a Hopf bifurcation. This bifurcation is subcritical, and this subcriticality extends to the Neimark-Sacker bifurcation so that quasi-periodic solutions exist alongside the yearly solutions above the curve. Combined with the quasi-periodic solution generated by curve NS2, this produces the shape of the two regions C and D in Figure 3.3(a).

In Figure C.2 we include all the bifurcation curves for each of the different period cycles that were found. For $2 - 5$ year cycles, these were studied individually in Figure 3.4 but we show them all together in Figure C.2 in order to see the full picture and the overlapping behaviour. This new bifurcation diagram includes all the fold bifurcation curves for all the cycles that were found between 3 and 9 years. There are further bifurcation curves within these bounded regions, as seen in Figure 3.4, denoting changes in stability to these solutions but we omit these in Figure C.2 in order to gain a clearer representation of existence of the cycles. Furthermore, there are undoubtedly more fold bifurcation curves indicating additional regions of multi-year cycles for any integer period, but we either didn't find these or they are too small to be traced.

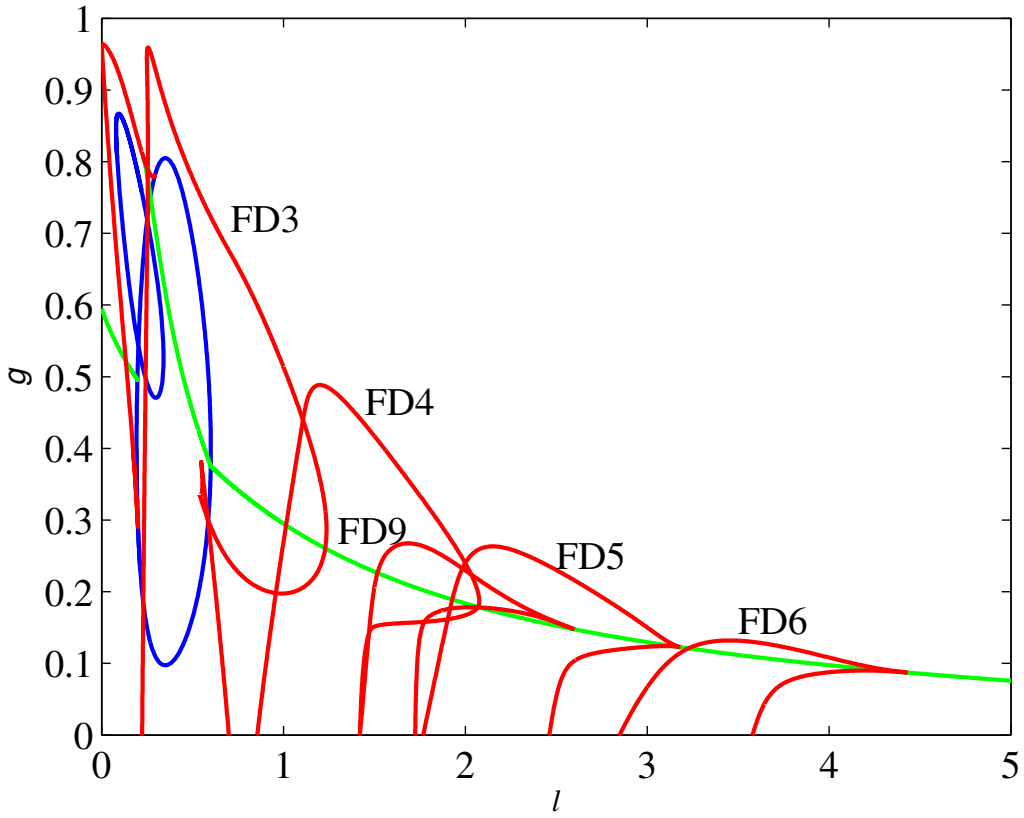

Figure C.2: Full bifurcation diagram in season length parameter (l) and extent of generalist predation (g). The curves which are labelled are those which are not in Figure C.1. All other details as in Figure C.1. For the 3 year and higher cycles, only the bifurcation curves indicating existence are shown and not any that only indicate changes in stability; these can be found in Figure 3.4.

Appendix D

Vole Model: Prey-only Forcing

In the model (B.2) we forced both the prey and predator growth rates with the same forcing term. Although weasels are able to breed throughout the whole year, this only happens in peak years of vole populations (King, 1989). Therefore, including a weasel breeding season is valid but it is unclear whether this should follow the same pattern as the vole breeding season, on which the forcing term was based. In order to understand the effects of different forcing in the predator growth rate, we consider the scenario where the prey growth rate is forced (B.2a) but there is no forcing in the predator equation (B.2b). We analyse the model using the same methods as in Chapter 3, namely through bifurcation and simulation analysis. The bifurcation diagram, Figure D.1, shows the Neimark-Sacker bifurcation curve, NS1, the period-doubling curve PD1 and the two fold curves, FD3 and FD4, for the model without predator forcing (which can be compared to Figure C.2 when both predator and prey are forced). We did not determine the higher period fold curves for this scenario. Whereas in Figure C.1 the period-doubling curve PD1 intersected the Neimark-Sacker bifurcation curve, NS1, for the case with no predator forcing this period-doubling curve does not exist and the Neimark-Sacker bifurcation curve is now continuous. Both the three year and four year cyclic regions have changed in shape, with the three year region shrinking and the four year region increasing in size. This indicates the potential for a large area of stable four year cycles. The Neimark-Sacker bifurcation has also moved up in the $l - g$ plane so that it now hits the $l = 0$ axis at $g = 1$. The upward shift in the Neimark-Sacker curve and the expansion of the period four fold curve indicates that when l is small, multi-year cycles are possible for more values of generalist predators, i.e. for a wider range of g values, compared to the predator forcing case in Chapter 3.

We also produced simulation results for this prey-only forcing case, showing both the cycle period and the dominant period (Figure D.2). The influence of the large four year fold curve as seen in Figure D.1 is clear, dominating the region containing multi-year cycles. However, 3, 7 and 8 year cycles are also found. This is interesting

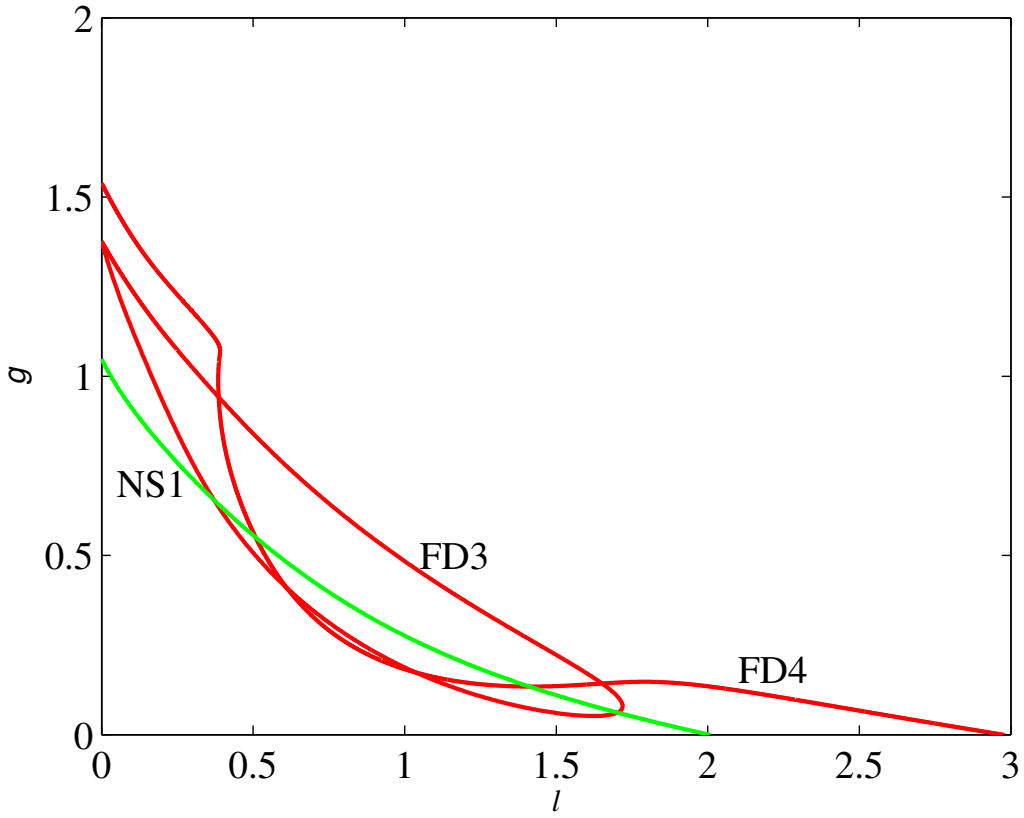

Figure D.1: Bifurcation diagram in season length parameter (l) and extent of generalist predation (g) when the predators are not forced. Only the four curves NS1, PD1, FD3 and FD4 were found, although the period-doubling curve, PD1, has in fact disappeared for this scenario. The different bifurcation curves shown by colour: red: fold, green: Neimark-Sacker bifurcation.

considering that the 7 and 8 year cycles were rare in the predator forcing case (see Figure 3.3(b)).

From these figures, it is clear that a number of results stated in Chapter 3 for the model with prey and predator forcing hold true when the forcing on the predator is removed. As before there is a diagonal split from top left to bottom right delineating multi-year cycles and annual cycles. As the extent of the generalist predation increases, such as when one moves south in Fennoscandia, there is a switch to annual cycles as expected. However, it is not a clear split and there is still the potential for 3 year cycles in a similar manner to the results in Figure 3.2. Also holding true is the fact that multi-year cycles exist for a wide range of values of l when g is small. The main difference between the results in Chapter 3 and these results for prey-only forcing is the fact that only annual cycles are indicated for the higher values of l, i.e. for breeding seasons around $3\frac{1}{2}$ months, although confirmation by simulation is needed to see if this continues for $l > 3$. This also ties in with the fact that the pattern of increasing period length for small g as l increases is less clearly defined. The

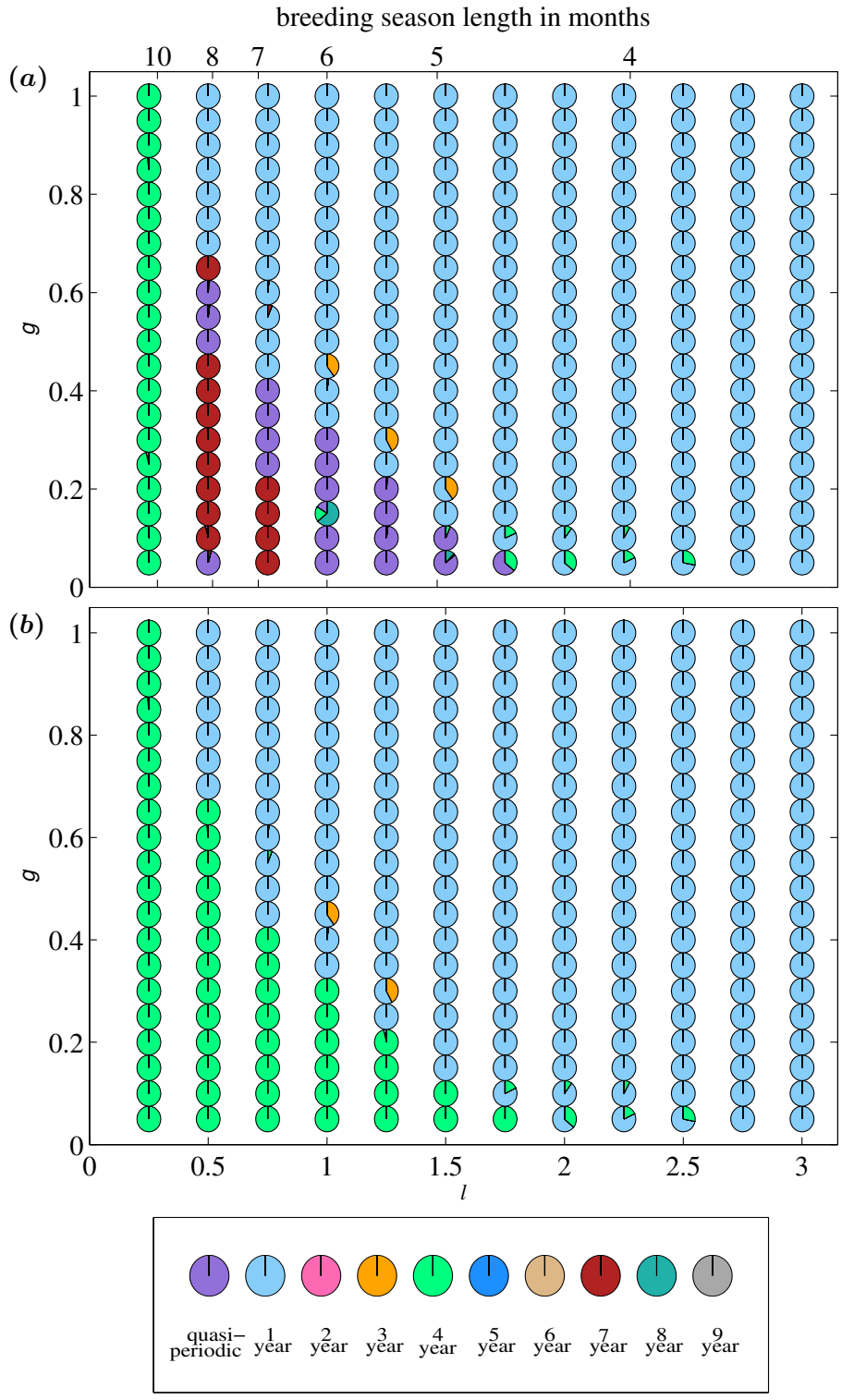

Figure D.2: Simulation results when the predators are not forced. The diagrams show season length parameter (l) against extent of generalist predation (g). The breeding season length is indicated on the top axis. In (a) a simulation diagram with a grid of pie charts showing what proportion of the 50 simulations had a particular period, indicated by the legend. Each simulation was run with random initial conditions (between 0 and 1 for both prey and predator) and the period was tested after 2000 years. In (b) these same simulations were tested using fast Fourier transforms to determine the dominant period of the solutions. Other parameter values are $r = 6$, $s = 1.25$, $d = 0.04$, $a = 15$, $h = 0.1$, $\epsilon = 0.95$.

dominance of the 4 year cycles makes it hard to determine this behaviour; identifying the bifurcation curves for the higher period cycles could clarify whether this pattern still holds.

Reducing forcing in the predator growth rate The case of no predator forcing above shows that the period-doubling curve has disappeared. It is possible that the curve does exist but we were unable to find it while doing the bifurcation analysis. However, confirmation of how the period-doubling curve, and the other curves, change can be found by analysing the system as it moves from the original scenario of both prey and predator being forced towards the case with prey-only forcing. We do this by tracing along a gradient of reduced forcing for the predator determined by a new parameter ξ, using the adapted forcing term $S^*(t)$ for the predator:

$$S^*(t) = 1 - \xi + \xi S(t). \tag{D.1}$$

Therefore, $\xi = 1$ is the case in Chapter 3 while $\xi = 0$ is the case of no forcing for the predator. By reducing ξ from 1 to 0 we can determine how the four curves (NS1, PD1, FD3 and FD4) change as we move towards prey-only forcing. We consider the bifurcation diagram for different values of ξ, as shown in Figure D.3.

Through consideration of the full range of ξ values (Figures C.2, D.1 and D.3) it is clear how the different curves change shape. The Neimark-Sacker bifurcation curve is increasing in g as ξ is reduced. The break between the two sections of the Neimark-Sacker bifurcation reduces in size as ξ decreases until $\xi = 0$ where it is now continuous (Figure D.1). This is due to the reduction in size of the period-doubling region as seen in Figure D.3. In fact, as ξ is reduced from 1 to 0, the period-doubling curve, PD1, gets smaller until it disappears just below $\xi = 0.155$. The three year fold curve, FD3, reduces in size and is no longer connected to the $g = 0$ axis. Figure D.3 also indicates that the Hopf bifurcation on the $l = 0$ axis is still subcritical (as in Figure C.2) because the three year fold curve hits the axis above the Neimark-Sacker bifurcation curve. The four year fold curve, FD4, lowers in g as ξ is reduced at first, although by $\xi = 0$ the fold curve has increased again so that for $\xi = 0$, it exists up to $g = 1.5$ for low values of l. It also exists for more values of l as ξ decreases.

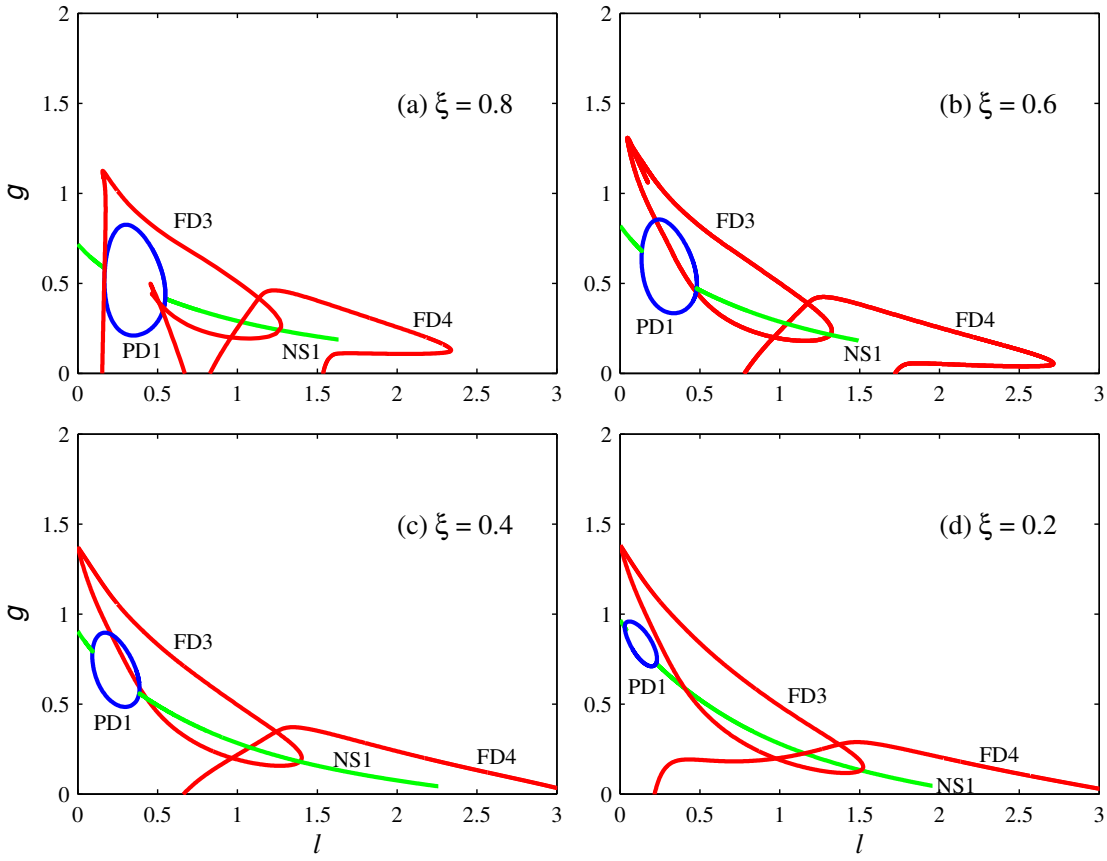

Figure D.3: Four bifurcation diagrams in season length parameter (l) and extent of generalist predation (g) as the level of forcing in the predator equation is reduced. Four different values of ξ are shown, namely (a) $\xi = 0.8$, (b) $\xi = 0.6$, (c) $\xi = 0.4$, (d) $\xi = 0.2$. For $\xi = 0$ see Figure D.1. The different bifurcation curves shown by colour: blue: period-doubling, red: fold, green: Neimark-Sacker bifurcation.

Appendix E

Macroparasite Model: Further Details

E.1 Non-Dimensionalising the Model

In this study we use a general model formulation which includes the larval stage explicitly, and the aggregation of parasite spread throughout hosts is represented by the commonly used negative binomial distribution (Anderson and May, 1978; Diekmann and Kretzschmar, 1991; Rosà and Pugliese, 2002). We present it here before rescaling:

$$\frac{dH}{d\tau} = (a^* - b)H - (\alpha + \delta^*)P \tag{E.1a}$$

$$\frac{dP}{d\tau} = \beta^* LH - (\mu^* + b + \alpha)P - \alpha\frac{P^2}{H}\left(\frac{k+1}{k}\right) \tag{E.1b}$$

$$\frac{dL}{d\tau} = \lambda P - \gamma^* L - \beta^* LH. \tag{E.1c}$$

$H(\tau)$ is the number of host species at time τ, $P(\tau)$ is the total number of adult parasites contained within all of the hosts at time τ and $L(\tau)$ is the number of free-living larval stage parasites. The host species undergoes exponential birth and death, with rates a^* and b respectively, as well as death, αP, and reduced fecundity, $\delta^* P$, caused by the parasite. The term $\beta^* LH$ denotes the rate of transmission of larvae to hosts leading to adult parasites. Parasites are lost due to natural mortality with rate μ^*, natural death of the host (rate b) and parasite induced death of the host. However, the loss of parasites due to host death requires knowledge of expected number of parasites within each host, and we assume a negative binomial distribution for the parasites with aggregation parameter k (which leads to the form of (E.1b)). Finally, the larvae are produced by adult parasites laying eggs at rate λ and die at rate γ^*.

We use the same parameter values as Dobson and Hudson (1992), which are: $a^* = 1.8$, $b = 1.05$, $\alpha = 3 \times 10^{-4}$, $\beta^* = 0.1$, $\mu^* = 1$, $k = 1$, $\lambda = 10$, $\gamma^* = 11$. However, we deviate with parameter δ^*. Dobson and Hudson (1992) let $\delta^* = 5 \times 10^{-4}$, which combined with the other parameter values leads to diverging cycles driving the hosts and parasites to extinction. Dobson and Hudson (1992) chose to counteract this by adding in host regulation through logistic growth. We instead keep this model but lower the value of δ^* to values which do not lead to extinction.

We non-dimensionalise this model, with the scalings, $h = \frac{\beta^* H}{b}$, $p = \frac{\alpha\beta^* P}{b^2}$, $l = \frac{\alpha\beta^* L}{\lambda b}$ and $t = b\tau$. The new parameters are $a = \frac{a^*}{b}$, $\delta = \frac{\delta^*}{\alpha}$, $\beta = \frac{\lambda}{b}$, $\mu = \frac{\mu^* + \alpha}{b}$ and $\gamma = \frac{\gamma^*}{b}$. Of particular note is that $a = 1.7$ and δ will vary about 0.8. This produces the following model, as seen in (4.1).

$$\frac{dh}{dt} = (a-1)h - (1+\delta)p \tag{E.2a}$$

$$\frac{dp}{dt} = \beta l h - (\mu+1)p - \frac{p^2}{h}\left(\frac{k+1}{k}\right) \tag{E.2b}$$

$$\frac{dl}{dt} = p - \gamma l - lh, \tag{E.2c}$$

E.2 Log-Transforming the Model

We log-transformed the equations to speed up computational time as the solutions spend a large proportion of each cycle very close to zero and it takes a long time for the transient dynamics to die out. Log-transforming the equations significantly improves both computational time in Matlab and accuracy in AUTO.

By letting $\hat{h} = \ln h$, $\hat{p} = \ln p$ and $\hat{l} = \ln l$, this transforms (E.2) into the following model:

$$\frac{d\hat{h}}{dt} = (a-1) - (1+\delta)\mathrm{e}^{\hat{p}-\hat{h}} \tag{E.3a}$$

$$\frac{d\hat{p}}{dt} = \beta \mathrm{e}^{\hat{l}+\hat{h}-\hat{p}} - (\mu+1) - \left(\frac{k+1}{k}\right)\mathrm{e}^{\hat{p}-\hat{h}} \tag{E.3b}$$

$$\frac{d\hat{l}}{dt} = \mathrm{e}^{\hat{p}-\hat{l}} - \gamma - \mathrm{e}^{\hat{h}}, \tag{E.3c}$$

We reverse this log-transformation before presenting results.

Appendix F

Macroparasite Model: The Unforced Dynamics

F.1 Investigating the Period at the Hopf Bifurcation

In Figure 4.4 we showed how the initial period at the Hopf bifurcation changes as both a and δ are varied. We stated that only by varying a (concurrently with any other parameter) was it possible to reduce the period to low period limit cycles at the Hopf bifurcation. Here we present the results for every parameter pair showing both the change in the initial period and the resulting change in the Hopf bifurcation curve in two-dimensional parameter space.

F.1.1 Parameter a

We show first of all the changes in the period when a is varied with each of the other parameters in turn.

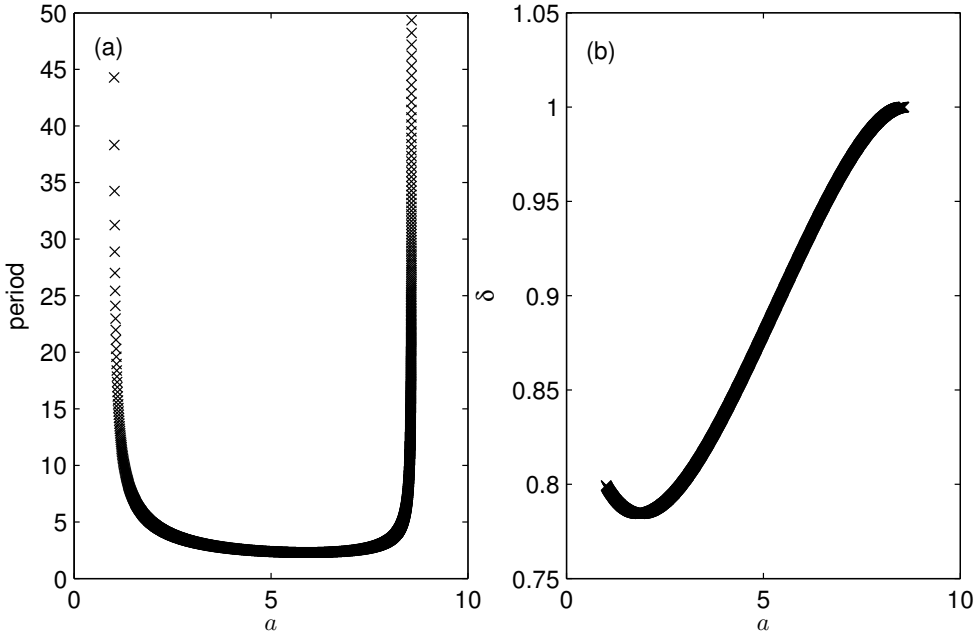

Figure F.1: Varying a and δ in the unforced system. In (a) the initial period at the Hopf bifurcation is shown. In (b), the Hopf bifurcation curve. All other parameters are kept constant at $\beta = \gamma = 10/1.05$, $\mu = 1.0003/1.05$ and $k = 1$.

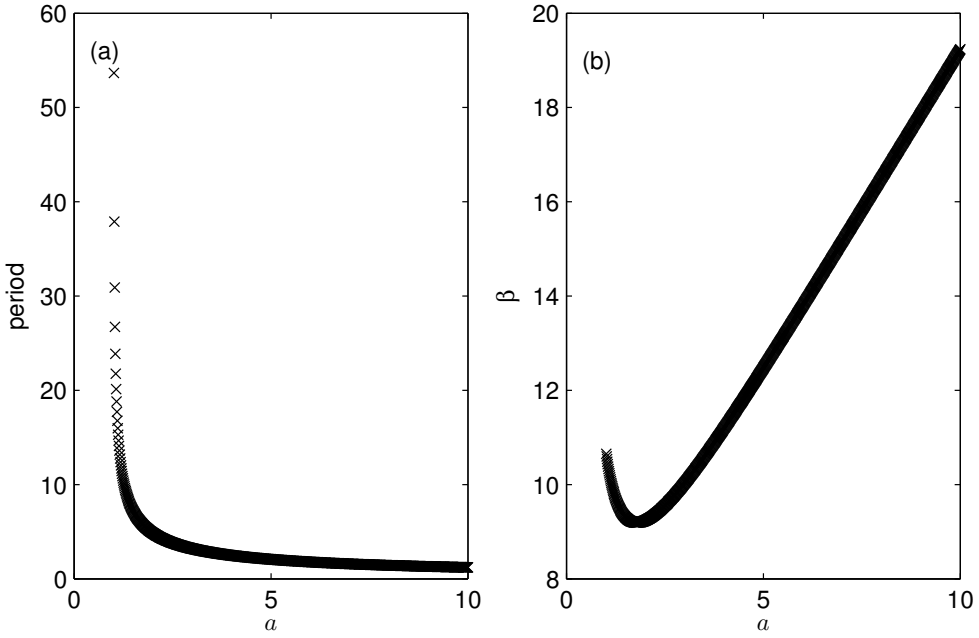

Figure F.2: Varying a and β in the unforced system. In (a) the initial period at the Hopf bifurcation is shown. In (b), the Hopf bifurcation curve. All other parameters are kept constant at $\delta = 0.789798$, $\gamma = 10/1.05$, $\mu = 1.0003/1.05$ and $k = 1$.

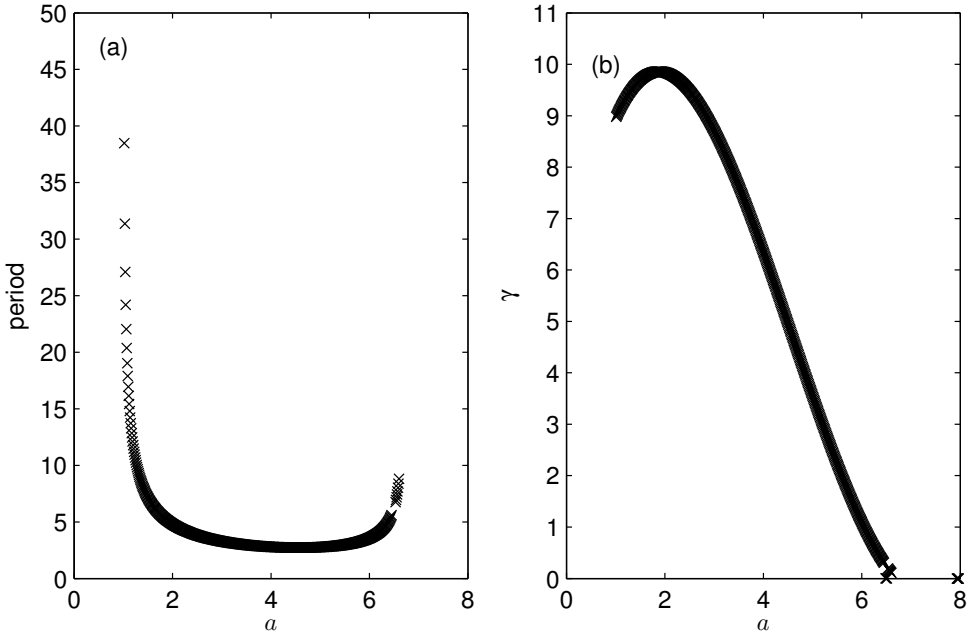

Figure F.3: Varying a and γ in the unforced system. In (a) the initial period at the Hopf bifurcation is shown. In (b), the Hopf bifurcation curve. All other parameters are kept constant at $\delta = 0.789798$, $\beta = 10/1.05$, $\mu = 1.0003/1.05$ and $k = 1$.

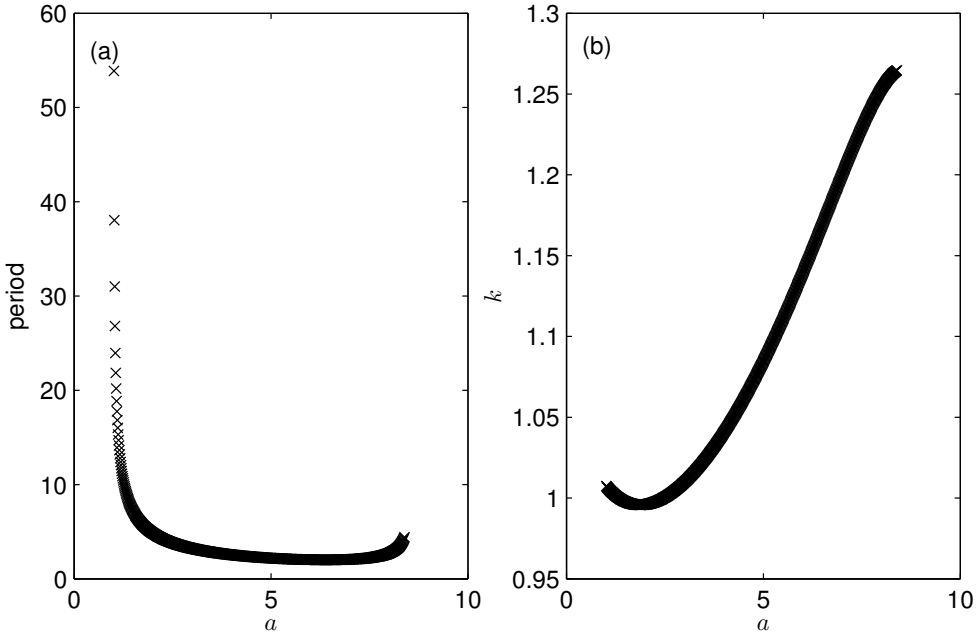

Figure F.4: Varying a and k in the unforced system. In (a) the initial period at the Hopf bifurcation is shown. In (b), the Hopf bifurcation curve. All other parameters are kept constant at $\delta = 0.789798$, $\beta = \gamma = 10/1.05$, and $\mu = 1.0003/1.05$.

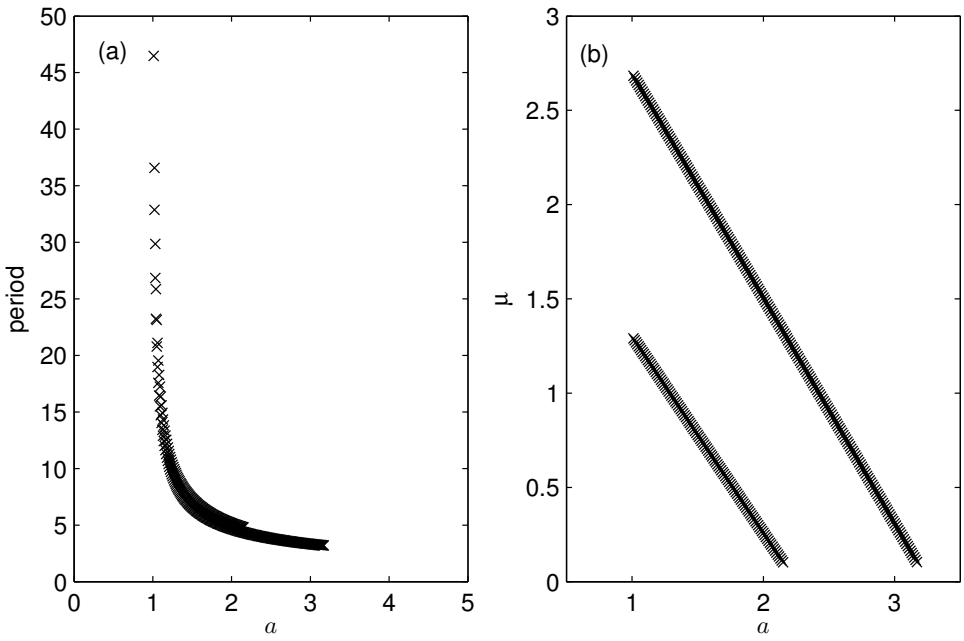

Figure F.5: Varying a and μ in the unforced system. In (a) the initial period at the Hopf bifurcation is shown. In (b), the Hopf bifurcation curve. All other parameters are kept constant at $\delta = 0.789798$, $\beta = \gamma = 10/1.05$ and $k = 1$.

F.1.2 Parameter β

We show the change in the Hopf bifurcation and the resulting change in the initial period when β is varied with each of the parameters in turn, apart from with a (that case is shown in Figure F.2).

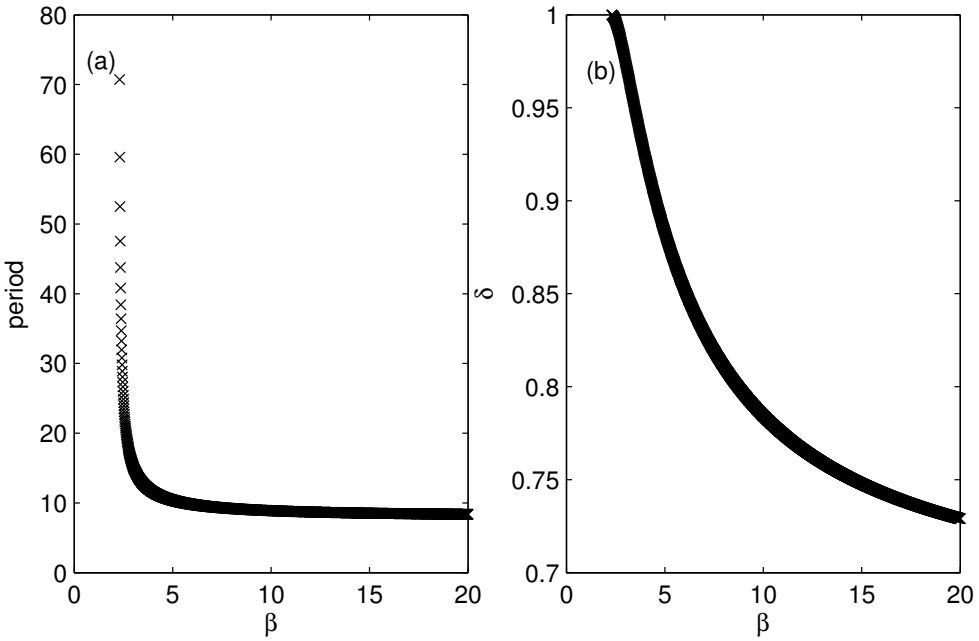

Figure F.6: Varying β and δ in the unforced system. In (a) the initial period at the Hopf bifurcation is shown. In (b), the Hopf bifurcation curve. All other parameters are kept constant at $a = 1.4/1.05$, $\gamma = 10/1.05$, $\mu = 1.0003/1.05$ and $k = 1$.

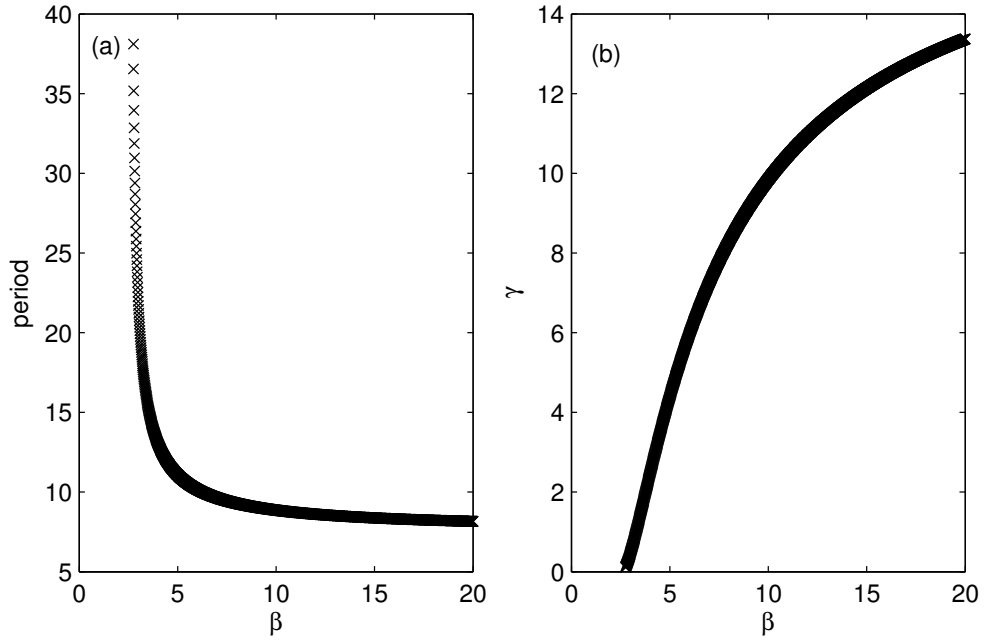

Figure F.7: Varying β and γ in the unforced system. In (a) the initial period at the Hopf bifurcation is shown. In (b), the Hopf bifurcation curve. All other parameters are kept constant at $a = 1.4/1.05$, $\delta = 0.789798$, $\mu = 1.0003/1.05$ and $k = 1$.

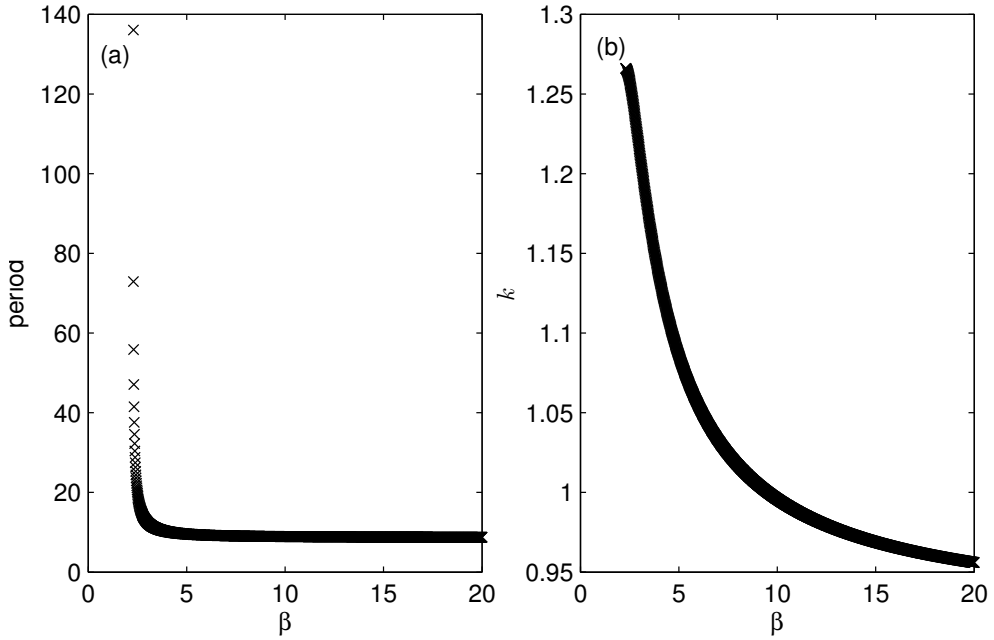

Figure F.8: Varying β and k in the unforced system. In (a) the initial period at the Hopf bifurcation is shown. In (b), the Hopf bifurcation curve. All other parameters are kept constant at $a = 1.4/1.05$, $\delta = 0.789798$ $\gamma = 10/1.05$, and $\mu = 1.0003/1.05$.

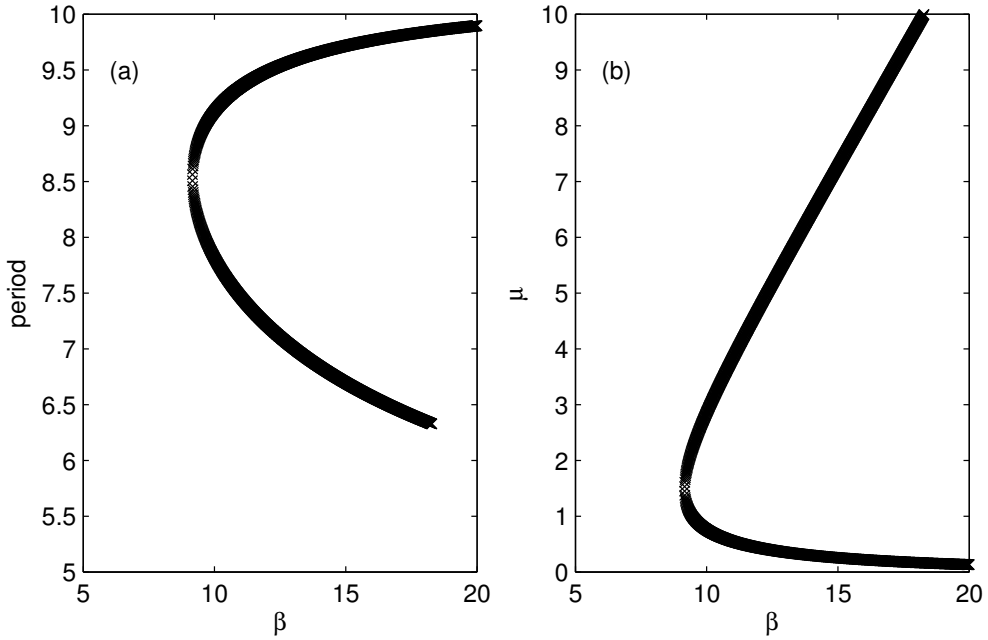

Figure F.9: Varying β and μ in the unforced system. In (a) the initial period at the Hopf bifurcation is shown. In (b), the Hopf bifurcation curve. All other parameters are kept constant at $a = 1.4/1.05$, $\delta = 0.789798$, $\gamma = 10/1.05$ and $k = 1$.

F.1.3 Parameter γ

We show the change in the Hopf bifurcation and the resulting change in the initial period when γ is varied with each of the parameters in turn, apart from with a and β, as these are shown in Figures F.3 and F.7 respectively.

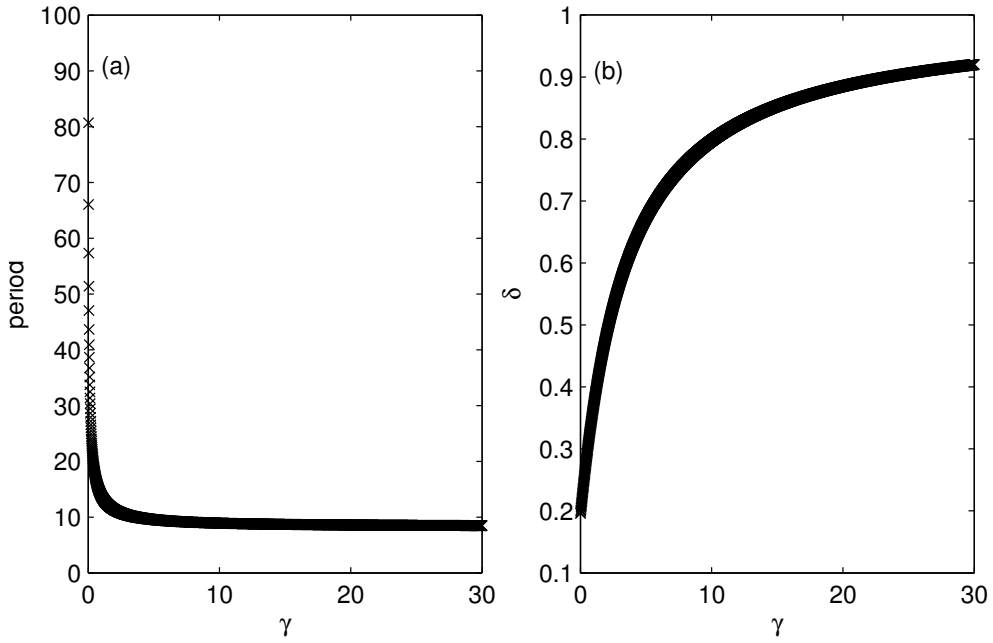

Figure F.10: Varying γ and δ in the unforced system. In (a) the initial period at the Hopf bifurcation is shown. In (b), the Hopf bifurcation curve. All other parameters are kept constant at $a = 1.4/1.05$, $\beta = 10/1.05$, $\mu = 1.0003/1.05$ and $k = 1$.

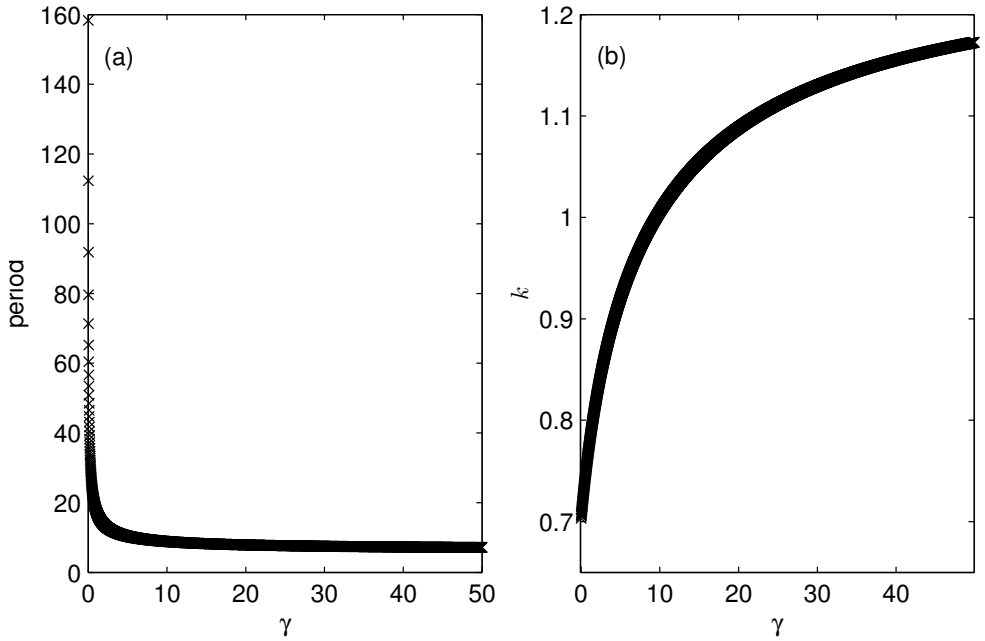

Figure F.11: Varying γ and k in the unforced system. In (a) the initial period at the Hopf bifurcation is shown. In (b), the Hopf bifurcation curve. All other parameters are kept constant at $a = 1.4/1.05$, $\delta = 0.789798$ $\beta = 10/1.05$, and $\mu = 1.0003/1.05$.

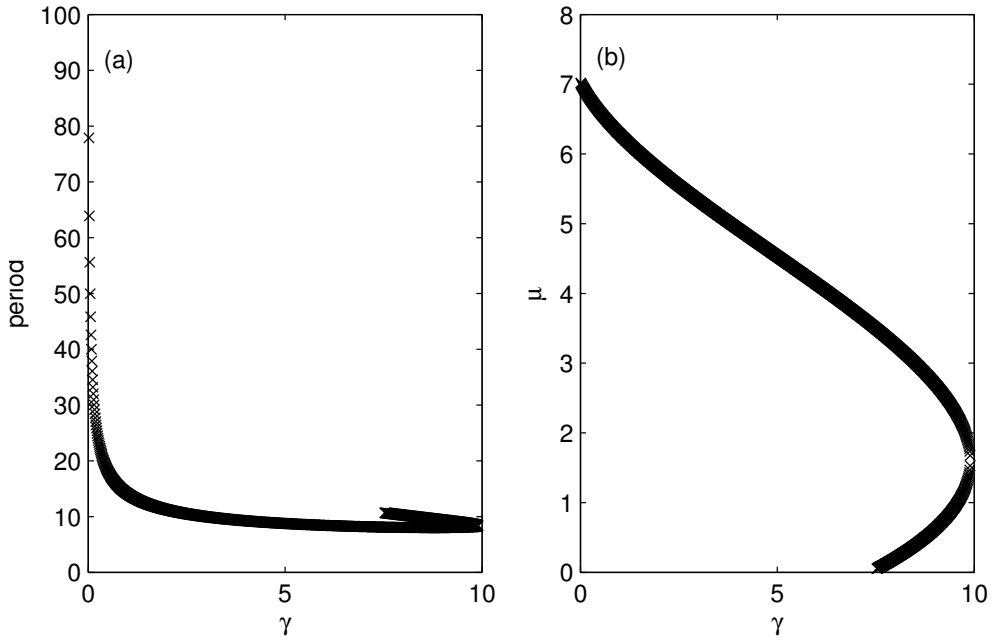

Figure F.12: Varying γ and μ in the unforced system. In (a) the initial period at the Hopf bifurcation is shown. In (b), the Hopf bifurcation curve. All other parameters are kept constant at $a = 1.4/1.05$, $\delta = 0.789798$, $\beta = 10/1.05$ and $k = 1$.

F.1.4 Parameter δ

We show the change in the Hopf bifurcation and the resulting change in the initial period when δ is varied with k and μ; δ varied with a, β and γ are shown in Figures F.1, F.6 and F.10 respectively.

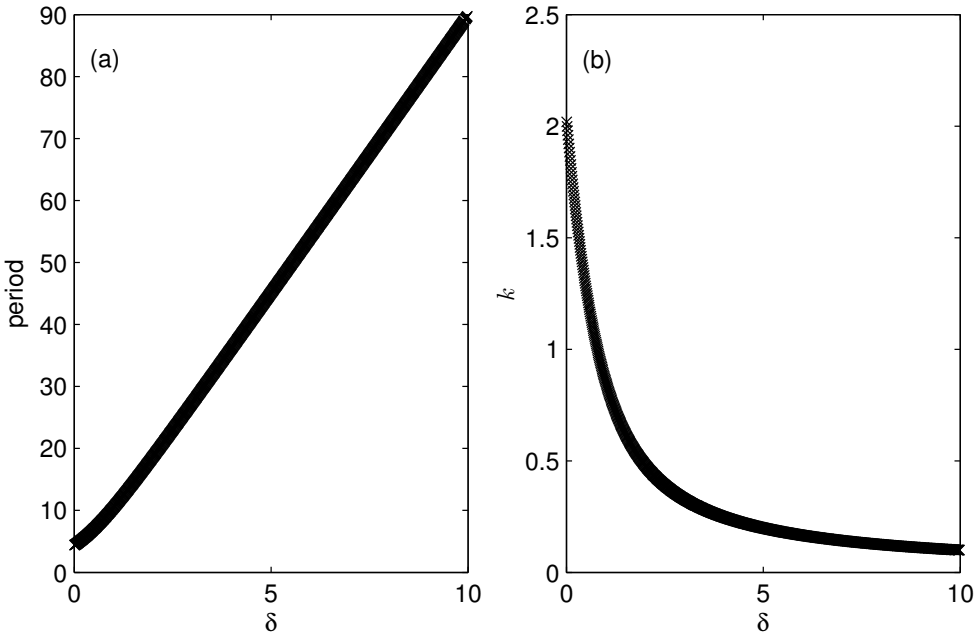

Figure F.13: Varying δ and k in the unforced system. In (a) the initial period at the Hopf bifurcation is shown. In (b), the Hopf bifurcation curve. All other parameters are kept constant at $a = 1.4/1.05$, $\beta = \gamma = 10/1.05$, and $\mu = 1.0003/1.05$.

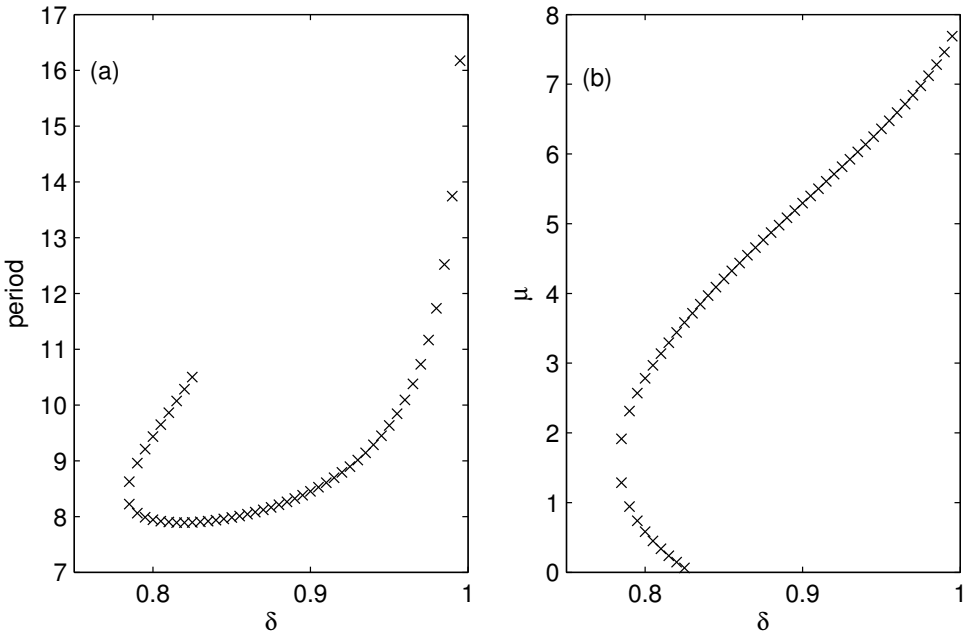

Figure F.14: Varying δ and μ in the unforced system. In (a) the initial period at the Hopf bifurcation is shown. In (b), the Hopf bifurcation curve. All other parameters are kept constant at $a = 1.4/1.05$, $\beta = \gamma = 10/1.05$ and $k = 1$.

F.1.5 Parameter k

We show the change in the Hopf bifurcation and the resulting change in the initial period when k is varied with μ in Figure F.15. Parameter k varied with a, β, γ and δ are plotted in Figures F.4, F.8, F.11 and F.13 respectively.

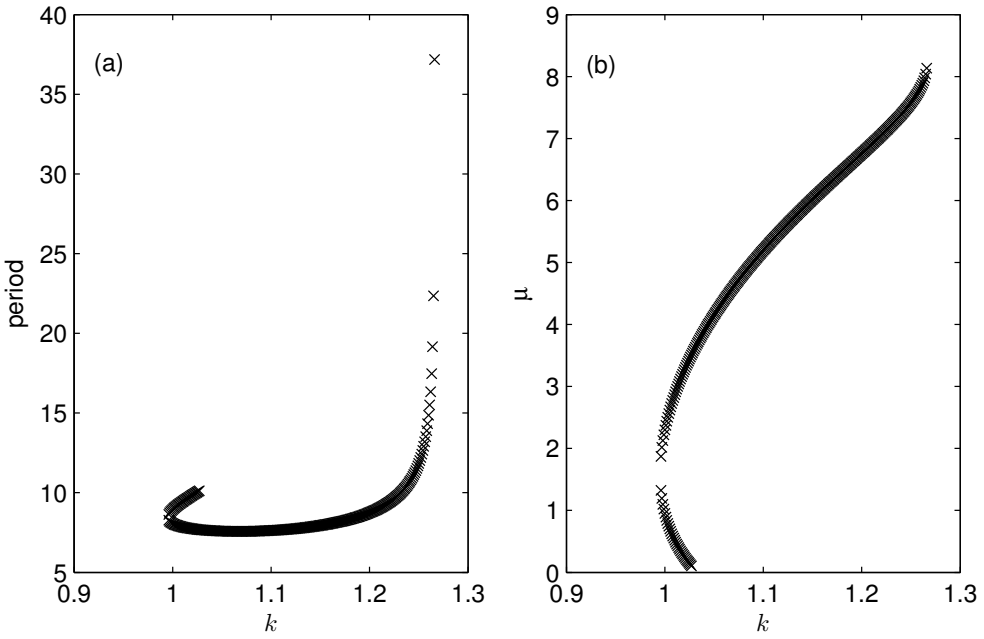

Figure F.15: Varying k and μ in the unforced system. In (a) the initial period at the Hopf bifurcation is shown. In (b), the Hopf bifurcation curve. All other parameters are kept constant at $a = 1.4/1.05$, $\beta = \gamma = 10/1.05$ and $\delta = 0.789798$.

F.1.6 Parameter μ

The change in the Hopf bifurcation and the resulting change in the initial period as μ is varied with each of the parameters in turn is shown in Figures F.5, F.9, F.12, F.14 and F.15.

F.1.7 Results

Figures F.1 - F.5 show that whenever parameter a is varied, concurrently with any other parameter, the initial period at the Hopf bifurcation decreases below 5 years. However, when any other parameter pair is considered, the initial period does not fall below 5 years at the Hopf bifurcation. As we are interested in the effect of seasonal forcing on lower period cycles, we chose to focus on varying a and let the location of the Hopf bifurcation also change with δ.